NTNU – Trondheim
Norwegian University of
Science and Technology

Seismic Response of Wind Turbines

Dynamic Analysis of a Wind Turbine in
Horizontal and Vertical Direction - Subject to
Earthquake, Wind & SSI

Remi André Kjørlaug

Civil and Environmental Engineering
Submission date: June 2013
Supervisor: Amir Kaynia, KT
Co-supervisor: Svein N. Remseth, KT

Norwegian University of Science and Technology
Department of Structural Engineering

Department of Structural Engineering
Faculty of Engineering Science and Technology
NTNU- Norwegian University of Science and Technology

ACCESSIBILITY:
OPEN

MASTER THESIS 2013

SUBJECT AREA:	DATE:	NO. OF PAGES:
STRUCTURAL DYNAMICS	07.06.13	165 + Cover

TITLE:

Seismic Response of Wind Turbines
Seismisk respons av vindturbiner

BY:

Remi André Kjørlaug

SUMMARY:
The main contributions and research within this thesis are based on a numerical model of a 5-MW wind turbine. Surrounding soil was modelled in order to investigate soil-structure interaction. The wind turbine was subject to various combinations of earthquake excitation and wind-induced load.

It is shown that the vertical excitation from an earthquake can produce severe vertical accelerations in the upper parts of the wind turbine. The vertical acceleration from earthquake motivates for future considerations regarding buckling in the steel tower (when combined with wind), disturbance of the fine-tuned machinery in the nacelle, and further considerations when designing the connection between nacelle and turbine tower.

Furthermore, results show that mainly higher order mode shapes were excited by horizontal earthquake excitation – due to the high natural periods of the structure.

A comparison between the statically applied wind and horizontal earthquake excitation concluded that soil-structure interaction can be of the uppermost importance for displacement of wind turbines. The same importance of soil-structure interaction was confirmed for base moment demand when combining earthquake and turbulent, dynamic wind – and in general throughout this thesis.

RESPONSIBLE TEACHER: Amir M. Kaynia

SUPERVISORS: Amir M. Kaynia and Svein N. Remseth

CARRIED OUT AT: Department of Structural Engineering, Faculty of Engineering Science & Technology, Norwegian University of Science & Technology

Department of Structural Engineering

FACULTY OF ENGINEERING SCIENCE & TECHNOLOGY
NTNU – Norwegian University of Science & Technology

Master Thesis 2013

by

Remi André Kjørlaug

Seismic Response of Wind Turbines

Seismisk respons av vindturbiner

Increasing focus on wind energy has lead to a need for knowledge on the dynamic response of wind turbines. Seismic response of wind turbines is a relative new field of research. This thesis will investigate the general response of wind turbines excited by earthquake alone, and in combination with wind-induced loads. The thesis will not focus on design, as it is a study of dynamic behavior and general trends in response. Effects from soil-structure interaction shall also be investigated throughout the work. In addition, the thesis does not include a thorough aerodynamic analysis.

The overall objectives can be summarized as follows:

i. Study and investigate existing research on the topic.
ii. Make careful and correct assumptions in order to utilize structural finite element methods rather than aerodynamic software.
iii. Obtain response from earthquake excitation.
iv. Study response from wind-induced loads, and compare with seismic response.
v. Present and discuss important finding and key aspects.

The thesis is organized in accordance with the current guidelines

Supervisors: Amir M. Kaynia and Svein N. Remseth

The thesis shall be submitted to the Department of Structural Engineering by June 10th, 2013.

NTNU, January 14th, 2013

Amir M. Kaynia
Responsible Teacher

Sammendrag

Denne oppgaven har undersøkt den dynamiske responsen av vindturbiner. Hovedsakelig har to forskjellige vindturbiner blitt undersøkt: en 65-kW vindturbin – som tidligere er blitt utsatt for ristebord-forsøk ved *University of California, San Diego* – samt en hypotetisk 5-MW vindturbin, produsert av *National Renewable Energy Laboratory* for å fungere som en referanseturbin i dimensjonering og forskning på vindturbiner. Numeriske modeller av begge vindturbinene ble laget i analyseprogrammet SAP2000.

Hovedmålet for modellen av vindturbinen på 65-kW var å sammenligne resultater fra påsatt jordskjelv i SAP2000 med resultater fra forskjellige fullskala, ristebord-forsøk. Resultatene presenteret i denne oppgaven for vindturbinen på 65-kW var meget tifredsstillende og lik resultatene fra forskningen ved *University of California, San Diego*. Dermed fungerte modellen (og tilhørende kalibrering) av vindturbinen på 65-kW som en kvalitetssikring av kandidatens evne til å produsere en tilfredsstillende, numerisk modell av en 5-MW vindturbin.

Hovedbidragene i denne oppgaven er basert på modellen av vindturbinen på 5-MW. En omfattende modell av jord og grunn laget for å studere påvirkningen av grunnen på konstruksjonen. Undersøkelser av egenfrekvensene for den sammenslåtte modellen (inkludert både grunn og vindturbin) viste resultater som samsvarte med grunnleggende teori om jord-struktur interaksjon.

Under analysene av vindturbinen på 5-MW ble den eksitert i én retning av gangen ved bruk av horisontal- og vertikal-komponenter fra jordskjelvet Nahanni (Canada) i 1985. Disse tidsseriene er modifisert og skalert for å tilpasses responsspektra som brukes i Eurocode 8. Vind ble påført konstruksjonen enten som; 1) statisk last; 2) en turbulent, dynamisk last; eller 3) ikke påført. Disse tre metodene sammenfaller med hovedmålsettingene for denne oppgaven; 1) å undersøke den generelle responsen av vindturbinene på 5-MW utsatt for kun jordskjelv; 2) responsen av jordskjelv kombinert med statisk eller dynamisk vindlast; og 3) en undersøkelse av når et jordskjelv kan likestilles med responsen fra statisk vind. I tillegg var det et hovedmål å undersøke responsen av vindturbinen utsatt for kun vertikal eksitasjon fra jordskjelv.

Hovedresultatene fra denne oppgaven er tredelt. Først ble det vist at vertikal

eksitasjon fra et jordskjelv kan føre til alvorlig høy akselerasjon øverst i vindturbiner. Følgende kan vertikal akselerasjon fra et jordskjelv føre til motivasjon for undersøkelser av lokal knekking i tårnet (når kombinert med vind), forstyrrelse av det finstemte maskineriet i nacellen, samt generelt flere hensyn under dimensjonering av koblingen mellom nacellen og tårnet.

Videre viste resultater fra analysene at hovedsakelig høyere ordens egenfrekvenser og svingeformer blir eksitert av jordskjelv (horisontalt) når det gjelder vindturbiner av denne størrelsen (5-MW) – hovedsakelig på grunn av de høye egenperiodene for disse konstruksjonene. Dermed vil den midterste delen av tårnet oppleve den høyeste akselerasjonen og relativt store utbøyninger. Disse resultatene viser at nøye overveielser bør utøves langs hele tårnet, og spesielt i de boltede skjøtene mellom de forskjellige tårn-seksjonene. Jordskjelv viste seg også veldig dominerende i horisontal akselerasjon langs tårnet sammenlignet med den påsatte dynamiske vinden.

Til slutt ble en sammenligning mellom statisk påsatt vindlast og horisontal eksitasjon fra jordskjelv gjennomført. Denne sammenligningen konkluderte med at grunnens påvirkning på konstruksjonen kan være veldig viktig for vindturbiners utbøyning. Jordskjelv klarte ikke å gi like høy respons som statisk vind – selv for høye spissverdier av grunnakselerasjon – når man antok stiv grunn. Men, for mykere grunn kunne utbøyningen og momentkrav i bunnen av turbintårnet bli lik (eller høyre) enn responsen fra statisk vind. Den samme konklusjonen angående jord-struktur interaksjon ble trukket for momentkravet i bunnen av turbintårnet ved kombinasjon mellom jordskjelv og den påsatt dynamiske vinden – og generelt gjennom hele oppgaven.

Abstract

This thesis conducted research in the structural dynamic response of wind turbines. Mainly, two different wind turbines were investigated: a 65-kW wind turbine – which has previously been subject to shake table testing at *University of California, San Diego* – and a hypothetical 5-MW reference wind turbine produced by *National Renewable Energy Laboratory* to serve as a baseline in wind turbine design and research. Finite element models were created of both these wind turbines in SAP2000.

The main objective of the modelled 65-kW wind turbine was to compare results from earthquake excitation in SAP2000 to the results obtained from various full-scale shake table tests. The results provided in this thesis from the 65-kW wind turbine matched previous research from *University of California, San Diego* very well. Thus, the 65-kW wind turbine model served as a quality assurance of the authors' ability to produce an adequate finite element model of the 5-MW wind turbine.

The main contributions and research within this thesis are based on the numerical model of the 5-MW wind turbine. Surrounding soil was modelled in order to investigate soil-structure interaction. A study of the natural frequencies for the combined model, containing both modelled soil and the wind turbine, revealed expected results from basic theory of soil-structure interaction.

For the purpose of analysis, the wind turbine (including modelled soil) was excited uni-axially by the horizontal and vertical component of the 1985 Nahanni, Canada earthquake. These records are modified and scaled in order to match response spectra from Eurocode 8. Further, depending on the analysis conducted, the wind load was applied as either; 1) a static load; 2) a turbulent, dynamic load; or 3) not applied. These three conditions coincides with the main objectives for the thesis; 1) investigating the general response of the 5-MW wind turbine subject to earthquake excitation alone; 2) the response of earthquake excitation combined with static or dynamic wind load; and 3) an investigation of when an earthquake can match the response from static wind. In addition, a main objective was to study the response of vertical excitation alone.

The *main* results produced from this thesis are three-folded. First, it is shown

that the vertical excitation from an earthquake can produce severe vertical accelerations in upper parts of a wind turbine. This vertical acceleration from earthquake motivates for future considerations regarding buckling in the steel tower (when combined with wind), disturbance of the fine-tuned machinery in the nacelle, and further considerations when designing the connection between nacelle and turbine tower.

Secondly, when considering a wind turbine of this size (5-MW), mainly the higher order mode shapes were excited by horizontal earthquake excitation – due to the high natural periods of this structure. As such, the middle parts of the tower will experience the highest accelerations and fairly high displacements. These results show that careful considerations must be shown along the tower height, and especially in the bolted connections between the different parts of the tower. Also, in terms of horizontal acceleration, earthquake proved to be very dominant compared to dynamic wind.

Lastly, a comparison between the statically applied wind and horizontal earthquake excitation concluded that soil-structure interaction can be of the uppermost importance in regards to the displacement of wind turbines. Observations showed that earthquake could not match the static wind-induced displacement – even for high PGAs (peak ground acceleration) – when considering stiff soils. However, for softer soils, the displacement and base moment demand from earthquake could very well match the static wind-induced response. The same importance of soil-structure interaction was confirmed for base moment demand when combining earthquake and turbulent, dynamic wind – and in general throughout this thesis.

Preface

This master thesis was written during the spring semester of 2013. It marks the end of my five year Master of Science degree in Civil and Environmental Engineering, with study towards a specialization in Structural Engineering. My degree will be obtained from Norwegian University of Science and Technology, NTNU, in Trondheim. This master thesis represents my chosen specialization (*TKT4920 - Structural Design*) for the Department of Structural Engineering.

Over the years as a student I have attended various courses in structural design, structural statics, structural dynamics, linear & non-linear finite element method, earthquake engineering and geotechnical dynamics among others. These courses, with the corresponding knowledge obtained, provides a solid foundation in order to produce this master thesis.

Mainly, SAP2000 was the computer software used to perform the structural analysis for this project. Assistance in the modelling was provided by the company Engineering Data Resources (EDR). Other programs like Matlab and Excel were also widely used. Lastly, the thesis was written in LaTeX.

Acknowledgements

Credit and acknowledgements must be awarded to Adjunct Professor Amir M. Kaynia of Norwegian Geotechnical Institute (NGI) and NTNU, for educational sessions and meetings on the topic, in addition to cumulative assistance in this thesis. In addition, Professor Svein Remseth of NTNU provided a daily support, answered questions and enlightened problems.

Associate Professor Michael Muskulus of NTNU provided some insight in the science and dynamics of wind turbines which was much appreciated.

I spent my fourth year abroad at *University of California, San Diego*. It was during this year I obtained great interest for dynamics and seismic design. Because of this, I would like to extend a thank you to the professors and staff at *UCSD* for introducing me to the topic. Especially Professor Ahmed Elgamal who also provided crucial material, dissertations, articles and guidance in this thesis. Also, Professor J. Enrique Luco provided some

materials on specific subjects, and Dr. Ian Prowell (now of MMI Engineering) provided some additional input and recommendations for this thesis.

Credit must be given to EDR for providing support and assistance for every challenge encountered in SAP2000 along the way. Also, Statkraft AS made room in their schedule to arrange a visit to a wind farm near Trondheim called Hitra. Acknowledgements is thus made to Hans Bolme and Frode Vitsø of Statkraft AS.

Lastly – but of the uttermost importance – is the acknowledgement towards the motivation and support provided by my friends and family over the years as a student. It kept me sane (more or less).

Building bridges
ain't the hardest part
it's trying to swim
once they fall apart

Israel Nash Gripka

Trondheim – June 7, 2013

Remi André Kjørlaug

Contents

List of Figures

List of Tables

List of Symbols & Abbreviations

Roman Letters & Symbols

$\sum U_i$	Summarized mass participation ratio in direction i
$\overline{V}(10)$	Reference wind velocity at z = 10 m
a_n	Second Fourier-coefficient
B	Bulk Modulus
b_n	Third Fourier-coefficient
c_0	First Fourier-coefficient
C_d	Drag coefficient
C_k	Fourier Amplitude Spectra Coefficient
c_n	Fourier Amplitude-coefficient
C_{rad}	Equivalent damping coefficient for radiation damping
D	Cross sectional depth of structure for wind pressure
E	Youngs Modulus
f	Frequency in Hz
f_0	Fixed-base natural frequency
f_{damp}	Force due to damping in dynamic equations
f_e	Equivalent natural frequency
f_v	Vertical natural frequency
G	Shear Modulus
H	Depth of soil layer above bedrock
k_{spring}	Spring stiffness coefficient
k_T	Terrain roughness coefficient
k_v	Vertical spring stiffness coefficient
L_e	Length of element in FEM
N_{mod}	Number of modes
P	Rotational frequency of wind turbine blades
$q_U(t)$	Velocity pressure induced by wind
R_n	Rotor radius for wind turbine n
S_e	Elastic Response Spectra Coefficient
T_n	Thrust force for wind turbine n
V_p	Pressure wave velocity
$V_{s,30}$	Average value of propagation velocity of Shear-waves in the upper 30 m of the soil profile at a shear strain of 10^{-5}

	or less.
$V_{s/p}$	Indicates pressure wave velocity or shear wave velocity
V_s	Shear wave velocity
z_0	Terrain roughness length
z_f	Cartesian flow axis
°C	Degree of Celsius
g	Acceleration of Gravity, 9,81 $[m/s^2]$
m	Meters
N	Newton
r	Radius of foundation system
s	Seconds
t	Time variable
z	Vertical (height) coordinate

Greek Letters & Symbols

$\alpha_{Joint-Base}$	Amplification factor from described joint to base of wind turbine
$\alpha_{Joint-EQ}$	Amplification factor from described joint to earthquake
α_0	Mass proportional Rayleigh damping coefficient
α_1	Stiffness proportional Rayleigh damping coefficient
α_b	Caughey damping coefficient number b
β	Angular frequency ratio
η	Hysteretic damping ratio
λ	Wavelength
λ_0	Average intensity (mean-squared acceleration)
μ	Rupture strength of the material along a fault
ν	Poisson's Ratio
ω_0	Fixed-base natural angular frequency
ω_e	Equivalent natural angular frequency
ω_n	Radian natural frequency number n
ω_v	Vertical natural angular frequency
ϕ_n	Fourier Phase number n
ρ	Mass density
ξ	Viscous damping ratio in general
ξ_{aero}	Viscous damping ratio induced by aerodynamics
ξ_n	Viscous damping ratio number n
ξ_{soil}	Viscous damping ratio induced by soil characteristics
ξ_{steel}	Viscous damping ratio in steel of the given structure
ξ_{tot}	Indicates total viscous damping ratio
°	Indicates orientation in N-S and E-W direction

Vectors & Matrices

$\ddot{u}_{wind+EQ}^{joint}$	Response in terms of acceleration due to simulated turbulent wind-induced load and earthquake in given joint
$\ddot{u}_{wind}^{joint}$	Response in terms of acceleration due to simulated turbulent wind-induced load in given joint
$\dot{u}_g$	Ground velocity
$\left[\tilde{\boldsymbol{C}}\right]$	Modal damping matrix
$\left[\tilde{\boldsymbol{K}}\right]$	Modal stiffness matrix
$\left[\tilde{\boldsymbol{M}}\right]$	Modal mass matrix
$[\Phi]$	Matrix of eigenvectors
$\left\{\tilde{\boldsymbol{L}}\right\}$	Modal vector for ground acceleration
$\{\ddot{\eta}\}$	Relative modal acceleration
$\{\ddot{u}\}$	Relative acceleration vector
$\{\ddot{u}_{tot}\}$	Total acceleration vector
$\{\dot{\eta}\}$	Relative modal velocity
$\{\dot{u}\}$	Relative velocity vector
$\{\dot{u}_{tot}\}$	Total velocity vector
$\{\eta\}$	Relative modal displacement
$\{\eta_{tot}\}$	Total modal displacement
$\{u\}$	Relative displacement vector
$\{u_{tot}\}$	Total displacement vector
$\overline{V}(z)$	Mean wind velocity
M_{Ed}^{base}	Moment demand in base of wind turbine
$U(z,t)$	Total wind velocity
$u(z,t)$	Turbulent wind velocity
u_{wind}^{nac}	Displacement of nacelle due to wind-induced load
$[-]$	Denotes a matrix or a unit
$\ddot{u}_g$	Ground acceleration
$\ddot{u}_i$	Acceleration peak i used for log decrement
$[\mathbf{C}]$	Damping matrix
$[\mathbf{K}]$	Stiffness matrix
$[\mathbf{M}]$	Mass matrix
$\{\mathbf{R}(t)\}$	Given principal external load
$\{\Phi_n\}$	Eigenvector number n
$\{r\}$	Influence coefficient vector for ground motion to structure DOFs
$\{-\}$	Column-vector
d	Displacement vector in FEM
F	Force vector in FEM

$F(\omega)$	Amplification function as a function of angular frequency
$F_{thrust,sim}(t)$	Simulated turbulent wind-induced thrust force, function of time
$F_{thrust,static}$	Static wind-induced thrust force, independent of time
F_z	Force in vertical direction
PF	Modal Participation Factor
$u^{x-dir}_{node\#n}(x_i, y_i, z_i)$	Nodal displacement value of node n in X-direction, with coordinates x_i, y_i, z_i
u_g	Ground displacement

Abbreviations & Terms

ADAMS	Automatic Dynamic Analysis of Mechanical Systems
DNV	Det Norske Veritas AS
DOF	Degree of Freedom
EDR	Engineering Data Resources (Company)
EQ	Earthquake
FAST	Fatigue, Aerodynamics, Structures and Turbulence
FEDEM	Fedem Technology AS (Company)
FEM	Finite Element Method
GL	Germanischer Lloyd
HAWT	Horizontal Axis Wind Turbine
HHT	The Hilber-Hughes-Taylor algorithm for numerical integration
IEC	International Electrotechnical Commission
Joint	Denotes point-of-interest along the height of a wind turbine
LDR	Load Dependent Ritz-vectors
LHPOST	Large High Performance Outdoor Shake Table
NGI	Norwegian Geotechnical Institute (Company)
Node	Denotes a node in a FEM-model
NREL	National Renewable Energy Laboratory
NTNU	Norwegian University of Science & Technology
OpenSees	Open System for Earthquake Engineering Simulation
PGA	Peak Ground Acceleration
RMS	Root Mean-Square Acceleration
RPM	Revolutions Per Minute
SSI	Soil-Structure Interaction
UCSD	University of California, San Diego

1. Introduction

Wind energy is a renewable form of energy. Focus on renewable and clean energy over the past decade has thus increased the motivation for wind energy using wind turbines. China is by 2011 the largest country in terms of globally installed wind power, followed by the U.S. Also, both India and Italy are large contributors to wind power in a global scale [Wiser and Bolinger, 2012] (See Appendix A for details on world rankings). These are all highly seismic active regions [Prowell and Veers, 2009; Hänler et al., 2006].

In the U.S., California had the highest increase of wind power in 2011, and is now the third state in terms of cumulative production. In addition, Oregon and Washington are both among the ten largest states in the U.S. in terms of MW installed [Wiser and Bolinger, 2012].

Indeed, wind turbines are already playing a critical role in the infrastructure of many countries and regions. By recognizing the fact that a wind farm is a collection of large, expensive, unique and homogeneous structures important to the infrastructure, it becomes imperative that the probability of total shut-down should be at a minimum. In the extreme event of a larger earthquake in a city the spread of different building will equally allocate the damage throughout the city. However, at a wind farm, an earthquake can cause a collapse of every turbine within a defined area. Consequently, some guidelines recommend designing the wind turbines (or at least some of its components) as *high safety class* [DNV, 2013; Risø, 2002; EC8-1, 2004].

1.1 Wind Turbine Type & History

Although the field of wind energy and wind turbines for producing electricity is relatively new, there has been some historical development in terms of the structure and types of wind turbines [Burton et al., 2011]. By now, the industry mostly produce the three bladed Horizontal Axis Wind Turbines (HAWTs) [Manwell et al., 2002; Risø, 2002]. A typical HAWT is displayed in Figure 1.1.

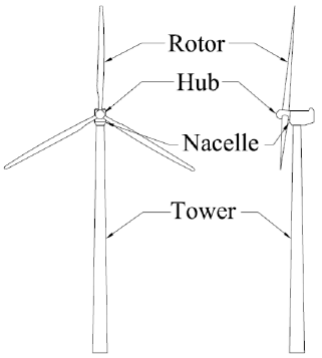

Figure 1.1: *Principle sketch of a HAWT [Prowell, 2011].*

The tower is typically a thin-walled steel tower, whilst the rotor blades are often made of some lighter polyester material. The nacelle contains the gearbox, generator, shafts and other fine-tuned machinery. The turbine tower is traditionally pre-fabricated in sections, and bolted together on site [Nuta, 2010].

In order to increase efficiency of the wind turbine, and in addition converting a degree of freedom to a fixed, controllable parameter, active yaw is implemented in most modern turbines [Prowell, 2011; Burton et al., 2011]. The active yaw will orient the rotor to face the wind.

The 65-kW and 5-MW wind turbines assessed for the analysis presented here is a HAWT and uses active yaw. The 65-kW wind turbine is a Danish wind turbine, produced by Nordtank [Prowell, 2011]. This turbine was highly utilized in California in the 1980s [Hau, 2006]. The 5-MW turbine is developed as a reference turbine, and only exists on paper.

Historically, modelling the structure would be conducted by a beam-like tower with a lumped mass on the top to represent the nacelle, rotor and blades. However, with increasing computer efficiency and rapidly growing dimensions of wind turbines more detailed models are desired in order to provide a realistic description of the turbine dynamics [Hänler et al., 2006]. The level of reliability grows naturally with the size and cost of the wind turbines.

1.2 Objectives & Scope

The main focus and objective of this thesis is the overall, global dynamic response of the wind turbine. The thesis has not focused on detailed design of neither wind turbines and its components, or the foundation systems.

This includes studying the effects of earthquake excitation, wind induced loads, and the effect of soil-structure interaction. To clarify, even though the effects of wind induced loads has been studied, this is *not* a study of aerodynamics as it is mainly a study of structural engineering.

1.2.1 Research Questions

Some of these research questions are justified in Chapter 2.2, by looking at previous work on the subject.

1) Vertical Acceleration: A study of the effect vertical, seismic acceleration has on a typical, modern HAWT. In civil structures the vertical component of seismic action is often very simplified as the capacity in vertical direction often exceeds this demand [Løset et al., 2010]. However, a wind turbine includes fine tuned machinery, and have a rather concentrated, complex load at the top (nacelle, rotor and blades).

2) General Seismic Response of Wind Turbines: Knowledge and understanding of the general seismic response of HAWTs are obtained and studied, mainly through base excitation using an actual time serie.

3) Effect of Wind & Earthquake: Wind induced loads are simplified in order to obtain some information of the demand created by wind. Further, the effect of wind induced loads together with an earthquake is investigated. Lastly, it is investigated when a typical earthquake can exceed the demand from simplified wind-induced loads.

1.3 Outline of Thesis

After a brief introduction – including an overview of modern wind turbines, some historical aspect and status of wind energy, followed by definitions of the main objectives – Chapter 2 presents existing guidelines, and some previous research related to this thesis.

Chapter 3 presents necessary theory for the subject. The subjects introduced vary from being general about earthquake engineering, to very specific on the design of wind turbines. Some additional theoretical aspects are continuously introduced and utilized throughout the thesis.

In order to obtain knowledge and verify the modelling of wind turbines in a structural software, Chapter 4 is dedicated to model a smaller wind turbine and compare obtained results with actual shake table data provided by *University of California, San Diego*. The level of detail provided from the shake table experiment ensured invaluable experience in correctly modelling a wind turbine in this type of software.

Chapter 5 presents the development of a numerical model of a large, megawatt-scale wind turbine. This numerical model includes modelled soil in order to fully include soil structure interaction. The soil required some special modelling techniques in order to match the theoretical behaviour of soil subject to bedrock excitation. Chapter 5 also contains an overview of different set-ups and configurations used in the different analysis' conducted.

Chapter 6 is a natural successor to Chapter 5, as it presents the natural frequencies and mode shapes of the modelled wind turbine. Also, the effect of different soil on the natural frequencies is investigated. Due to some ambiguous results, the utilization of another soil-structure interaction approach is needed to obtain data on certain natural frequencies.

Due to the magnitude and amount of analysis' of interest, Chapter 7 is purely dedicated to describing the loads (earthquake and wind), load combinations, assumptions in the different analysis, procedure in the software and the approach concerning damping.

The results are presented in Chapter 8. This chapter has been divided into several parts: Chapter 8.1:*Results from Vertical Set-Up* which presents results concerning vertical response, mainly due to vertical excitation. Further, Chapter 8.2:*Results from Horizontal Set-Up* presents the results concerning horizontal excitation and wind-induced load – both alone and combined. The responses obtained vary from acceleration, displacement, vertical forces

in wind turbine, and moment demand in the base. Throughout, the level of effect from earthquake compared to wind-induced loads is investigated.

In addition, Chapter 8 contains two extra parts: a study of the effect from earthquake compared to static wind, and a *brief* comparison to existing work and recommendations in current codes and guidelines.

Lastly, Chapter 9 contains the concluding remarks, and recommendations for further research on the topic.

Appendix

As a note, the Appendices mainly contains elaborated information on the wind turbines (both experimental data from previous research and additional information from the models in this study), theoretical definitions, and various obtained results from this thesis not directly shown in Chapter 8.

Also, some Matlab-scripts essential for calculations are included in the Appendix. No CD or .zip file is enclosed for this thesis. Direct contact with the author is preferred if more information is of interest.

2. Previous Work

There have been conducted some amount of research in the field of wind turbines and seismic activity, and already a number of guidelines have been developed.

2.1 Codes & Guidelines

There exists a number of standards for design of wind turbines:

- Guidelines for Design of Wind Turbines [Risø, 2002], created through cooperation of DNV and Risø National Laboratory.
- Certification of Wind Turbines [GL, 2010].
- IEC 61400-1: Wind Turbines - Part 1: Design Requirements [IEC, 2005].

In addition, with the growth of offshore wind industry there exist some specific standards for these:

- Design of Offshore Wind Turbines [DNV, 2013].
- Guideline for the Certification of Offshore Wind Turbines [GL, 2012].
- IEC 61400-3: Wind Turbines - Part 3: Design Requirements for Offshore Wind Turbines [IEC, 2009].

NREL 5-MW Reference Turbine

Recognising that wind turbines are more or less confidential information kept by the manufacturers, *National Renewable Energy Laboratory* (herein NREL) has developed a numerical 5-MW reference wind turbine as reported in Jonkman et al. [2009]. This turbine was developed by using any public available information on the structural, operational and other aspects of wind turbines that existed at the time.

2.2 Previous Research

University of California, San Diego (herein UCSD) has conducted extensive work on several wind turbines, with focus on seismic response and other dynamic properties:

The 65-kW Wind Turbine:

The research done at UCSD regarding the 65-kW wind turbine presented in this research includes, among others:

- Study of seismic response of a 65-kW wind turbine at the Large High Performance Outdoor Shake Table (LHPOST)@UCSD in 2004 [Prowell et al., 2009; 2008].
- A more extensive study of the same 65-kW wind turbine at the same location that included parked and operating states, configuration and levels of shaking and denser instrumentation in 2010 [Prowell et al., 2012; 2013].
- Modifying the FAST code (an open source software capable of modelling turbine dynamics [Jonkman and Buhl Jr., 2005]) to enable base shaking in addition to other loads. The results from analysis in FAST are compared through a validated OpenSees (an open source computational platform [Mazzoni et al., 2006]) model of the 65-kW wind turbine developed from the previous research [Prowell et al., 2010a].

The 5-MW Reference Wind Turbine:

Regarding the NREL 5-MW reference turbine, it has been conducted a fair amount of research from various institutions. Some of the work from UCSD on this matter include:

- Estimating the seismic load demand for a wind turbine in time domain, using the FAST code [Prowell et al., 2010d].
- Checking soil-structure interaction effects using OpenSees [Prowell et al., 2010b].

Other Research

The most relevant research, concerning some of the topics in this thesis is presented below:

- An investigation of turbines ranging from 65-kW to 5-MW concluded that consideration of aerodynamics and operational state becomes increasingly important with size [Prowell, 2011]. Thus, one motivation for this research has been to study how more structural based software, such as SAP2000, can produce adequate results by using the correct assumptions concerning the aerodynamics and other factors which are better obtained in software like FAST, FEDEM and others.
- An early Ph.D. dissertation [Kühn, 2003] on offshore wind energy systems suggested that considerable research was "needed to develop reliable means of computing the extreme response of offshore wind energy converters".
- Prowell [2011] concluded that soil-structure interaction was important, especially for large machines. This Ph.D. dissertations also expressed the need for "tools capable of modelling an operational turbine, foundation, and soil systems subjected to a *turbulent wind field*" in order to fully understand the implications of possible soil structure interaction.
- Prowell et al. [2010b] stated that it was important to conduct further soil-structure interaction research as an integral component of seismic response studies.
- An article concerning damping of an offshore wind turbine [Damgaard et al., 2012], concluded that, in general, significant research is needed within the field of determining the dynamic properties of offshore wind turbine structures.
- Kiyomiya et al. [2002] concerned the combination of wind and earthquake. The mean wind velocities and large-scale earthquake events were simulated from a Weibull distribution. The occurrence probability of the mean wind velocities and large-scale earthquake events can be calculated from these Weibull distributions. The probability of the simultaneous occurrence of storms and large-scale earthquakes was proven extremely small. Thus, it was concluded that the use of mean-wind velocity was reasonable when combining wind and earthquakes.

  The article examined a wind turbine with pile foundation. They suggested that other types of foundations should be checked for seismic

capacity. Furthermore, Kiyomiya et al. [2002] concluded that dynamic analysis is required to consider a dynamic behaviour of not only the earthquake, but also the wind.

To the knowledge of the author, very little attention has been given to the vertical response of wind turbines due to seismic loads. It is common practice in earthquake engineering to concentrate more on the horizontal excitation, because the vertical excitation might be small and structures in general have more capacity in the vertical direction [Løset et al., 2010; Ritschel et al., 2003]. However, Ritschel et al. [2003] briefly reported of high response in vertical direction due to earthquake excitation.

Also, most of the existing research on the topic of wind-induced loads and earthquake in structural based software have simplified the wind as a static horizontal load [Kiyomiya et al., 2002; Prowell et al., 2010a].

However, some of the work done at UCSD which included the use of a turbulent wind field [Prowell et al., 2010d; Prowell, 2011], concluded that ignoring aerodynamic effects (e.g. by simplifying the wind as a static load), may result in inaccurate predictions of extreme loads. Further, questions was raised about the accuracy and level of conservatism when conducting these simplified simulations.

3. Theory

A typical wind turbine is a highly dynamic structure. It is a tall and slender structure, with a rather concentrated mass on the top and low overall weight [Damgaard et al., 2012]. In addition there is a lot of aerodynamics and complex effects from the rotating blades, wind loading, yawing of the rotor and pitching of the blades [Burton et al., 2011]. Indeed, under normal operating conditions the loads on wind turbines is strongly dominated by wind-induced loads.

However, research has concluded that these structures must be designed carefully against any overloading, as they have little capacity beyond its elastic limit. Especially with the tendency for taller wind turbines, the seismic response may become more critical [Nuta, 2010].

3.1 Wind-Induced Loads

Although it is not the main focus in this thesis, some basic wind theory is presented. Wind loads on a structure can be superimposed by a quasi-static part and a turbulent part [Strømmen, 2010]:

$$U(z,t) = \overline{V}(z) + u(z,t) \tag{3.1}$$

Here $U(z,t)$ is the total wind velocity, $\overline{V}(z)$ is the mean wind velocity and $u(z,t)$ the turbulent wind velocity. The mean wind velocity is assumed purely as a function of the height coordinate, z. As such, only the turbulent part contributes to variety in the time domain for a given height. This principle is shown in Figure 3.1.

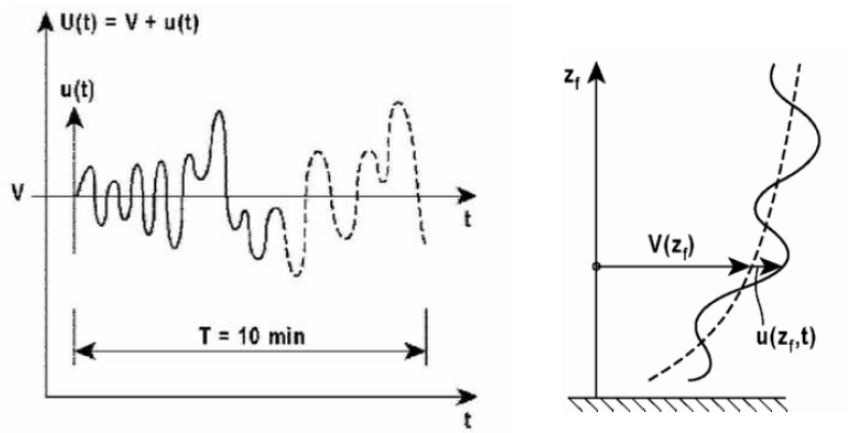

(a) Principles of wind velocities in time. *(b) Principles of wind velocities at in space.*

Figure 3.1: *Basic principles of wind velocities [Strømmen, 2010].*

Data for the mean wind velocity is typically provided in codes and guidelines, such as Eurocode 1: Part 1-4 (herein EC1-4 [2004]). To obtain $U(z,t)$ for a given height, some functions exists which can be applied to assess the mean wind velocity, $\overline{V}(z)$, at the height of interest. Summarized, EC1-4 [2004] recommends a logarithmic function:

$$\overline{V}(z_f) = \overline{V}(10)k_T \cdot ln\left[\frac{z_f}{z_0}\right] \tag{3.2}$$

In Equation (3.2), $\overline{V}(10)$ is a reference wind velocity (often at the height of 10 m and averaged over 10 min), k_T is the terrain roughness coefficient and, lastly, z_0 denotes the terrain roughness length. Furthermore, using Bernoulli's equation yields the wind velocity pressure [Strømmen, 2010]:

$$q_U(t) = \frac{1}{2}\rho\left[U(t)\right]^2 C_d D \tag{3.3}$$

$$q_U(t) = \frac{1}{2}\rho\left[\overline{V}^2 + 2\overline{V}u(t)\right] C_d D \tag{3.4}$$

In Equation (3.4), the higher order term of $[u(t)]^2$ has been neglected. Thus, the wind induced pressure will also consist of a quasi-static and turbulent part, as well as the wind induced forces and wind induced structural response, as shown in Figure 3.2.

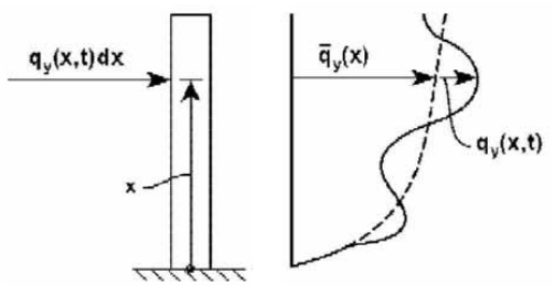

(a) *Principles of a line-like structure.* ***(b)*** *Principles of wind induced pressure on structure.*

Figure 3.2: *Basic principles of wind induced pressure [Strømmen, 2010].*

Note that the coordinate along the structures axis in Figure 3.2a is x, whereas it is generally denoted z in this work.

3.1.1 Wind-Induced Loads on Wind Turbines

DNV [2013] lists direct and indirect wind-induced loads to be considered for wind turbines:

- Direct wind-generated loads:
  - Aerodynamic blade loads.
  - Aerodynamic drag forces on tower and nacelle.
- Indirect wind-generated loads:
  - Gravity loads on the rotor blades, vary with time due to rotation.
  - Centrifugal forces and Coriolis forces due to rotation.
  - Gyroscopic forces due to yawing.
  - Braking forces due to braking of the wind turbine.

As the objective of this study is mainly global responses, these loads have been simplified or neglected as further explained in Chapter 4.3 and Chapter 7.3.

3.2 Seismic Loads

DNV [2013] mainly focuses on using a simplified model with a lumped mass on the top and earthquake excitation defined as response spectra in terms of pseudo response spectra, thus reducing the procedure to a static problem [Chopra, 2012]. DNV [2013] further recommends to analyse the turbine in one vertical and two horizontal directions, but implies that it is normally sufficient to run just one horizontal analysis due to symmetry. Also, it is suggested that the scope of the vertical analysis can be limited to a static capacity for buckling induced by the largest vertical acceleration (i.e. largest vertical load by earthquake).

IEC [2005] does not require an earthquake assessment in locations that are excluded by the local seismic code (e.g. EC8-1 [2004] or IBC [2006]) due to weak seismic action. However, in locations with high seismicity, the seismic load must be combined with a specified operational loading. The seismic load shall be based on the ground acceleration for a 475-year recurrence period. IEC [2005] gives opportunities to carry out evaluation both in frequency- and time-domain.

GL [2010] is very similar to IEC [2005], and specifies that wind loads shall be combined with the earthquake acceleration with a return period of 475 years, which is also the given return period for earthquake acceleration in EC8-1 [2004].

3.2.1 Equation of Motion

Earthquakes produce excitation of the ground which the structure is built on. Assuming that the given structure is linear elastic and time-invariant, applying Eulerian formulation and considering dynamic equilibrium of a given structure yields the dynamic equation for earthquakes [Humar, 2005; Irgens, 2008]:

$$[\mathbf{M}]\{\ddot{u}_{tot}\} + [\mathbf{C}]\{\dot{u}_{tot}\} + [\mathbf{K}]\{u_{tot}\} = 0 \tag{3.5}$$

[**M**] denotes the mass matrix of the system, and [**C**] denotes the damping matrix of the system – discussed further in Chapter 3.3. [**K**] represents the stiffness matrix of the system considered. Furthermore:

$$\{u_{tot}\} = \{u\} + \{r\}\, u_g(t) \tag{3.6}$$

Here $\{u\}$ and u_g denotes the displacement relative to the ground, and displacement of the ground itself, respectively. $\{r\}$ is a vector of influence coefficients. Further, $\{\dot{u}_{tot}\}$ and $\{\ddot{u}_{tot}\}$ denotes the derivatives with respect to time (i.e. velocity and acceleration).

Assuming that internal forces and damping forces are only induced by deformations within the structure, i.e.:

$$[\mathbf{C}]\{\dot{u}_g\} = [\mathbf{K}]\{u_g\} = 0 \tag{3.7}$$

This assumption is valid for uniform and "stiff" buildings (not recommended to be applied structures immersed in water and structures subject for high air friction).

Thus, Equation (3.5) becomes [Humar, 2005]:

$$[\mathbf{M}]\{\ddot{u}\} + [\mathbf{C}]\{\dot{u}\} + [\mathbf{K}]\{u\} = -[\mathbf{M}]\{r\}\,\ddot{u}_g(t) \tag{3.8}$$

In Equation (3.8) inertia forces due to the ground accelerations has been moved over to the right hand side of the equal sign in order to act as an forced-motion [Humar, 2005].

Assessing the undamped, unloaded equation of motion yield the natural frequencies of the structure by solving Equation (3.9) for ω_n^2 [Chopra, 2012]:

$$\left|\,[\mathbf{K}] - \omega_n^2\,[\mathbf{M}]\,\right| = 0 \tag{3.9}$$

$$\omega_n^2 \neq 0 \tag{3.10}$$

When ω_n^2 is obtained, the corresponding eigenvectors (mode shapes) can be found by solving Equation (3.11) for $\{\Phi_n\}$ [Chopra, 2012]:

$$\left[[\mathbf{K}] - \omega_n^2\,[\mathbf{M}]\right]\{\Phi_n\} = 0 \tag{3.11}$$

$$[\Phi] = [\{\Phi_1\}\{\Phi_2\}...\{\Phi_{N_{mod}}\}] \tag{3.12}$$

Further, the following relations can be applied:

$$\{u_{tot}\} = \{\Phi\}\{\eta_{tot}\} \tag{3.13}$$

$$[\Phi]^T[\mathbf{M}][\Phi] = \left[\tilde{\boldsymbol{M}}\right] \tag{3.14}$$

$$[\Phi]^T[\mathbf{K}][\Phi] = \left[\tilde{\boldsymbol{K}}\right] \tag{3.15}$$

$$[\Phi]^T[\mathbf{M}]\{r\} = \left\{\tilde{\boldsymbol{L}}\right\} \tag{3.16}$$

And assuming that the modal damping matrix is defined as shown in Equation (3.17):

$$[\Phi]^T [\mathbf{C}] [\Phi] = \left[\tilde{\boldsymbol{C}}\right] \tag{3.17}$$

Then the equation of motion becomes uncoupled due to modal orthogonality, yielding the modal equation [Humar, 2005]:

$$\left[\tilde{\boldsymbol{M}}\right] \{\ddot{\eta}\} + \left[\tilde{\boldsymbol{C}}\right] \{\dot{\eta}\} + \left[\tilde{\boldsymbol{K}}\right] \{\eta\} = -\left\{\tilde{\boldsymbol{L}}\right\} \{\ddot{u}_g\} \tag{3.18}$$

Thus, Equation (3.8) becomes Equation (3.18) – the modal equilibrium equation. Pre-multiplying Equation (3.18) by $\left[\tilde{\boldsymbol{M}}\right]^{-1}$ produces the modal participation factor:

$$PF = \left[\tilde{\boldsymbol{M}}\right]^{-1} \left\{\tilde{\boldsymbol{L}}\right\} \tag{3.19}$$

This modal participation factor obtains the level of contribution to the total response for given modes of interest.

3.3 Damping

The matrices [**M**] and [**K**] are straight forward to define, and are not given much focus in this study. The challenge really lies in the matrix [**C**].

3.3.1 Damping Algorithms

SAP2000 uses modal damping, hysteretic-proportional damping or Rayleigh damping. Hysteretic-proportional damping is not widely used in classical time domain analysis, but often used in steady-state (frequency domain) analysis. It is briefly introduced in Chapter 5.2. Modal damping is used in modal analysis, but has one major disadvantage: it leads to zero damping for the modes for which the modal damping ratios are not specified [Luco, 2008b].

Rayleigh Damping

Rayleigh damping is a mass-proportional and stiffness-proportional damping matrix defined as [Humar, 2005]:

$$[\mathbf{C}] = \alpha_0 [\mathbf{M}] + \alpha_1 [\mathbf{K}] \tag{3.20}$$

Where α_0 and α_1 are quantities to be calculated.

In general the α_1 coefficient will be more significant than α_0 for damping [Bergan et al., 1993]. The Rayleigh damping matrix is simple and banded, however one can only assign damping ratios for two frequencies [Luco, 2008b].

Caughey Series Damping

One alternative algorithm of assigning damping is the use of Caughey series. Whereas the Rayleigh damping matrix uses only two frequencies to assign damping, the Caughey damping matrix can use n number of frequencies [Humar, 2005]. The Caughey damping matrix is presented in Equation (3.21):

$$[\mathbf{C}] = \sum_{b=0}^{n-1} \alpha_b [\mathbf{M}] ([\mathbf{M}]^{-1} [\mathbf{K}])^b \tag{3.21}$$

Selecting $n = 4$ as an example, produces the four first terms of the Caughey series:

$$\begin{aligned} [\mathbf{C}] = {} & \alpha_0[\mathbf{M}] + \alpha_1[\mathbf{K}] + \\ & \alpha_2[\mathbf{K}][\mathbf{M}]^{-1}[\mathbf{K}] + \alpha_3[\mathbf{K}][\mathbf{M}]^{-1}[\mathbf{K}][\mathbf{M}]^{-1}[\mathbf{K}] \end{aligned} \tag{3.22}$$

Equation (3.22) exhibits that the Caughey damping matrix with only two terms is the same as Rayleigh damping [Chopra, 2012]. However, the Caughey damping algorithm does have a few drawbacks. With the use of more than two terms (i.e. extended Rayleigh damping), the damping matrix becomes fully populated [Chopra, 2012], which entails a computational cost. Also, the determination of damping ratios may include solving an ill-condition system of equations (see Appendix B.1 for further details on the ill-conditioned system of equations) [Luco, 2008a].

Lucos' Algorithm

An alternative damping matrix that leads to classical normal modes and that depends explicitly on prescribed modal damping ratios are presented in Equation (3.23) and Equation (3.24) [Luco, 2008b]:

$$[\mathbf{C}] = \sum_{n=1}^{m} 2\xi_n \omega_n \left[\mathbf{L}_n^{m-1}\right], \quad (n = 1, N_{mod}), \ (m \leq N_{mod}) \tag{3.23}$$

$$\left[\mathbf{L}_n^{m-1}\right] = \frac{[\mathbf{M}] \prod_{s=1, s\neq n}^{m} \left([\mathbf{M}]^{-1}[\mathbf{K}] - \omega_s^2[\mathbf{I}]\right)}{\prod_{s=1, s\neq n}^{m} (\omega_n^2 - \omega_s^2)}, \quad (r \leq m) \tag{3.24}$$

This algorithm removes the drawback of solving a possibly ill-conditioned system of equations to obtain the different damping ratios. In addition it produces non-zero damping for the modes where there is no prescribed damping ratios provided [Luco, 2008b].

Classical & Non-Classical Damping

All of the above are examples of *classical damping* matrices – best applied when the structures considered are fairly uniform in material and components. *Non-classical damping* should be applied when considering a system with components differing significantly in level of damping [Chopra, 2012], e.g. soil-structure interaction when dealing with structures with very short natural periods. The structures in this thesis will very likely have rather high natural periods, thus making them suitable for classical damping.

Obviously damping is a challenging area. Rayleigh damping has some major drawbacks (for further reading on the disadvantages and controversy of Rayleigh damping, see Wilson [2002]), and it could be desirable to include different algorithms in SAP2000. Nevertheless, Rayleigh damping is assumed and applied in most practical analyses [Chopra, 2012], and it is also the algorithm applied in SAP2000 when direct integration is used [CSI, 2013].

3.3.2 Damping Ratios of Wind Turbines

As described in Damgaard et al. [2012], the total system viscous damping ratio can be expressed as a linear combination of the following parts:

$$\xi = \xi_{steel} + \xi_{aero} + \xi_{soil} \tag{3.25}$$

Damgaard et al. [2012] considered an offshore turbine with a oscillation damper installed in the tower. The contributions from the tuned damper and surrounding water are neglected in this study as this is a land-based structure with no damper installed. However, tuned slosh dampers can be very useful for these high, slender structures [Fujii et al., 1990] and have proved to also be effective against seismic action [Nanda and Biswal, 2011].

Directivity of Damping in Wind Turbines & Guideline Recommendations

For a parked turbine of the size considered in the first part of this study (65-kW), damping can easily go below 1% [Prowell, 2011]. Furthermore, some research showed that a theoretical approach can lead to "negative" damping ratios [Riziotis et al., 2004], and it appears that new pitch controlled turbines have higher damping in the first natural frequency. In addition, most of the published work on damping of wind turbines shows that damping is higher in the fore-aft direction than in the side-side direction [Prowell, 2011; Riziotis et al., 2004]. Especially when regarding operating condition vs. parked condition the damping values in the fore-aft direction can get doubled when operating – while the side-side direction remains relative constant [Prowell et al., 2013]. This directivity of damping justifies both the need for consideration of seismic response in both directions, and somewhat argues against the recommendations of DNV [2013] as explained in Chapter 3.2 [Prowell et al., 2013].

Neither GL [2010], Risø [2002] or DNV [2013] provide any guidance as to the level of critical structural damping to be applied for the first bending modes of wind turbines. IEC [2005] however, suggest a damping of 1% for the first tower mode, if a design response spectrum is used.

As a note, DNV [2013] recommends that the damping in soil should be taken as both internal and radiation damping, i.e. dissipation of energy through layers of soil or soil-rock boundary [Kramer, 1996].

3.4 Operating Frequencies of Wind Turbines

In addition to natural frequencies related to the global structure (i.e. the structure resembling a cantilever beam [Laura et al., 1974]), wind turbines have natural frequencies strongly related to the operational states. For the three-bladed HAWTs in this study, natural frequencies from operating condition are *1P* and *3P*. 1P is associated with the cyclic loading from mass imbalances in the blades while rotating. 3P is associated with the shadowing effect: i.e. each time a blade passes the tower it causes a load on the structure [Andersen et al., 2012].

It is a driving factor to avoid correlation between the tower natural frequencies and the natural frequencies from the rotating blades in order to prevent self-excitation. This has lead to three design approaches for wind turbines [Kühn, 2003]:

- Soft-soft design: Tower frequency is less than 1P.
- Soft-stiff design: Tower frequency is between 1P and 3P.
- Stiff-stiff design: Tower frequency is higher than 3P.

This principle is schematically illustrated in Figure 3.3.

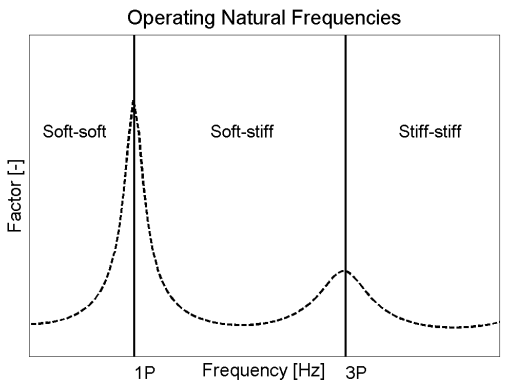

Figure 3.3: *Principles of natural frequencies for a typical HAWT.*

3.5 Soil-Structure Interaction (SSI)

Earthquakes produce a movement from the bedrock, but different soils between the bedrock and the structure will transform the movement (i.e. waves) differently [Kramer, 1996; Wilson, 2002; Bachman, 2003]. The 1985 Mexico City earthquake and other recent earthquakes exhibit the importance of this fact. These earthquakes were greatly (by over a factor of five) amplified because of the weak soil they are built on [Wilson, 2002].

Soil Material Parameters

To account for different ground-types the shear and pressure wave velocity (V_s and V_p) of the soil has been changed, and results obtained. Listed below are different material quantities, applicable for soil:

$$Shear\ Modulus : G = \rho V_s^2 \tag{3.26}$$

$$Youngs\ Modulus : E = 2G(1+\nu) \tag{3.27}$$

$$Bulk\ Modulus : B = \frac{E}{3(1-2\nu)} \tag{3.28}$$

$$Poisson's\ Ratio : \nu = \frac{E}{2G} - 1 \tag{3.29}$$

Also, the pressure wave velocity should be explicitly mentioned:

$$Pressure\ Wave\ Velocity : V_p = \sqrt{\frac{B + \frac{4}{3}G}{\rho}} = \sqrt{\frac{G(2-2\nu)}{\rho(1-2\nu)}} \tag{3.30}$$

The ratio between pressure waves and shear waves is presented in Equation (3.31):

$$\frac{V_p}{V_s} = \sqrt{\frac{2-2\nu}{1-2\nu}} \tag{3.31}$$

The Poisson's Ratio could be changed in order to account for different soil qualities, but is remained constant throughout this thesis as 0.25. Thus, this produces a relation of $V_p/V_s = 1.73$. However, this thesis is not an extensive study of different soil-types, but changing V_s will provide a fair variation of the soil. Also, these equations explicitly exhibits context between shear wave velocity and soil mechanics.

Amplification Functions of Soil

Amplification functions that calculates the ratio between bedrock and free surface response can be derived in order to compute the design response at the base of a structure. Theoretical solutions exist for uniform, undamped soil; uniform, damped soil; layered, damped soil etc. [Kramer, 1996]. A relevant amplification function is introduced in Chapter 5.2.

3.6 Earthquake Statistics & Design Principles

Registration of seismic activity provides the foundation of applying statistics in order to obtain some design principles on the topic. Measuring *Peak Ground Acceleration* (i.e. the largest ground acceleration in any direction of an earthquake) and calculating the response of different structures with different natural periods yields *Response Spectra*. This type of analysis is commonly used, both in Eurocode 8 and International Building Code (herein EC8-1 [2004] and IBC [2006] respectively).

SAP2000 can conduct code checks using different load combinations and response spectrum-analysis. SAP2000 also allows for the possibility of shaking the modelled structure with an actual record of an earthquake (i.e. time domain), and obtain results from this using either modal combination or direct integration. EC8-1 [2004] approves the possibility of using a time serie analysis in seismic design, as long as the time series is representative for the location of the structure of interest.

4. Validating SAP2000 with a 65-kW Wind Turbine

4.1 65-kW Wind Turbine

Recognizing the fact that most previous studies have been conducted using software like FAST and OpenSees, the need for some validation with existing results was desired in order to validate the use of SAP2000. Thus, a model of the 65-kW wind turbine was created based on its geometry, mass and materials. Its natural frequencies were compared to existing results, and the wind turbine was shaken with the Landers earthquake [PEER, 2013]. The true wind turbine is further elaborated in Appendix C. The data for the turbine is presented in Table 4.1:

Table 4.1: *65-kW wind turbine properties [Prowell et al., 2008].*

Property	**Values**
Rated power	65-kW
Rated wind speed	11,9 m/s
Operational RPM	45 - 55 RPM
Rotor diameter	16,0 m
Tower height	21,9 m
Lower section length	7,9 m
Lower section diameter	2,0 m
Middle section length	7,9 m
Middle section diameter	2,0 m
Top section length	6,0 m
Top section diameter	1,1 m
Tower wall thickness	5,314 mm
Rotor hub height	22,6 m
Tower mass	6400 kg
Nacelle mass	2400 kg
Rotor mass (with hub)	1900 kg

The tower was modelled as a cylindrical shell of steel, the nacelle was modelled as solid elements of a user-defined material with the correct mass

and size. The blades were modelled as cylindrical sections of a fibreglass reinforced polyester material defined through a user-defined material. In order to match the given data and natural periods for the turbine the mass density and stiffness had to be somewhat modified, but the overall mass is correct. The turbine was assumed fixed to its base. A summary of the different components are given in Table 4.2, and the resulting model to represent the wind turbine is shown in Figure 4.1.

Table 4.2: *Component data of 65-kW model in SAP2000.*

Component [-]	**Material** [-]	**Mass density** $[kg/m^3]$	**Youngs Modulus** $[MPa]$
Tower	Steel, S275	9891	200 000
Nacelle	User-defined	1529	210 000
Rotor	Steel, S275	1101	210 000
Blades	Polyester	1101	10 000

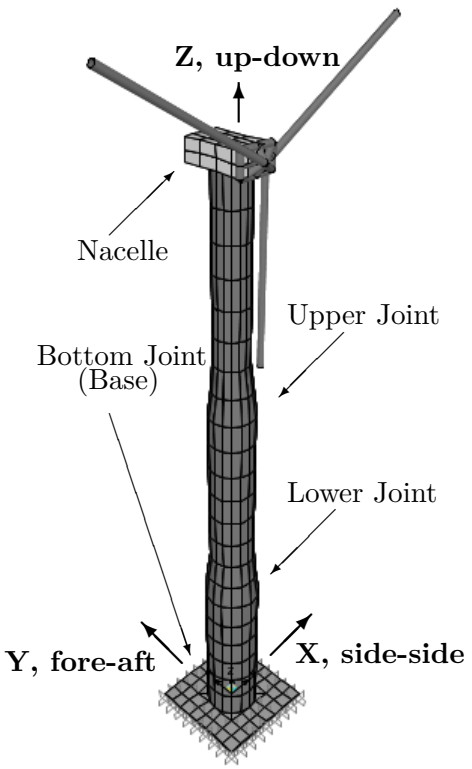

Figure 4.1: *Model of the 65-kW wind turbine in SAP2000.*

Coordinate system is also shown in Figure 4.1. Traditionally the X-direction is named side-side direction and the Y-direction is named fore-aft direction or upwind-downwind direction [Burton et al., 2011; Prowell et al., 2009]. Z-direction is up-down direction.

4.2 Natural Frequencies & Mode Shapes

Referring to Chapter 3.4 and Table 4.1, the system natural frequencies due to rotating blades can be obtained (averaged RPM):

$$\frac{50\ RPM}{60\ s} = 0,83\ s \tag{4.1}$$

$$1P: \quad \frac{1}{0,83\ s} = 1,20\ Hz \tag{4.2}$$

$$3P: \quad \frac{3}{0,83\ s} = 3,60\ Hz \tag{4.3}$$

As mentioned in Chapter 3.4, it is desirable to design the tower to not have natural frequencies near these operational frequencies in order to avoid self excitation.

Modal eigenvector analysis in SAP2000 will produce unloaded, undamped natural frequencies and mode shapes. The structural natural frequencies obtained by SAP2000 are presented and compared with existing results from Prowell et al. [2009; 2012] in Table 4.3 and the four first global mode shapes are shown in Figure 4.2.

Table 4.3: *Natural frequencies of the 65-kW wind turbine, compared to previous work.*

	2004 [Prowell et al., 2009]				**2010 [Prowell et al., 2012]**		**This study**	
f_n	***ShakeTable***		***Model***		***ShakeTable***		***Model***	
#	**Type**	**f [Hz]**	**Type**	**f [Hz]**	**Type**	**f [Hz]**	**Type**	**f [Hz]**
1	Side-Side	1,70	Side-side	1,68	Fore-Aft	1,70	Fore-aft	1,66
2	Combined	11,7-12,3	Fore-aft	1,68	Side-Side	1,71	Side-side	1,68
3	...	...	Torsional	9,20	...	...	Torsional	9,16
4			Side-side	10,8	Fore-Aft	11,9	Fore-aft	11,9
5			Fore-aft	10,9	Side-Side	12,4	Side-side	11,9

Note that the more recent natural frequencies from 2010 are obtained from analysis conducted at LHPOST@UCSD only, while the natural frequencies

from 2004 are both from LHPOST@UCSD and from a computational model developed at the time.

Table 4.3 shows that the model developed in SAP2000 exhibits quite a good match with previous work. Especially compared to the shake table tests performed, while the numerical model developed in Prowell et al. [2012] shows a bit more deviation in the 2^{nd} side-side and fore-aft natural frequencies. However, the difference is not too large, and the focus of this validation has been to match the actual wind turbine (i.e. the natural frequencies obtained from shake table testing). Also, the structural natural frequencies does not coincide with the operational natural frequencies presented in Equation (4.2) and (4.3), and the wind turbine is a soft-stiff design. The corresponding mode shapes are shown in Figure 4.2:

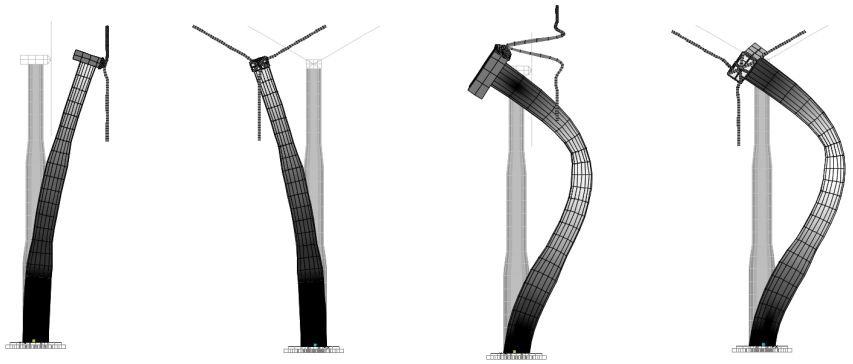

(a) 1^{st} *(fore-aft: 1,66 Hz).* ***(b)*** 2^{nd} *(side-side: 1,68 Hz).* ***(c)*** 3^{rd} *(fore-aft: 11,9 Hz).* ***(d)*** 4^{th} *(side-side: 11,9 Hz).*

Figure 4.2: *First four mode shapes of the 65-kW model obtained from SAP2000.*

Figure 4.2 clearly shows the classic mode shapes of a cantilever beam with a point mass at the end [Laura et al., 1974]. Figure 4.2c shows some unnatural movement of the blades. This is due to some tweaking and modifying of the model and rigidity of the blades in order to better match the dynamic properties from previous research. This study has focused on global responses, and responses of the blades are not of interest in this thesis. In addition, previous research has shown that loads on the blades caused by earthquake is significantly lower than the designed value of an extreme wind load [Ritschel et al., 2003].

4.3 Wind-Induced Load

Recognizing the fact that SAP2000 is not an aerodynamic software, the wind (when of interest) is applied as an equivalent thrust-force working on the rotor with a load value depending on the wind speed. Since there is no information on thrust-force as a function of wind speed available for the 65-kW wind turbine, scaling has been applied from the NREL 5-MW wind turbine presented in Chapter 2.1. According to Manwell et al. [2002] the relation in Equation (4.4) can be applied to scale the thrust force:

$$\frac{T_1}{T_2} = \left[\frac{R_1}{R_2}\right]^2 \tag{4.4}$$

Where T_n is the thrust-force for wind turbine n and R_n is its rotor radius. The scaled thrust-curve for the 65-kW wind turbine is presented in Figure 4.3.

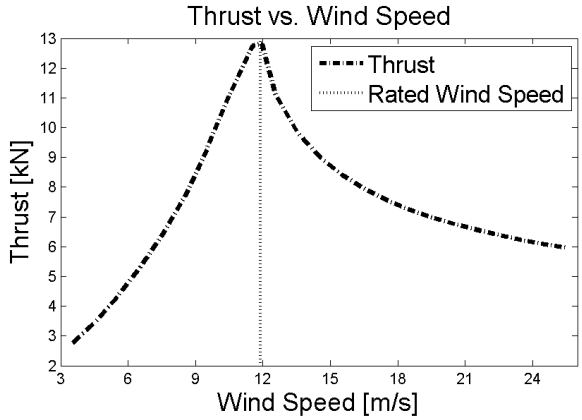

Figure 4.3: *Thrust curve for the 65-kW wind turbine.*

The thrust peak clearly coincides with the rated wind speed for the wind turbine, i.e. the wind speed which rated power is achieved [Prowell, 2011].

For the analysis and validation process in this chapter, the lack of data concerning wind conditions during the shake table test of Prowell et al. [2009] yielded motivation for investigating wind data provided in the extended research done in Prowell et al. [2013], presented in Chapter 2.2.

The meteorological data from Prowell et al. [2013] is presented in Table C.2, with the wind speed ranging from 2,5 m/s to 5,1 m/s. For this validation

analysis, the averaged wind speed of 3,5 m/s was used. Referring to Chapter 3.1, the analysis was only performed using a mean wind velocity. Thus, a static thrust force of 2,8 kN as the horizontal force at the nacelle, in the positive fore-aft direction.

4.4 Earthquake Record & Analysis Procedure

In the original shake-table test program, the turbine was parked with one blade oriented downward (as the model exhibited in Figure 4.1) and the turbine was shaken with a uni-axial, horizontal base motion, imparted to the side-side direction [Prowell et al., 2009]. The numerical analysis will imitate these conditions: referring to Figure 4.1, the modelled turbine was shaken in the X-(side-side)-direction.

4.4.1 Earthquake Record

The time-series selected for the test program was the East-West component of the Landers earthquake, dated 1992-06-28 [PEER, 2013]. Some selected data for this earthquake is presented in Table 4.4 (some of these earthquake quantities are elaborated in Appendix B.2):

Table 4.4: *Landers earthquake and derived data.*

Parameter	**Data**
Name	Landers
Date	26^{th} June, 1992
Country	USA
Station	CDMG 12149 Desert Hot Springs
Station Direction	DSP090 (east-west)
Fault Distance	23 [km]
$V_{s,30}$	345,40 [m/s]
M_w	7,28 [-]
PGA	0,154 [g]
RMS Acceleration	0,266 [g]
Arias Intensity	0,678 [m/s]
Relative Significant Duration	31,980 [s]

The original work in Prowell et al. [2009] also included scaled records of this earthquake to 100%, 150% and 200%. However, this work is only a

validation; therefore, only the "normal" record was utilized.

The time series is plotted in Figure 4.4, and includes Arias Intensity and Fourier Amplitude Spectra of the record. In addition, the calculated pseudo acceleration response spectrum for the Landers record is shown (using the Matlab script `Respons_Spec.m` provided in Appendix B.4), as well as the design spectrum for ground type A from EC8-1 [2004].

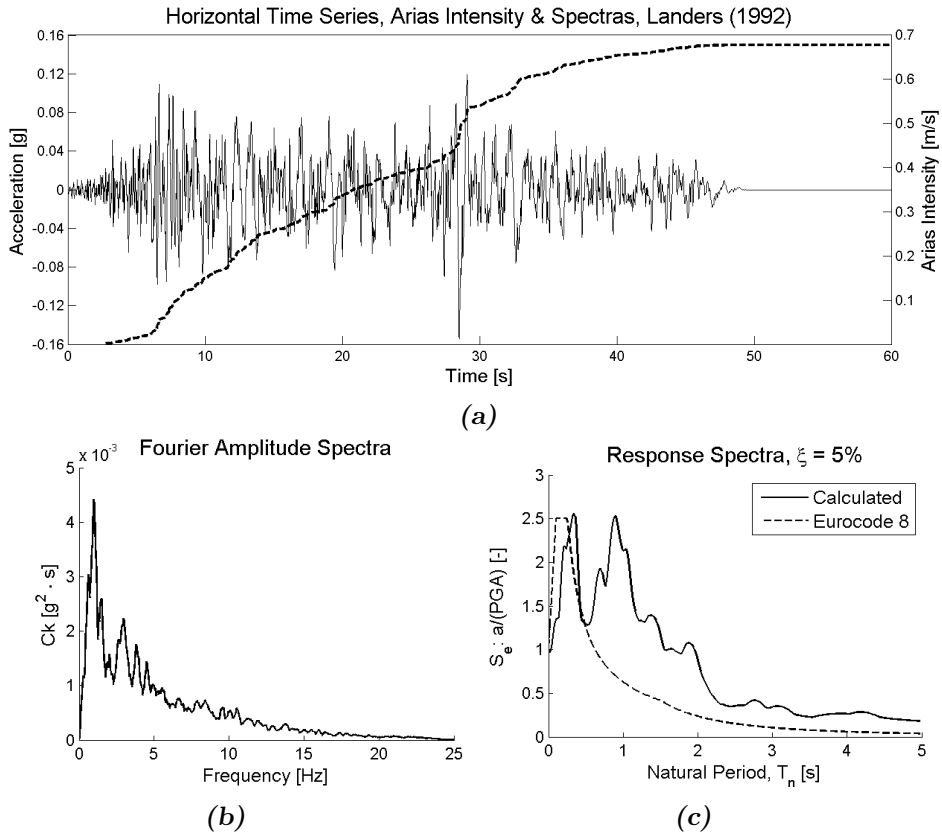

Figure 4.4: *Time series & Arias, Fourier amplitude spectra and response spectra for the Landers earthquake.*

As can be seen on Figure 4.4b, this records contains mostly frequencies from approximately 1-10 Hz. Note that the first natural frequencies were found to be from 1,6 $\sim$ 12 Hz (Table 4.3).

4.4.2 Method & Analysis

Modal combination was used as algorithm for the analysis, and the first 10 modes were included. Higher modes contained frequencies well beyond frequencies of a normal earthquake [Chopra, 2012; Kramer, 1996]. Modal participation table for the 10 first modes is given in Appendix C.3. As seen on Figure 4.5, approximately 10 seconds were added at the end of the time series to observe a free-vibration phase of the structure.

Modal damping ratios were assigned according to the modal damping ratios for the parked 65-kW wind turbine, obtained from LHPOST@UCSD [Prowell, 2011] presented in Table 4.5:

Table 4.5: *Assigned modal damping ratios.*

Mode #	**Type**	ξ
1	1^{st} Fore-aft	1,0 %
2	1^{st} Side-side	1,1 %
3	1^{st} Torsional	3,5 %
4	2^{nd} Fore-aft	1,5 %
5	2^{nd} Side-side	2,2 %
⋮	⋮	⋮
n	...	3,5 %

Note that an overall modal damping ratio of 3,5% was assigned to all other modes in this study when nothing else is specified. In Prowell et al. [2009], a modal damping ratio of 3,5% was assigned to the rest of the modes in form of Rayleigh damping in the numerical model. However the work in this thesis is purely compared with the specific wind turbine and shake table test conducted in Prowell et al. [2009].

4.5 Seismic Response

In order to compare the numerical model developed in SAP2000 to the shake table test in Prowell et al. [2009], response along the height of the 65-kW wind turbine was collected in terms of acceleration. Figure 4.1 indicates the joints were the output was collected (acceleration was also registered from the top of the nacelle). Note that the bottom joint (base) as indicated in Figure 4.1 was not used for output in this analysis.

Figure 4.5 exhibits the results gather from the numerical analysis in SAP2000. Clearly, the nacelle experiences severe amplification of the base input acceleration.

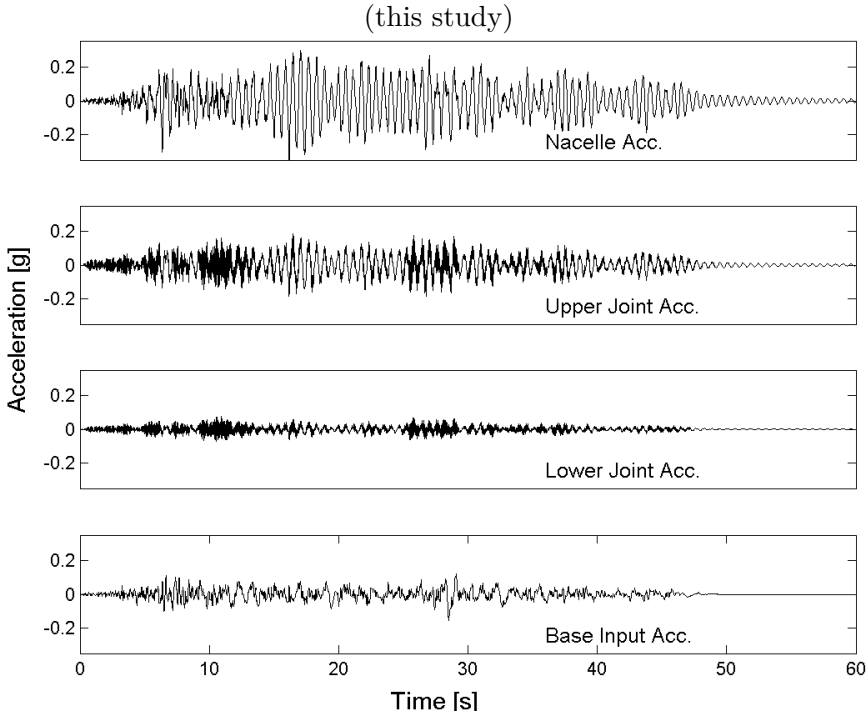

Figure 4.5: *Time series response from SAP2000 for the Landers earthquake.*

In order to compare with Prowell et al. [2009], Figure 4.6 exhibits the results gathered in Prowell et al. [2009] in the same terms as explained above (i.e. accelerations along the height of the 65-kW wind turbine).

(previous study, Prowell et al. [2009])

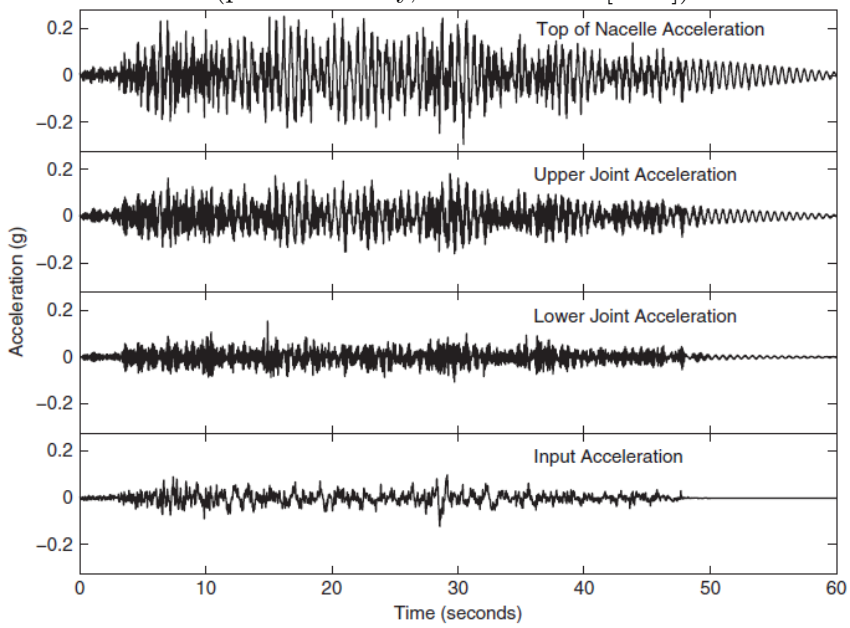

Figure 4.6: *Results from shake table testing of the 65-kW wind turbine [Prowell et al., 2009].*

It appears that the lower joint in this study does not experience as much amplification of the base input movement as expected, and is not to consistent with the results presented in Prowell et al. [2009]. This could be due to some difference in the way the mode shapes behaves in SAP2000 vs. the real wind turbine.

Furthermore, it seems that the nacelle mostly experiences rather low-frequency motion. This coincides with the dominant first side-side mode-shape, which mainly consists of uniform, almost linear side-side movement of the nacelle and the entire tower in general (Figure 4.2b). To further validate the model, a check of the overall structural damping was performed in the free vibration phase (approximately 50-60 s in Figure 4.5) using the log decrement method [Chopra, 2012; Humar, 2005]:

$$\xi \approx \ln\left(\frac{\ddot{u}_i}{\ddot{u}_{i+1}}\right)/2\pi \tag{4.5}$$

$$\xi \approx \ln\left(\frac{0,0202}{0,019}\right)/2\pi \approx 0,975\% \tag{4.6}$$

A result of a damping of less then 1% coincides with the work done in Prowell et al. [2009].

Transfer Functions of Seismic Response

To further elaborate, Figure 4.7 shows the transfer functions for the *base to different joints and nacelle*. The peaks in Figure 4.7 clearly coincides with the natural frequencies presented in Table 4.3. In addition, the dominance of nacelle movement in the first peak shows, yet again, the first mode shape and low-frequency movement (as discussed above).

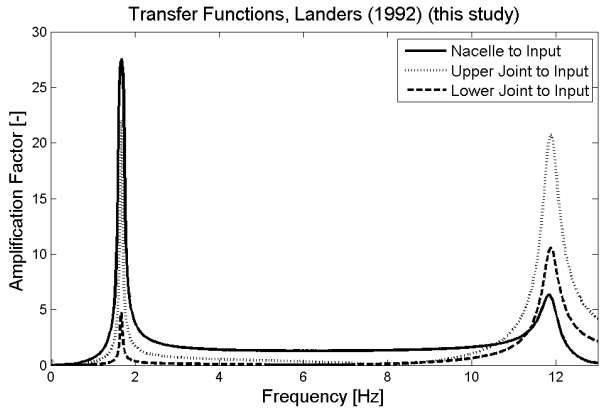

Figure 4.7: *Transfer functions for Landers earthquake response.*

To compare, Figure 4.8 shows an averaged transfer function of *base to nacelle* acceleration from test performed in Prowell et al. [2009].

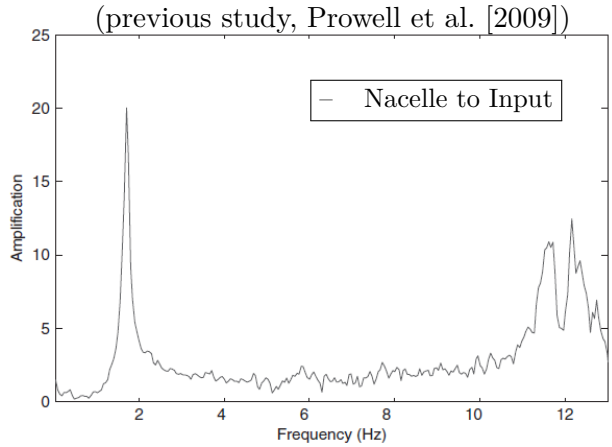

Figure 4.8: *Averaged transfer function from base to nacelle [Prowell et al., 2009].*

In general the transfer function from this study shows approximately the same results as the shake table test, but there exist some difference in the magnitude of amplification. The SAP2000 model presented in this work has a higher peak for the first natural frequency than Prowell et al. [2009], and lower peak at the second natural frequency. This could be due to the complexity of recreating the geometry from the real structure in a numerical model, and getting the mode shapes to behave exactly as the mode shapes of the real turbine.

Further, the fact that the previous research (Figure 4.8) shows two peaks near 12 Hz, could be due to some beating phenomenon near the second frequency of resonance [Mansfield and O'Sullivan, 2008]. This can be caused by poor measurement sensors, etc. As explained, the work conducted in Prowell et al. [2009] was the first shake table test of a wind turbine and was state-of-the-art, but somewhat limited. However, Prowell et al. [2009] was followed by a more extensive and elaborated shake table test in Prowell et al. [2012].

4.6 Conclusion & Discussion

This chapter presented a study of a numerical model in SAP2000, which was shaken with an earthquake record at its base. Comparing the response from SAP2000 with existing results from a shake table using the actual wind turbine, yielded both motivation and invaluable knowledge about adjusting and correctly modelling this type of structure in a non-aerodynamic software.

The responses obtained in this study matched the results from previous research very well. Thus, the confidence and experience from this chapter will be of great value in the rest of this thesis.

5. Numerical Model of a 5-MW Wind Turbine

After achieving fairly satisfactory results in Chapter 4 for the 65-kW wind turbine, and gaining knowledge and ensuring the quality of modelling a wind turbine in SAP2000, the idea to develop a model of a larger and more modern wind turbine was pursued.

5.1 5-MW Reference Turbine

As introduced in Chapter 2.1, NREL created a 5-MW reference turbine [Jonkman et al., 2009]. This model serves as a baseline for research and development in the field of wind turbines. Some of the data for the turbine is presented in Table 5.1:

Table 5.1: *5-MW wind turbine properties [Jonkman et al., 2009].*

Property	**Values**
Rated power	5MW
Rated wind speed	11,4 m/s
Operational RPM	12,1 RPM
Rotor diameter	126 m
Tower height	87 m
Lower section diameter	6 m
Top section diameter	3,87 m
Hub diameter	3 m
Tower wall thickness	27 - 19 mm
Rotor hub height	90 m
Tower mass	347 460 kg
Nacelle mass	240 000 kg
Rotor mass (with hub)	110 000 kg
Total wind turbine mass	697 460 kg

The tower diameter linearly decreases towards the top, along with the tower wall thickness.

Even though previous research suggest that beam-column models of wind turbines can produce results that are consistent with detailed models containing shells in the tower [Bazeos et al., 2002], and in the turbine blades [Malcolm and Laird, 2003], the same techniques used for the 65-kW turbine presented in Chapter 4 was utilized. That is, the tower were modelled as a cylindrical shell of steel and the nacelle was modelled as solid elements of a user-defined material with the correct mass and size. The blades were modelled as cylindrical sections of a fibreglass reinforced polyester material defined through a user-defined material.

Even though it is not described in Jonkman et al. [2009], stiffening rings have been added within the turbine tower, at approximately every 3 m along the tower height in order to prevent buckling of the tower. This agrees with previous similar work [Lavassas et al., 2003; Bazeos et al., 2002]. The stiffener rings are made of the same material as the tower. Material parameters are summarized in Table 5.2:

Table 5.2: *Component data of 5-MW model in SAP2000.*

Component [-]	**Material** [-]	**Mass density** $[kg/m^3]$	**Youngs Modulus** $[MPa]$
Tower	Steel, S275	10500	210 000
Nacelle	User-defined	1578	210 000
Rotor	Steel, S275	152 905	210 000
Blades	Polyester	158	10 000

Overall, the mass of the entire turbine is correct. The extremely high mass density of the rotor might be surprising, but this is due the fact that the rotor and hub is not modelled as a massive point, but as a discrete number of beams connecting the nacelle and blades.

Figure 5.1 shows the numerical model of the 5-MW wind turbine developed in SAP2000 and points of interest – consistent with the model of the 65-kW wind turbine presented in Figure 4.1.

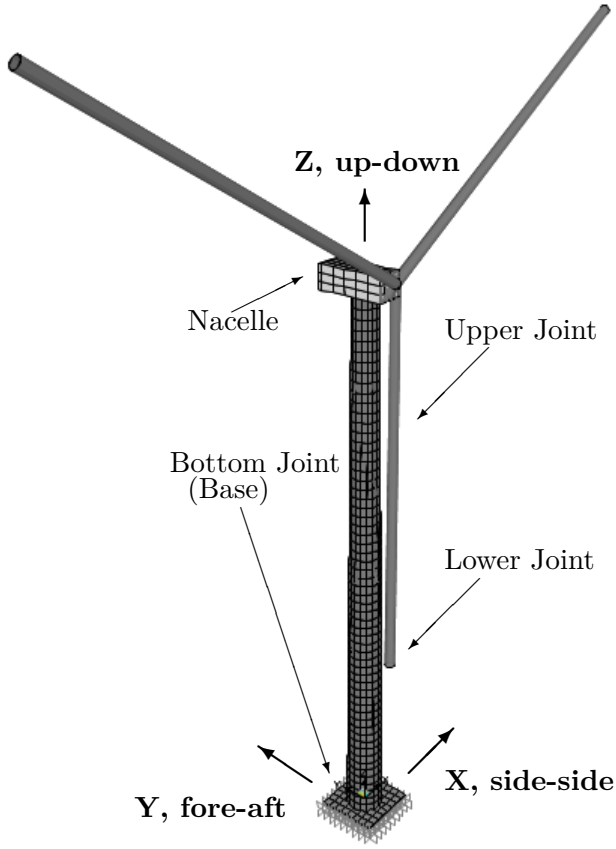

Figure 5.1: *Model of the 5-MW wind turbine in SAP2000.*

Coordinate system is also shown in Figure 5.1, and is consistent with the coordinate system presented in Figure 4.1.

5.2 Modelling Soil

Previous research has shown that this type of tall and slender structure can be prone to significant soil-structure interaction effects, especially for soil with $V_s \leq 750m/s$ [Luco, 1986]. Zhao and Maißer [2006] conducted numerical simulations on the SSI effects on the dynamic characteristics of wind turbine towers, using linear springs to encompass any flexibility present in the soil. It was concluded that SSI effects is particularly important in the

analysis of wind turbine structures located on relatively flexible soil, yielding further motivation for including SSI in this study.

Springs and dampers are often the preferred approach, but errors may occur in the response at resonance of the system [Ghaffar-Zadech and Chapel, 1983]. In order to include the effect of SSI in this study, a mass of the soil is included in the model to the depth of 30 m and 80 m in the direction of uni-axial shaking. The direct solution method is applied as the entire soil-foundation-structure system is modelled and analysed in a single step [Kramer, 1996]. Figure 5.2 shows the modelled soil with measurements and directions of uni-axial and vertical shaking.

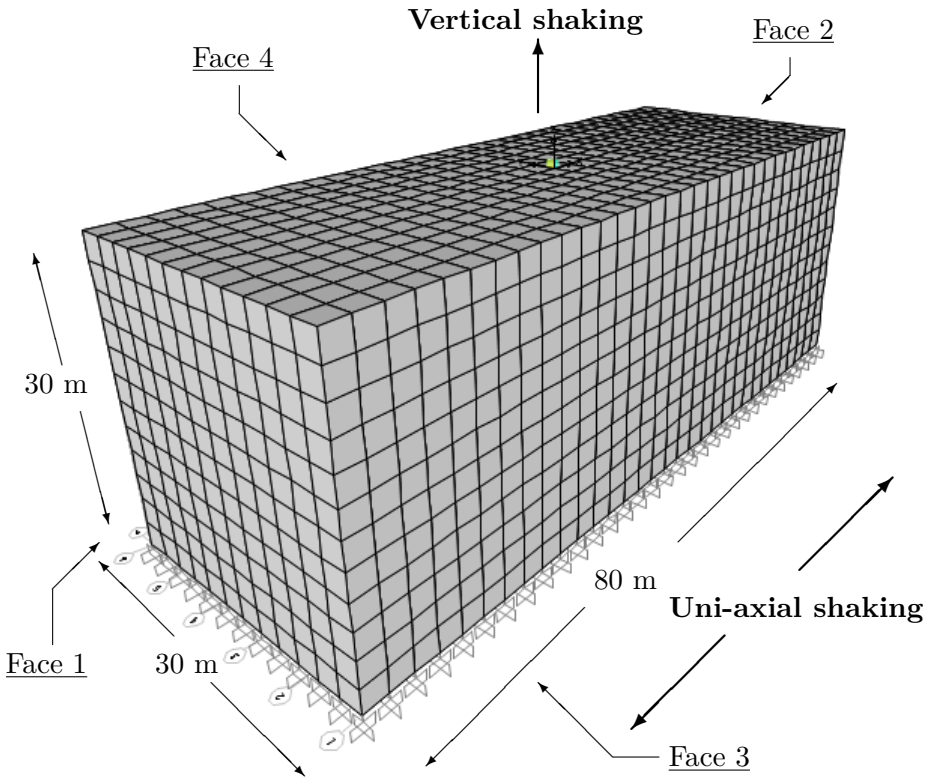

Figure 5.2: *Modelled soil in SAP2000.*

All the 5328 solid elements shown in Figure 5.2 are eight-noded with six equal quadrilateral faces [CSI, 2013]. The length of the elements are all set to 2,5 m in order to accurately describe waves, [Hughes, 1987; Cook et al.,

2002]:

$$\lambda = \frac{V_{s/p}}{f} \tag{5.1}$$

$$L_e = \frac{\lambda}{10}\,[m] \tag{5.2}$$

Here, f is the highest, realistic frequency of interest in (for this study) the input earthquake motion. $V_{s/p}$ is either shear wave velocity or pressure wave velocity (depending on the analysis at interest), and is used with f to obtain the wavelength, λ. The factor of 10 in Equation (5.2) is determined by experience and careful judgement of the problem at hand in order to obtain L_e; the desired element length.

Conferring with the spectra of frequencies in Figure 4.4b, and the characteristics of other earthquakes, the highest frequency of numerical interest is assumed to be 15 Hz [Chopra, 2012; Kramer, 1996]. The lowest wave velocity is taken as 300 m/s, yielding:

$$\lambda = \frac{300\ m/s}{15\ s^{-1}} = 20\ m \tag{5.3}$$

$$L_e = \frac{20\ m}{10} = 2\ m \tag{5.4}$$

Although this indicates that the size of the solid elements in Figure 5.2 should be decreased, the thought of saving computational time and the fact that errors will first come at hand at high frequencies and soft soil, the model preserved its element length of L_e of 2,5 m. This is further justified in the next section.

5.2.1 Validating Modelled Soil

In order to verify the modelling of the soil, a comparison to analytical theory of an uniform, damped soil on rigid rock has been performed. The amplification function from bedrock motion to free surface motion is given by Equation (5.5) [Kramer, 1996]:

$$|F(\omega)| = \frac{1}{\sqrt{\cos(\omega H/V)^2 + [\xi(\omega H/V)]^2}} \tag{5.5}$$

where H is the depth of soil layer, V is the wave velocity of interest in the uniform soil (pressure or shear waves) and ξ is the viscous damping ratio in the uniform soil. Further, $\omega = 2\pi f$ is the angular frequency. However,

the results in this work is presented as f [Hz]. Theoretically, the n^{th} natural angular frequency of the modelled soil is given by:

$$\omega_n \approx \frac{V_{s/p}}{H}\left(\frac{\pi}{2} + n\pi\right) \qquad n = 0, 1, 2, \ldots, \infty \tag{5.6}$$

That is, when the denominator in Equation (5.5) approaches zero. At each of these natural frequencies, a standing wave develops in the soil, imitating mode shapes of the modelled soil (shown later in Figure 5.6). Theoretical solutions for the first six natural frequencies for different soils are presented in Appendix D.1.

As mentioned, the theoretical solution utilizes the viscous damping ratio. On the contrary, a steady state solution in the frequency domain in SAP2000 utilizes a hysteretic damping [Humar, 2005; CSI, 2013]:

$$f_{damp} = \frac{\eta\,[\boldsymbol{K}]}{\omega}\dot{u} \tag{5.7}$$

Equivalent viscous damping is given by Equation (5.8):

$$\xi_{eq} = \frac{\eta}{2\beta} \tag{5.8}$$

Where $\beta = \frac{\omega}{\omega_n}$, and ω and ω_n is defined as the angular load-frequency and natural angular frequency respectively. As Equation (5.8) shows, choosing a $\eta = 0{,}04$ equals a viscous damping ratio (ξ_{eq}) of 0,02 in frequencies of resonance.

Validation of the soil has been performed both for horizontal excitation (with V in Equation (5.5) being V_s; shear wave velocity) and vertical excitation (with V in Equation (5.5) being V_p; pressure wave velocity). The theoretical and steady-state solution from SAP2000 for the soil with a depth of $H = 30m$, and $\xi_{eq} = 0,02$ is given below for the three different shear-wave velocities of $V_s = 1000$, 500 and 300 m/s.

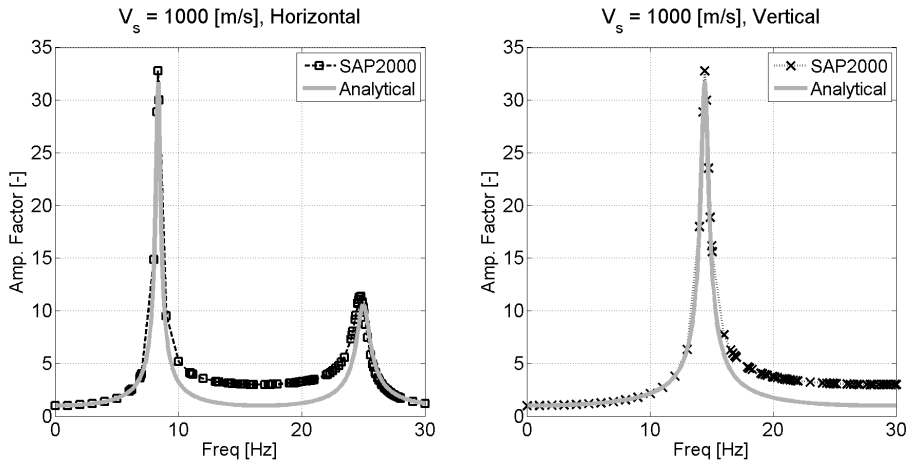

(a) Horizontal. *(b) Vertical.*

Figure 5.3: *Validation for soil with $V_s = 1000$ [m/s] in SAP2000.*

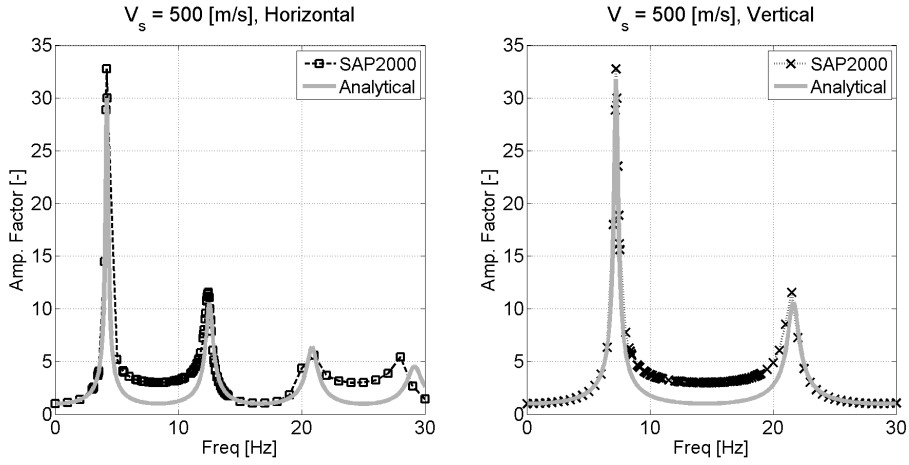

(a) Horizontal. *(b) Vertical.*

Figure 5.4: *Validation for soil with $V_s = 500$ [m/s] in SAP2000.*

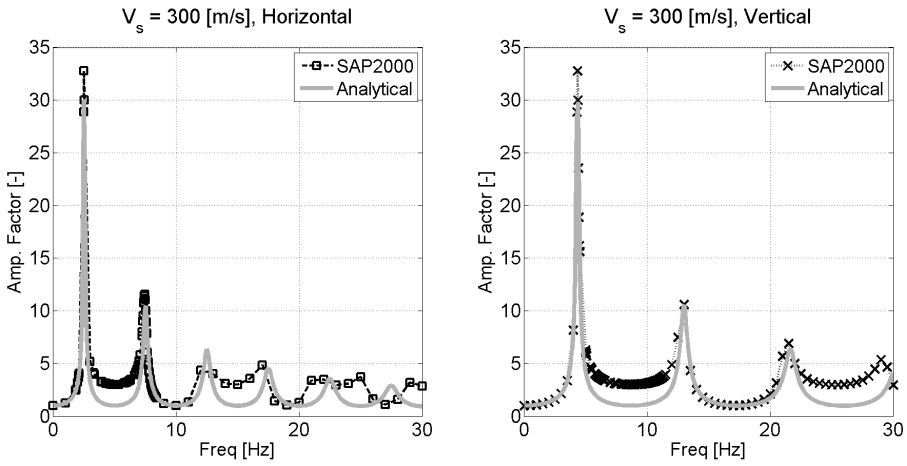

(a) *Horizontal.* ***(b)*** *Vertical.*

Figure 5.5: *Validation for soil with $V_s = 300$ [m/s] in SAP2000.*

As Figure 5.3 - 5.5 exhibits, quite satisfactory results were obtained in SAP2000. However, some additional amplification were observed between every second natural frequency in the SAP2000 model. Troubleshooting was performed, and some effort were given in order to find the source of this numerical difference, but with no success. It still remains an unsolved question, much so due to the objectives and scope of this thesis. Some further validations for the modelled soil is provided in Appendix D.1.

Modelling Techniques

In order to closely match the theoretical solution some assumptions has been made for the modelled soil: For the horizontal set-up, the vertical faces normal to the direction of shaking (Face 1 and Face 2 in Figure 5.2) have been restrained for displacements in the Z-direction. Further, the nodes of the same vertical faces with the same Y&Z coordinates have been tied to move together (i.e. constrained) in the direction of shaking. Thus, as the shaking is performed in the X-direction:

$$u^{x-dir}_{node\#n}(x_n, y_i, z_i) \;=\; u^{x-dir}_{node\#m}(x_m, y_i, z_i)$$

Then the horizontal layers of the soil will move as shear-beams, a well known approach to dynamic responses [Kramer, 1996], as shown in Figure 5.6:

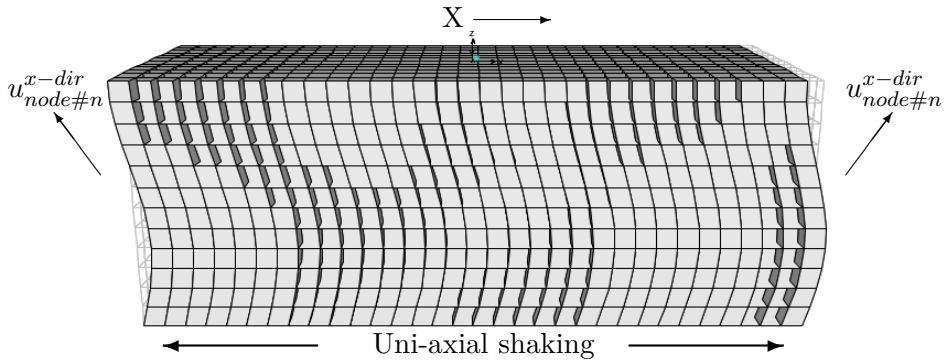

Figure 5.6: *Modelled soil showing shear-beam behaviour.*

A standing wave (i.e. mode shape) in the modelled soil, and the effect of the nodes being tied to move together in the direction of shaking is quite clear in Figure 5.6, and the modelled soil acts as having the shearing characteristics of a Kelvin-Voigt solid [Kramer, 1996].

Lastly, for the vertical set-up, all the vertical boundaries (Face 1-4) where restrained against horizontal displacement. The different set-ups are summarized in Table 5.3.

Table 5.3: *Summary of the horizontal and vertical assumptions for modelled soil.*

		Set-Up	
		Horizontal	**Vertical**
Face:	**1**	Restrained in Z-dir	Restrained in Y- & X-dir
	2	Restrained in Z-dir	Restrained in Y- & X-dir
	3	Assigned shear-behaviour	Restrained in Y- & X-dir
	4	Assigned shear-behaviour	Restrained in Y- & X-dir

As a note, other meshes and different levels of restraining were tested in order to utilize the best approximation for the modelled soil.

5.2.2 Monopile Foundation

In order to provide some foundation for the wind turbine when its submerged into the soil, a monopile foundation was modelled. Essentially, it was modelled as a continuous steel tower to the depth of 25 m, with the same material, outer diameter and thickness as the turbine tower at the ground

surface. This type of monopile foundation is one of the normal foundation types, together with a variety of slab foundations and multi-pile foundations [Burton et al., 2011; Kiyomiya et al., 2002]. Note that many monopile foundations are constructed using concrete instead of steel.

Figure 5.7 shows the principal of the monopile foundation, along with the a steel plate modelled at the ground surface. This plate is modelled to imitate a ground floor of the wind turbine, which often is a slab of concrete containing equipment such as transformers, elevators and computers. [Manwell et al., 2002; Burton et al., 2011].

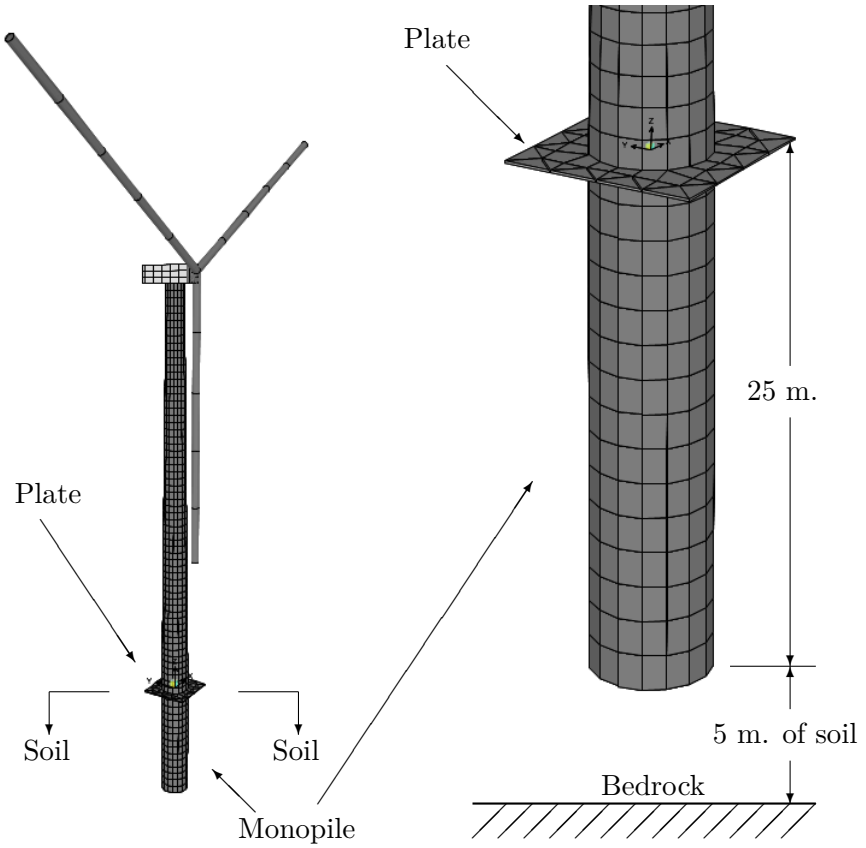

(a) *Wind turbine and monopile foundation.* ***(b)*** *Detail of monopile foundation.*

Figure 5.7: *Model of monopile foundation for 5-MW wind turbine in SAP2000.*

As shown in Figure 5.7b, the monopile extends 25 m into the soil, thus leaving 5 m between the end of the foundation and the bedrock. Also, the monopile is completely embedded in the soil, both on the inside and outside of the hollow steel section.

As presented in Chapter 1.2:*Objectives*, some previous research had included a foundation of piles, and suggested research using another type of foundation [Kiyomiya et al., 2002]. Thus, further motivation is presented for using the monopile foundation introduced in this section.

5.3 Combined Model

Combining the soil shown in Figure 5.2 with the turbine including monopile foundation as shown in Figure 5.7 produced the combined model. The wind turbine was placed in the middle of the soil. As will be explained in Chapter 7, uni-axial shaking was imparted to the combined model. This motivated the use of two configurations of the model (Configuration I & II), essentially rotating the wind turbine 90 degrees, as shown in Figure 5.8.

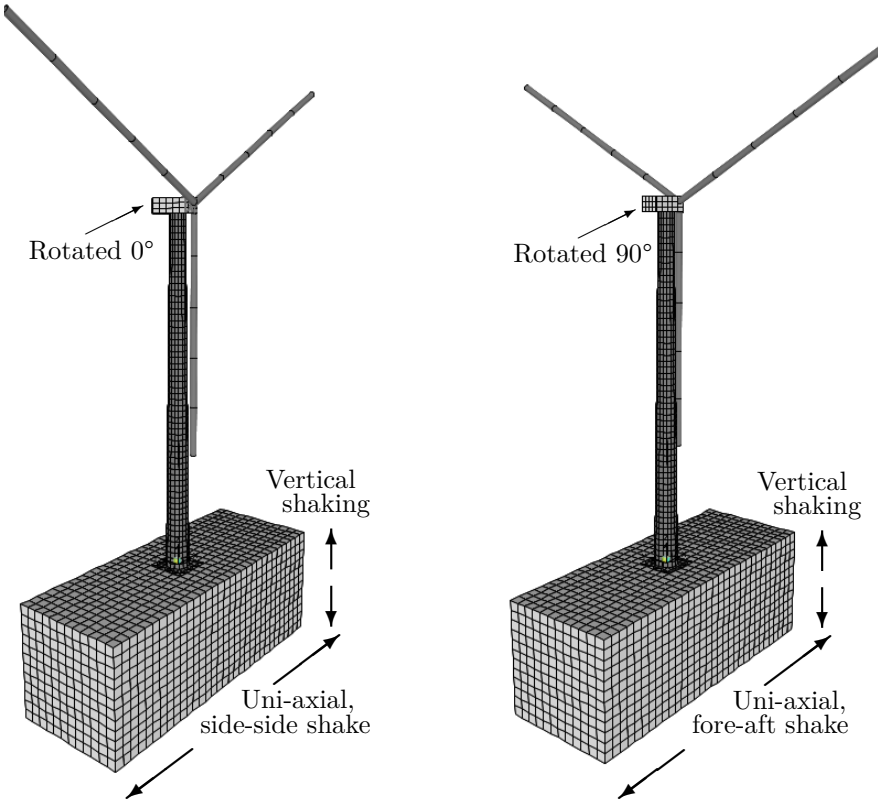

(a) *Configuration I.* ***(b)*** *Configuration II.*

Figure 5.8: *Combined model in SAP2000.*

As Figure 5.8a exhibits, Configuration I yields side-side shaking of the soil and wind turbine. And Configuration II yields fore-aft shaking of the soil and wind turbine, as shown in Figure 5.8b.

Also remembering that the model will have a vertical set-up as explained in the previous Section, a summary of the total number of varieties for the combined model is presented in Table 5.4:

Table 5.4: *Summary of modeltype for the combined model.*

		Configuration I	**Configuration II**
Set-Up:	**Horizontal**	Modeltype I-H	Modeltype II-H
	Vertical	Modeltype I-V	Modeltype II-V

5.4 Discussion of Model

Even though it will not be given much focus, some weaknesses of the numerical model should be mentioned:

- The modelled soil is (more or less) isotropic, while real soil is highly anisotropic. Also, the modelled soil is able to take tension, while real soil have very little capacity in tension [Kramer, 1996].
- The modelled soil does not account for shear induced pore pressure. An earthquake does not last long, or induce to much relative motion in the ground, but can build up excess pore pressure – degrading the strength and deformability of the soil [Egglezos and Bouckovalas, 1998]. Furthermore, a wind turbine is constantly (when wind is present) affecting the soil with dynamical behaviour. This may lead to important considerations near the base and foundation of the wind turbine.
- Closely related to the last item, the model and analysis' performed does not account for cyclic shear strain, which can reduce the damping ratio and strength of the soil [Ishibashi and Zhang, 1993; Hardin and Drnevich, 1972].
- The wind turbine does not contain any door near the base, as is usually present. The presence of a door could lead to some additional local effects in the response of the turbine tower [Bazeos et al., 2002; Lavassas et al., 2003].
- The model and procedure in this thesis is assumed purely linear elastic. This may be good enough for the wind turbine itself, but the soil (especially when applying the weakest soil) may yield and become non-linear, even at small loads. This could very well lead to both

dissipation of energy and movement from the bedrock, and lasting deformations of the wind turbine.

- And, in line with the objectives presented in Chapter 1.2, the model is not a detailed model of the different components of the wind turbine; both the geometry and functions of the rotor and blades are simplified.
- In a direct method type of model as presented in this chapter, radiation damping is difficult to assess correctly [Clough and Penzien, 2003; Wilson, 2002]. Ideally, the soil should be modelled towards infinity in horizontal directions in order to suppress the reflection of waves, or the vertical boundaries should be modelled differently [Kramer, 1996]. However, due to computational costs and the scope of the thesis, this is not preferable.

These are all fairly normal weaknesses of this type of FEM-model, and is acceptable for the structural aspect. Many of the weaknesses of the model is geotechnical aspects, and goes beyond the scope of this thesis.

6. Natural Frequencies & Mode Shapes

Obtaining (and studying) the natural frequencies and mode shapes for the modelled 5-MW wind turbine both in conditions with no soil (fixed-base) and with modelled soil is essential. Note that the only valid comparisons for the structural dynamic properties of the 5-MW wind turbine can be made with Jonkman et al. [2009], which did not utilize any structural software, but more wind energy-based software.

6.1 Natural Frequencies & Comparison to Guideline Work

Referring to Chapter 3.4 and Table 5.1, the system natural frequencies due to rotating blades can be obtained:

$$\frac{12,10\ RPM}{60\ s} = 0,20\ s \tag{6.1}$$

$$1P: \quad \frac{1}{0,20\ s} = 4,96\ Hz \tag{6.2}$$

$$3P: \quad \frac{3}{0,20\ s} = 14,88\ Hz \tag{6.3}$$

As mentioned in Chapter 3.4, it is desirable to design the tower to not have natural frequencies near these operational frequencies in order to avoid self excitation.

6.1.1 Structural Natural Frequencies

The structural natural frequencies obtained by eigenvector analysis in SAP2000 are presented and compared with provided data from Jonkman et al. [2009] in Table 6.1:

Table 6.1: *Natural frequencies of the 5-MW wind turbine, compared to guideline work.*

f_n #	NREL [Jonkman et al., 2009] Type	FAST [Hz]	ADAMS [Hz]	f_n #	This study Type	SAP2000 [Hz]	Mass PF	[%]
1	Fore-aft	0,324	0,320	1	Side-side	0,294	U_{s-s}	68,24 %
2	Side-side	0,312	0,316	2	Fore-aft	0,295	U_{f-a}	68,88 %
3	Torsion	0,621	0,609	3	Torsion	0,647	R_z	91,40 %
⋮	(Blades)	⋮	⋮	⋮	(Blades)	⋮		⋮
12	Fore-aft	2,900	2,859	10	Fore-aft	2,434	U_{f-a}	12,57 %
13	Side-side	2,936	2,941	11	Side-side	2,534	U_{s-s}	12,03 %
				⋮	⋮	⋮		⋮
				21	Vertical	9,646	U_z	77,24 %

FAST [Jonkman and Buhl Jr., 2005] and ADAMS [Laino and Hansen, 2001; Moriarty and Hansen, 2005] are two different aerodynamic software used in the documentation of the 5-MW reference turbine. Note that the natural frequencies are obtained from the SAP2000-model with no soil (as shown in Figure 5.1).

The natural frequencies obtained in this study closely matches the natural frequencies provided in Jonkman et al. [2009] for the first three types. Notice, however, that the type of mode shape for the two first natural frequencies are different. But the frequencies are very close, and the difference is of low significance.

On the contrary, some difference is observed for the 2^{nd} order fore-aft and side-side natural frequencies. Effort was made in modifying the sectional stiffness of the turbine tower at different heights in order to match these frequencies. But the modification proved to be fairly high in order to match these, and seemed unrealistic. Considering that both FAST and ADAMS are not structural software as SAP2000 is, and does not model the geometry explicitly, the deviation presented in Table 6.1 was accepted. The model also exhibited some mode shapes which can only be described as "semi" 2^{nd} order fore-aft and "semi" 2^{nd} order side-side. This fact was led to believe that some coupling or spreading effects of the mode shapes was present.

Also, the structural natural frequencies does not coincide with the operational natural frequencies presented in Equation (6.2) and (6.3), and the wind turbine is a soft-soft design.

6.1.2 Mode Shapes

The different mode shapes for natural frequency 1, 2, 10 and 11 in Table 6.1 are shown in Figure 6.1:

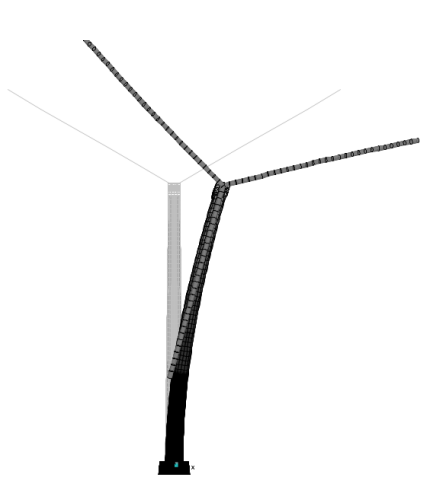

(a) 1^{st} *(side-side: 0,294 Hz).*

(b) 2^{nd} *(fore-aft: 0,295 Hz).*

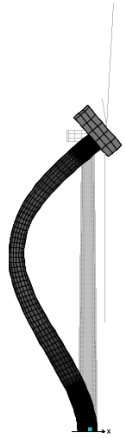

(c) 10^{th} *(fore-aft: 2,434 Hz).*

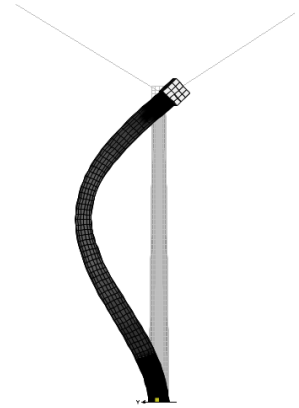

(d) 11^{th} *(side-side: 2,534 Hz).*

Figure 6.1: *First four global mode shapes of the 5-MW model obtained from SAP2000.*

The blades have been removed for the purpose of illustrating the mode

shapes of the tower better in Figure 6.1c and Figure 6.1d. As for the 65-kW wind turbine, the mode shapes for the 5-MW wind turbine resembles a cantilever beam with a point mass at the end [Laura et al., 1974].

Note also the first natural frequency in the vertical direction at 9,65 Hz (frequency number 21 in Table 6.1), with the corresponding mode shape shown in Figure 6.2:

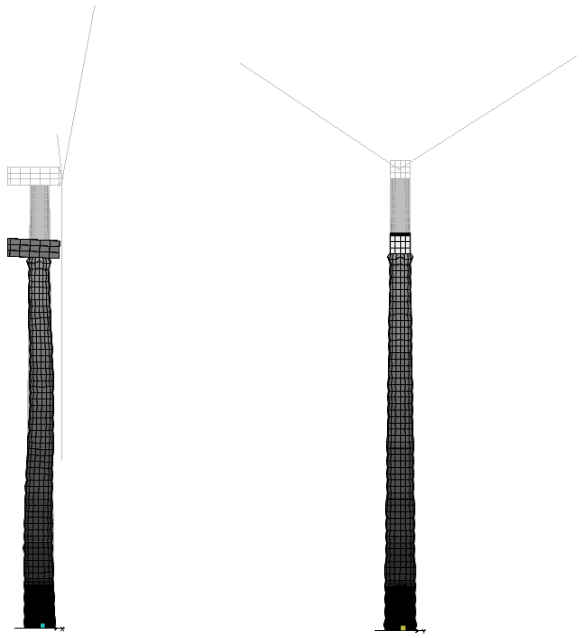

(a) *21^{st} (vertical: 9,646 Hz) fore-aft plane view.* ***(b)*** *21^{st} (vertical: 9,646 Hz) side-side plane view.*

Figure 6.2: *The first vertical mode shape of the 5-MW wind turbine.*

The blades have also been removed in Figure 6.2 in order to better illustrate the vertical mode shape of the tower.

6.2 Natural Frequencies & SSI

As explained in Chapter 5.2, the wind turbine is modelled on top of a layer acting as soil. Furthermore, the material of the soil will have varying qualities

in order to study the spread of ground types in soil-structure interaction. Different ground types used in EC8-1 [2004] is presented in Table D.2.

6.2.1 Horizontal Natural Frequencies

Varying the shear wave velocity as 1000, 800, 500, 300 and 100 m/s, and obtaining some of the first natural frequencies will provide some indications of the dynamic effect from the modelled soil. The results are presented in Figure 6.3 through Figure 6.6. Referring to Chapter 5.3, both Configuration I and Configuration II were analysed. The dotted line represents the corresponding natural frequency with no modelled soil included, that is: fixed-base natural frequencies as presented in Table 6.1.

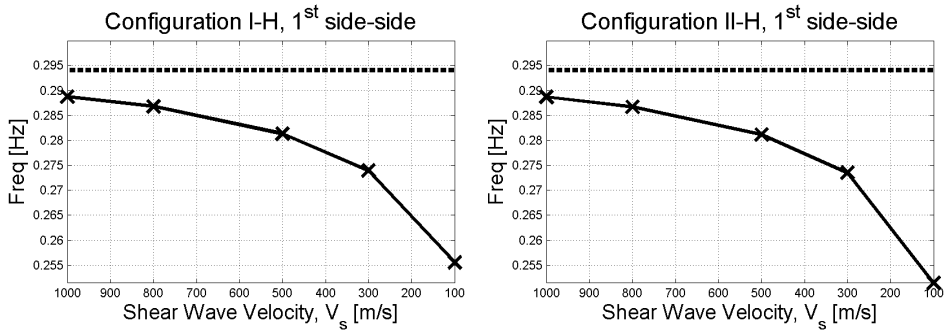

Figure 6.3: *1^{st} side-side natural frequency as function of V_s.*

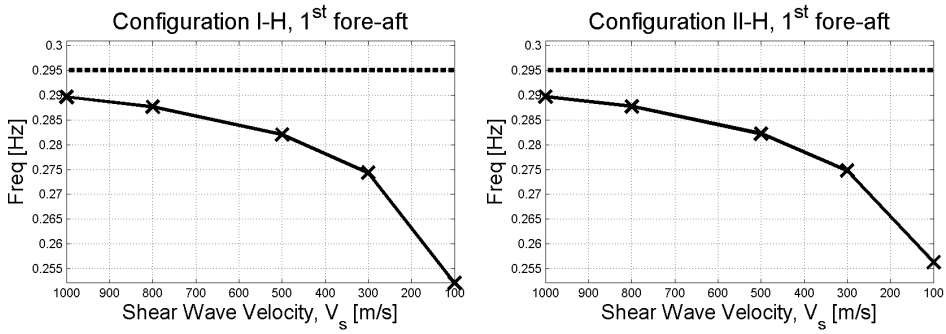

Figure 6.4: *1^{st} fore-aft natural frequency as function of V_s.*

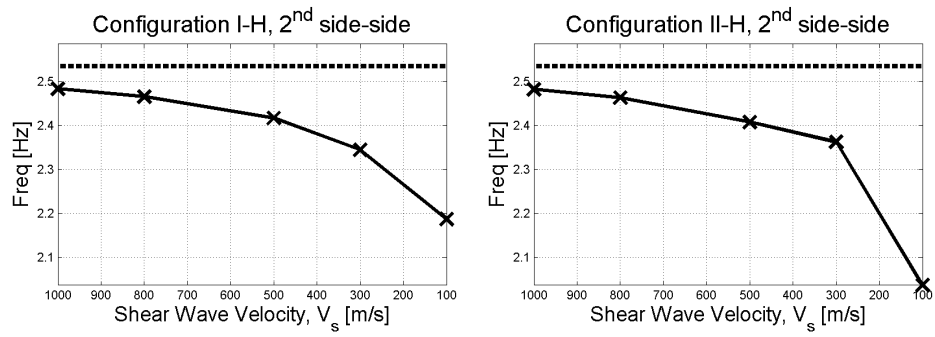

Figure 6.5: *2^{nd} side-side natural frequency as function of V_s.*

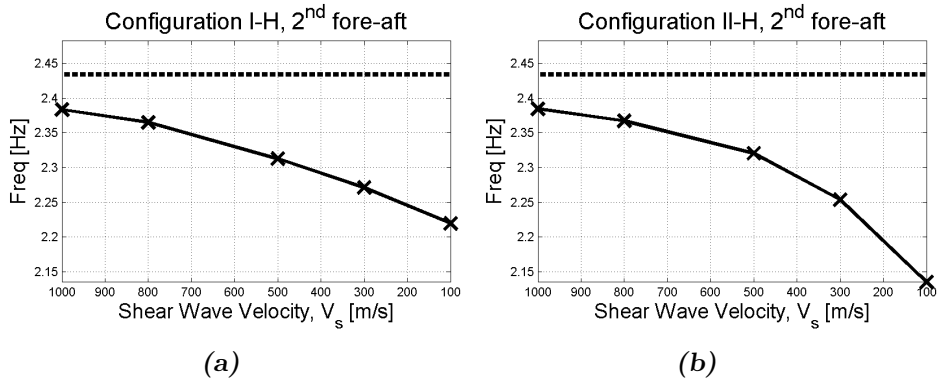

Figure 6.6: *2^{nd} fore-aft natural frequency as function of V_s.*

In general, all the results show the expected trend: the natural frequencies decreases as the shear wave velocity decreases (i.e. the soil gets softer, weaker) and converges against the fixed-base natural frequencies for stronger soil. Also, the correlation between Configuration I and Configuration II is quite good, with only some deviation in the weakest soil ($V_s = 100$ m/s).

6.2.2 Special Concerns for Vertical Natural Frequencies & SSI

Investigating the first vertical natural frequency and corresponding vertical mode shape of the wind turbine was also of interest. These results are presented in Figure 6.7. (Note that this analysis was only performed to a

soil of $V_s = 300$ m/s, due to the difficulty of identifying the correct mode shapes in further weaker soils). Again, the dotted line represents the natural frequency of the modelled wind turbine alone (as presented in Table 6.1).

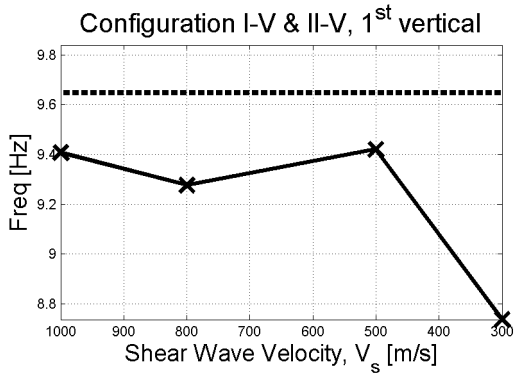

Figure 6.7: *1^{st} vertical natural frequency as a function of V_s.*

Accurately and confidently identifying the correct vertical mode shapes proved a difficult task. The coupling of mode shapes between the soil and wind turbine was evident, as the wind turbine will experience some rigid body translation due to the mode shapes of the modelled soil. This uncertainty may be one of the reasons for the somewhat surprising result of the fact that the natural frequency is not monotonously decreasing.

Note the title of the plot in Figure 6.7: this is due to the fact that the results were identical in both Configuration I and II.

The Equivalent Spring Approach

Motivated by the rather ambiguous results in Figure 6.7, a different approach was pursued. Using SSI theory from Kramer [1996], a simpler model for the study of vertical natural frequencies was created, and natural frequencies were studied for further different V_s:

Using the classical linear, one-dimensional, elastic spring equation [Cook et al., 2002]:

$$k_{spring} d = F \tag{6.4}$$

(where k_{spring} is the stiffness of a linear-elastic spring, d is the resulting displacement and F is the external force acting on the system), an equiva-

lent vertical stiffness of the soil and monopile foundation can be obtained. Removing all of the structure above ground level in Figure 5.8, and applying a unit area load on the plate, the vertical stiffness (k_v) of the modelled soil can be expressed using Equation (6.5):

$$k_v = Fd^{-1} \tag{6.5}$$

Thus, the vertical natural frequency of the modelled soil, including a mass representing the rigid wind turbine, can be defined as [Kramer, 1996]:

$$f_v = \frac{\omega_v}{2\pi} = \frac{1}{2\pi}\sqrt{\frac{k_v}{m}} \tag{6.6}$$

Where m is the total mass of the wind turbine (see Table 5.1).

Further, the equivalent natural frequency (f_e) can be expressed as the summation of the fixed-base (i.e. no soil) natural frequency (f_0) and vertical natural frequency (f_v) from the soil and a rigid wind turbine – i.e. the equivalent natural frequency is estimated as two springs in series [Kramer, 1996]:

$$\frac{1}{\omega_e^2} = \frac{1}{\omega_0^2} + \frac{1}{\omega_v^2} \tag{6.7}$$

or

$$\frac{1}{f_e^2} = \frac{1}{f_0^2} + \frac{1}{f_v^2} \tag{6.8}$$

$$\Downarrow$$

$$f_e = \frac{f_0}{\sqrt{1 + \frac{f_0}{f_v^2}}} \tag{6.9}$$

The approach is summarized in Figure 6.8:

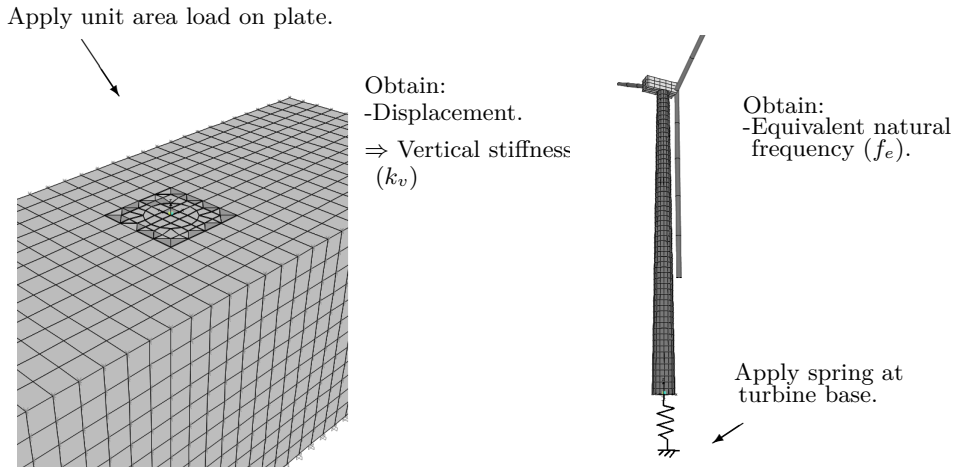

(a) *Unit load on plate and monopile foundation.* ***(b)*** *Applying spring on wind turbine, and obtaining f_e.*

Figure 6.8: *Summary of the equivalent spring approach.*

The equivalent natural frequency was both calculated using Equation (6.6) and Equation (6.9), and obtained through applying a spring at the base in SAP2000 (Figure 6.8b). Results are presented in Table 6.2:

Table 6.2: *Vertical natural frequencies from the equivalent spring approach.*

Soil V_s $[m/s]$	**Spring-stiffness** k_v $[kN/m]$	**Fixed-base Nat. Freq** f_0 $[Hz]$	**Calculated Nat. Freq** f_e $[Hz]$	**SAP2000 Nat. Freq.** $f_{e,SAP}$ $[Hz]$	**Diff** [%]
1000	$7,70 \cdot 10^7$	9,65	9,50	9,53	0,35
800	$5,13 \cdot 10^7$	9,65	9,42	9,47	0,52
700	$4,04 \cdot 10^7$	9,65	9,37	9,43	0,66
600	$3,09 \cdot 10^7$	9,65	9,29	9,36	0,84
500	$2,25 \cdot 10^7$	9,65	9,16	9,27	1,12
300	$9,70 \cdot 10^6$	9,65	8,62	8,83	2,42

The difference between the calculated equivalent frequencies and those obtained in SAP2000 are very small, and the results are satisfactory. The differences can be due to cumulative numerical errors in the process, or weakness of the method itself. Indeed, the model in SAP2000 is more complex than the 1DOF model this method is derived from. Also keep in mind, the vertical stiffness was obtained by very simple, static methods.

For graphical purposes, the results are plotted in Figure 6.9, including the

previous results from the combined SAP2000 model in Chapter 6.2.2. Again, the horizontal dotted line represents the natural frequency with no soil (f_0).

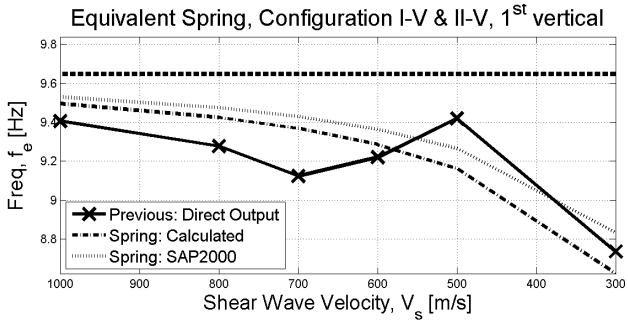

Figure 6.9: *1^{st} vertical natural frequency as a function of V_s, using equivalent spring method.*

The results from the equivalent spring approach clearly exhibits a smooth trend of decreasing the natural frequency as the soil gets weaker. The same trend is also seen in the previous result, but not so smooth due to the unexpected result at $V_s = 500$ m/s. Again, the difficulty of correctly identifying the mode shapes were precarious in the vertical set-up. Thus, the equivalent spring approach provided some additional reassurance of the model.

6.3 Conclusion & Discussion

Overall, the natural frequencies agreed with common theory of dynamics and SSI; converging against the fixed-base value for stiffer soil, and decreasing as the soil got weaker [Chopra, 2012; Kramer, 1996; Humar, 2005]. Also, the model did not exhibit to much difference from the two Configurations defined, thus eliminating a source of uncertainty in the different analysis conducted later.

Due to turbine geometry, the independent fore-aft and side-side natural frequencies were very close. This is similar to previous results, [Hänler et al., 2006; Bazeos et al., 2002; Zhao et al., 2007]. Also, the natural frequency of the fundamental mode was observed in the range of 0-1 Hz – agreeing with other results [Hänler et al., 2006; Bazeos et al., 2002; Lavassas et al., 2003]. Summed, this chapter provided further validation of the modelled soil and wind turbine.

7. Description of Analysis

It is normal practice to investigate different sets of ground motions in order to account for the variability in the ground motion [Wilson, 2002]. However, if a given structural site is indeed near a fault it is important to focus on near-fault ground motions in order to account for the specific near-fault effects. Nevertheless, this thesis does not focus on design, but on dynamical properties – thus only one record is utilized.

7.1 Considerations Regarding Directivity & Damping

Using a non-aerodynamic software like SAP2000 makes it difficult to assess the significant aerolastic damping i both directions for an operating turbine [Riziotis et al., 2004] in a correct manner. Thus, damping must be applied either as modal damping when a modal analysis can be run, or Rayleigh damping when direct integration methods are used – derived by and based on previous work and research.

Furthermore, due to the significant difference in damping in wind turbines from still and operational conditions, previous research has shown that analysis running in time-domain is in fact preferred over analysis running in frequency-domain (i.e. a response spectra approach) [Witcher, 2005]. The complexity and directivity of damping in wind turbines – as explained in Chapter 3.3.2 – is difficult to assess with Rayleigh damping. Recognising this fact yields motivation and justification of analysing the model uni-axial, i.e. only considering one direction in each analysis, and using modal analysis to approach damping more correctly.

7.2 Selected Earthquake

The Nahanni earthquake is selected as time series for the seismic analysis of the 5-MW wind turbine. The time series provided has been somewhat

modified and scaled in order to match response spectra for ground type A in EC8-1 [2004]. Thus, only some trivial facts are presented in Table 7.1 regarding the earthquake event [PEER, 2013].

Table 7.1: *Nahanni earthquake and derived data.*

Parameter	Data
Name	Nahanni
Date	23rd December, 1985
Country	Canada
M_w	6,76

7.2.1 Horizontal Component

As explained in the previous section, the provided horizontal component of the earthquake record has been scaled in order to match response spectra in EC8-1 [2004] of soil type A, and in order to have a PGA of 0,05 [g]. In later stages of the analysis, this record will be scaled upwards to represent (for instance) a higher PGA.

Nonetheless, some numerical data derived from the horizontal time series provided is presented in Table 7.2:

Table 7.2: *Derived data for the horizontal component of the Nahanni earthquake.*

Parameter	Derived Data
PGA	0,045 [g]
RMS	0,077 [g]
Arias Intensity	0,038 [m/s]
Relative Significant Duration	12,100 [s]

The time series for the horizontal component of the Nahanni earthquake is plotted in Figure 7.1, and includes Arias Intensity, Fourier Amplitude Spectra and Response Spectra.

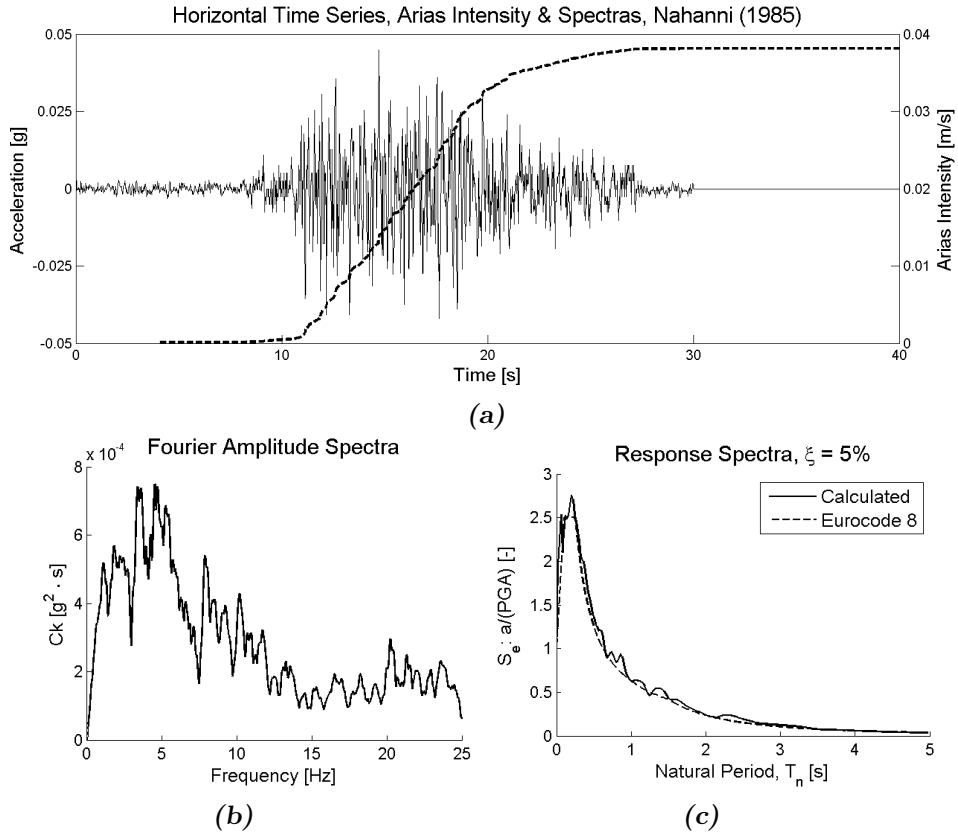

Figure 7.1: *Time series & Arias, Fourier amplitude spectra and response spectra for the Nahanni earthquake in horizontal direction.*

Note the added time from 30-40 sec in Figure 7.1a – the idea was to obtain some information about the free-vibration phase of the wind turbine.

Also note the extreme similarity between the calculated response spectra for the horizontal component, and the response spectra for ground type A in EC8-1 [2004] shown in Figure 7.1c, as expected.

7.2.2 Vertical Component

As for the horizontal component, the provided vertical component of the earthquake record has been scaled in order to match response spectra in EC8-1 [2004], and in order to have a PGA of $0,6 \cdot 0,05[g] = 0,03[g]$. In later

stages of the analysis, this record will be scaled upwards to represent (for instance) a higher PGA.

Table 7.3: *Derived data for the vertical component of the Nahanni earthquake.*

Parameter	Derived Data
PGA	0,028 [g]
RMS	0,049 [g]
Arias Intensity	0,012 [m/s]
Relative Significant Duration	11,560 [s]

The time series for the vertical component of the Nahanni earthquake is plotted in Figure 7.2, and includes Arias Intensity, Fourier Amplitude Spectra and Response Spectra.

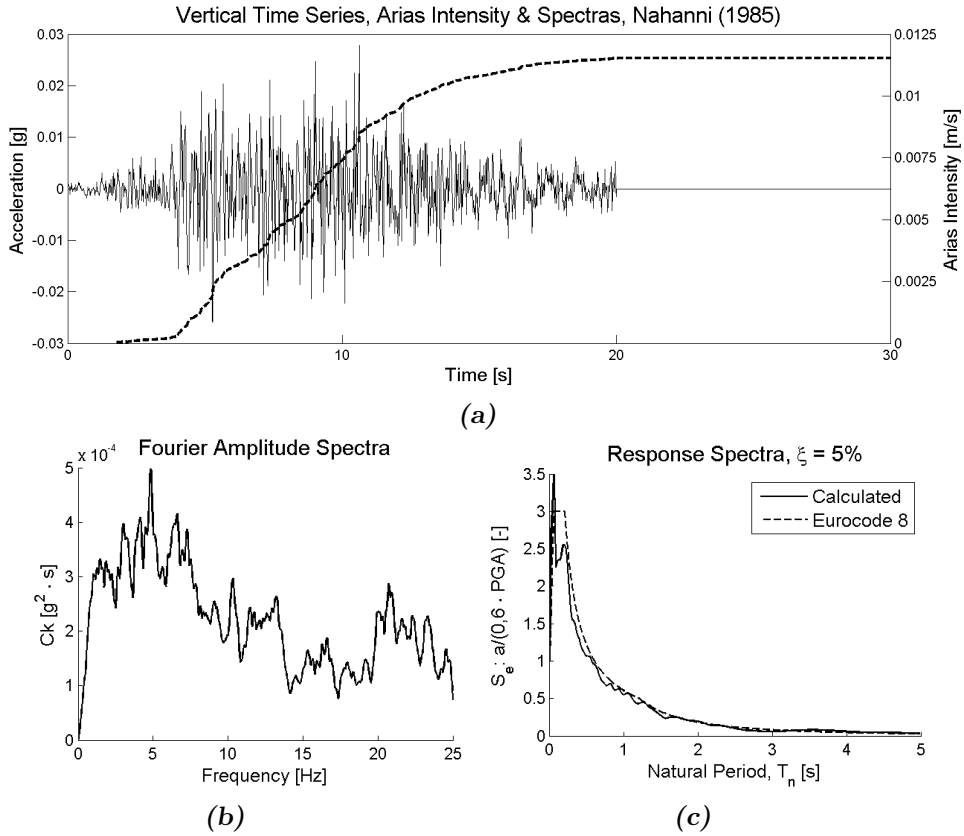

Figure 7.2: *Time series & Arias, Fourier amplitude spectra and response spectra for the Nahanni earthquake in the vertical direction.*

As for the horizontal component, note the added time from 20-30 sec in Figure 7.2a – the idea was to obtain some information about the free-vibration phase of wind turbine.

The calculated response spectra contains a peak higher then the response spectra obtained from EC8-1 [2004]. However, this peak does not coincide with the vertical natural frequencies of either soil, wind turbine or the combined model.

7.3 Wind-Induced Load

As explained in Chapter 4.3, SAP2000 is not an aerodynamic software, thus the wind-induced forces is applied as a horizontal force at the rotor. In the documentation for the NREL 5-MW wind turbine, Jonkman et al. [2009] have given numerical data for the equivalent thrust force to apply for given wind conditions. Figure 7.3 presents the thrust and generated power curve for the NREL 5-MW wind turbine.

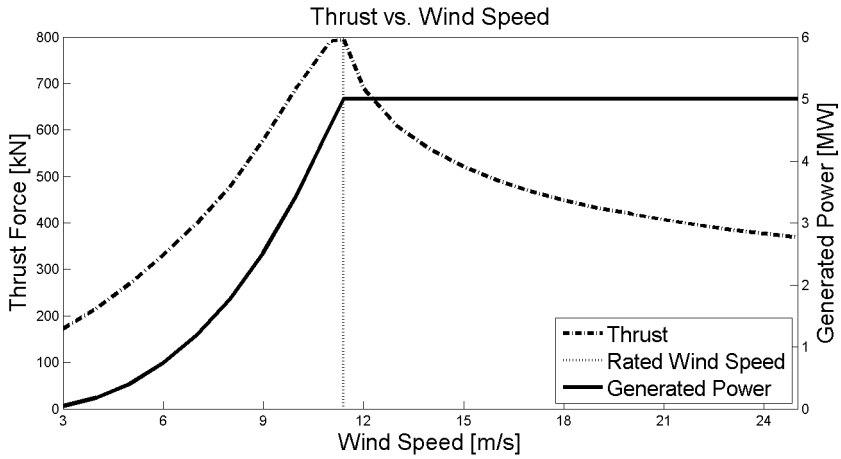

Figure 7.3: *Thrust curve for the 5-MW wind turbine.*

As for the 65-kW thrust curve presented in Figure 4.3, the peak of the thrust force (and, naturally, generated power) in Figure 7.3 also coincides with the rated wind speed at 11,4 m/s.

Previous research has concluded that the probability of the simultaneous occurrence of storms and large-scale earthquakes is extremely small [Kiyomiya

et al., 2002], and the use of the operating, mean-wind should be sufficient. Using the Matlab script `wind_simulation.m` (provided in Appendix D.2) a simulation of a turbulent wind field, with corresponding thrust force is obtained:

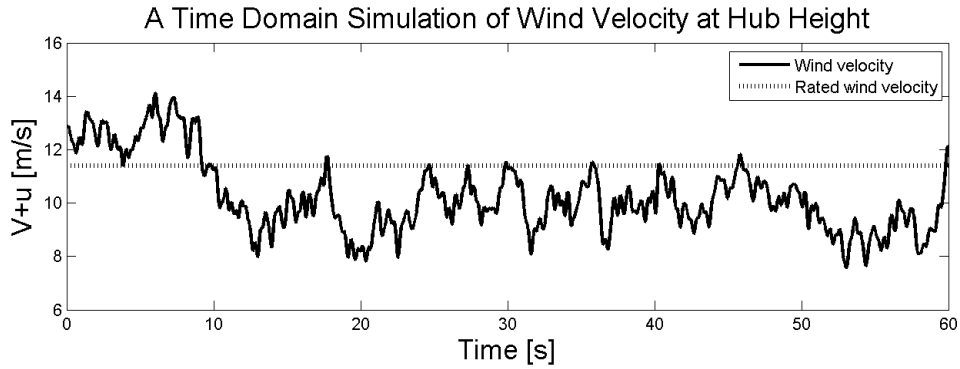

Figure 7.4: *Simulated turbulent wind velocity at hub height.*

And thus scaling this wind speed to an equivalent thrust force, using the data from Jonkman et al. [2009], yields a time history for the thrust force to be applied in the analysis:

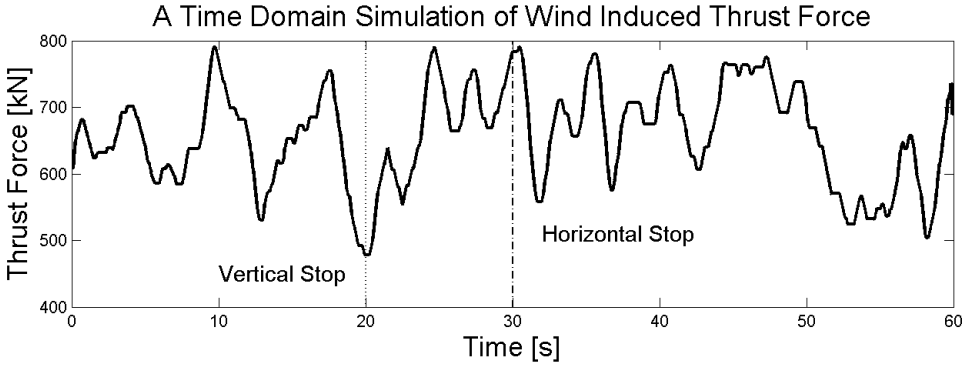

Figure 7.5: *Simulated wind-induced thrust force.*

7.3.1 Considerations

The wind induced thrust force is applied in two ways: Either as a static load of 800 kN at the nacelle in the fore-aft direction (i.e. the thrust force at the rated wind speed), or as a time-serie. That is, a time serie with a mean

wind velocity and a turbulent wind field presented in Figure 7.4-7.5. This is due to a range of interest in different type of combinations and responses, as will be introduced in the next section.

As explained in Chapter 7.2.1-7.2.2, a free-vibration phase is of interest in order to investigate the dynamic properties of the 5-MW wind turbine. Thus, the simulated wind-induced thrust force (Figure 7.5) is forced to stop after the same time the excitation stops (30 s and 20 s for the horizontal and vertical analysis, respectively). This sudden release of a "force" is a well known technique conducted in model experiments in order to obtain information and knowledge about natural frequencies, damping and mode shapes [Lauffer et al., 1988; Carne and Nord, 1983].

7.4 Load Cases & Load Combinations

Mainly four load cases and combinations have been investigated.

- The vertical responses due to the vertical component of the earthquake.
- The general dynamic response of a the 5-MW wind turbine subject to excitation, without wind induced loads. This is mainly done in the side-side direction.
- The general dynamic response from wind induced load only (both static and including turbulent wind field). This is mainly done in the fore-aft direction.
- The combined dynamic response of both wind induced loads and earthquake.

And, as a main focus throughout this thesis, studying the effects of varying stiffness in the modelled soil is of interest.

7.5 SAP2000 Procedure

While the analysis performed in Chapter 4, and obtaining of natural frequencies in this thesis in general were performed with modal analysis using eigenvectors, the analysis for the 5-MW wind turbine will be performed using Load Dependent Ritz-vectors (herein LDR) [CSI, 2013].

7.5.1 Load Dependent Ritz-Vectors

The advantages of using LDR-vectors are many. It only solves for frequencies and mode shapes excited by the external loading, thus fewer modes are needed to reach some target mass participation factor [Leger et al., 1986]. The latter argument is especially justified in analysis concerning vertical excitation (as one of the main focuses in this thesis) [Wilson, 2002]. As a consequence it converges faster then normal eigenvectors, and saves computational time. Also, it is not necessary to be concerned about errors introduced by higher mode truncation of a set of exact eigenvectors [Wilson, 2002].

Whereas the eigenvectors are solved by assessing the undamped, unloaded equation of motion (presented in Equation (7.1)), LDR-vectors are solved by assessing the undamped, but loaded equation of motion, presented in Equation (7.2):

$$[\mathbf{M}]\{\ddot{u}\} + [\mathbf{K}]\{u\} = 0 \tag{7.1}$$

$$\Downarrow$$

$$[\mathbf{M}]\{\ddot{u}\} + [\mathbf{K}]\{u\} = \{\mathbf{R}(t)\} \tag{7.2}$$

Thus adapting only the vectors of interest in regards to the external loading (e.g. earthquake excitation, wind, waves etc.). Further explanation goes beyond the scope of this thesis, see Wilson [2002]; Chopra [2012]; Leger et al. [1986].

Table 7.4 presents number of modes used in each analysis together with summarized mass participation ratio in different directions (confer with Table 5.4 for modeltype).

Table 7.4: *Number of modes utilized for analysis in SAP2000.*

Vs $[m/s]$	**Model Type**	**Number of modes**	$\sum \boldsymbol{U_x}$ [%]	$\sum \boldsymbol{U_y}$ [%]	$\sum \boldsymbol{U_z}$ [%]
1000	I-H	40	99,6	99,8	-
	II-H	40	99,9	-	-
	I-V & II-V	50	-	99,4	99,9
500	I-H	50	99,99	99,99	-
	II-H	50	99,9	-	-
	I-V & II-V	60	-	99,7	99,9
300	I-H	60	99,9	99,9	-
	II-H	60	99,9	-	-
	I-V & II-V	70	-	99,9	99,9

Some of the directions are not of interest (-) depending on the configuration in the analysis. The effectiveness of LDR-vectors is clearly exhibited from the modal mass participation ratios provided in Table 7.4.

7.5.2 Modal Damping Ratios

Modal damping ratios were assigned in order to simulate an *operating* turbine. Lacking experimental data for the NREL 5-MW wind turbine, these modal damping ratios are based on investigating previous research on wind turbines in the megawatt-scale (damping values for the first bending natural frequencies):

- For a 900-kW wind turbine, Prowell [2011] reported a mean damping of 4,7-5,9% from in-situ observations – operating at 22 RPM. The shear wave velocity at the site was estimated to increase from 300 m/s at the surface, to up to 650 m/s 10 meter below ground surface.

- Prowell [2011] also reported a mean damping of 7,6-7,9% from in-situ observations of an 1.5-MW wind turbine, operating at 17,4 RPM. However, this wind turbine had sloshing dampers installed to provide additional damping. The site was the same as mentioned above, thus the shear wave velocity of the soil was also the same.

- Damgaard et al. [2012] studied a offshore wind turbine of, what seems to be, around 2.3-MW (based on tower height, as the rated power is not provided). This turbine had a monopile foundation, and an oscillation damper installed just below the nacelle. The study obtained a damping of 2,25% for the first natural frequency. The soil conditions varied from loose sand to very stiff clay in the first 10 meter below seabed.

- Bazeos et al. [2002] used a viscous damping of 0,5% in the finite element models of a 450-kW wind turbine. The authors created one model with extensive finite element modelling (shells in tower, doors included etc.) and one simplified model using beam-column elements at turbine tower. Ishihara and Sarwar [2008] also utilized the same percentage of damping for turbines of size 400-kW and 2-MW, and showed underestimations in seismic response from response spectrum methods from codes, due to the assumptions of high damping in the codes (1-5%).

Keep in mind that a wind turbine of this size (5-MW) also is more than likely to have some tuned damper for the first natural frequencies. However, for a wind turbine in the megawatt-scale, the rather low first natural frequencies does not coincide too much with earthquakes [Prowell, 2011; Hänler et al., 2006; Ishihara and Sarwar, 2008], but possibly rather the frequency of turbulent winds.

As explained in Chapter 3.3, not much direct recommendations is provided in the current guidelines. Only IEC [2005] suggest a damping value; 1% of critical damping in the first natural frequency. Obviously there is some significant spread in recommendations and results on damping, especially for the first bending natural frequencies. Thus, some discussion can be justified on the matter of assigned modal damping ratios in this thesis, summarized in Table 7.5:

Table 7.5: *Principal of assigned modal damping ratios.*

Mode	**Type**	ξ
1^{st}	Fore-aft	4,0 %
1^{st}	Side-side	3,0 %
2^{nd}	Fore-aft	2,0 %
2^{nd}	Side-side	1,3 %
1^{st}	Vertical	1,7 %
⋮	⋮	⋮
n	...	2,0 %

Referring to Chapter 6.2, the natural frequencies will both vary in frequency for different soils, as well as the numbering of the mode shapes. But effort is made to identify the fundamental mode shapes, and apply damping as assumed. Note that an overall modal damping ratio of 2,0% was assigned to all other modes in this study when nothing else is specified. This is equal to the overall damping applied in Prowell et al. [2010b] for the 5-MW wind turbine including SSI.

Also note that the vertical natural frequency is based on $\xi_{steel} = 0.19\%$ from EC1-4 [2004] and ξ_{soil} taken as 1,5%. This is a similar approach as conducted in Damgaard et al. [2012] and Damgaard et al. [2013].

All in all, the arguments listed above shows that the applied modal damping ratios for the 5-MW wind turbine is neither very high, or overly conservative.

8. Results & Discussion

This chapter presents the results from the various analysis introduced in the previous chapter. A brief overview of the organization in this chapter is an advantage:

8.1: ***Results from Vertical Set-Up*:** This section presents results from the vertical set-up – focusing on vertical acceleration and vertical forces in the tower.

8.2: ***Results from Horizontal Set-Up*:** Presents results from the horizontal set-up. This includes the response from earthquake alone, wind-induced load alone (both static and dynamic) and the combination of wind-induced loads and earthquake. Response parameters include acceleration, displacement and base moment demand.

8.3: ***Static Wind Induced Response & Effect of Earthquake*:** Lastly, an investigation of the response from earthquake compared to static wind is conducted, in terms of displacement and base moment demand as a function of earthquake PGA.

8.4: ***Comparison to Existing Work:*** As a natural completion of this chapter, a comparison to the limited existing research, previous work and existing guidelines is included.

Mostly, the results are presented for V_s = 1000, 500 and 300 m/s. This is somewhat sufficient in order to study the SSI effects. However, for the results from the vertical set-up, some special considerations has been done. Thus, the results from the vertical set-up are presented for V_s = 800, 700 and 600 m/s – in addition to V_s = 1000, 500 and 300 m/s.

8.1 Results from Vertical Set-Up

The wind turbine was excited by the vertical component of the Nahanni earthquake, and was not subject to any wind load. Referring to Table 5.4, the results were rather identical for Configurations I-V and II-V.

8.1.1 Vertical Acceleration in Turbine Tower

Even though the vertical component of the Nahanni earthquake has a rather low PGA, the *amplification* of the responses is of interest. Studying the theoretical natural frequencies of the modelled soil (Table D.1), it became evident that studying the modelled soil with V_s = 800, 700 and 600 m/s was of major interest. Furthermore, in order to be consistent with the results presented in the reminder of this thesis, results are also presented for V_s = 1000, 500 and 300 m/s.

Table 8.1 shows the maximum of responses along the turbine height, in terms of vertical acceleration, as well as the amplification factor for nacelle to PGA, that is:

$$\alpha_{Nac-EQ} = \frac{max(\ddot{u}_{Nacelle})}{PGA} \tag{8.1}$$

Table 8.1: *Summary of acceleration in the vertical direction (I-V & II-V).*

V_s [m/s]	PGA (EQ) [g]	Base Jnt. [g]	Lower Jnt. [g]	Upper Jnt. [g]	Nacelle [g]	α_{Nac-EQ} [-]
1000	0,028	0,066	0,083	0,126	0,220	7,916
800		0,063	0,128	0,246	0,383	13,664
700		0,092	0,277	0,508	0,790	28,225
600		0,142	0,298	0,461	0,644	23,000
500		0,130	0,204	0,284	0,373	13,410
300		0,093	0,101	0,114	0,126	4,547

All the models ranging from a shear wave velocity of 1000 to 500 m/s experienced *severe* amplification of the input acceleration. Figure 8.1 shows the response in terms of vertical acceleration, along the turbine tower height for the model with V_s = 700 m/s.

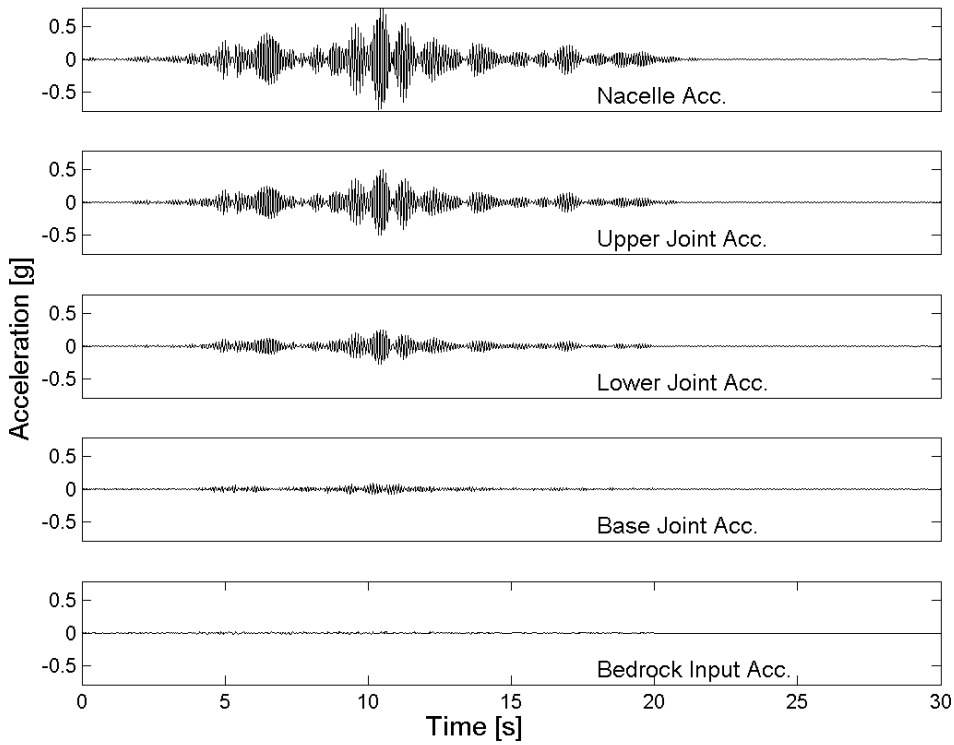

Figure 8.1: *Vertical time serie response from SAP2000 for the Nahanni earthquake, V_s = 700 m/s (I-V & II-V).*

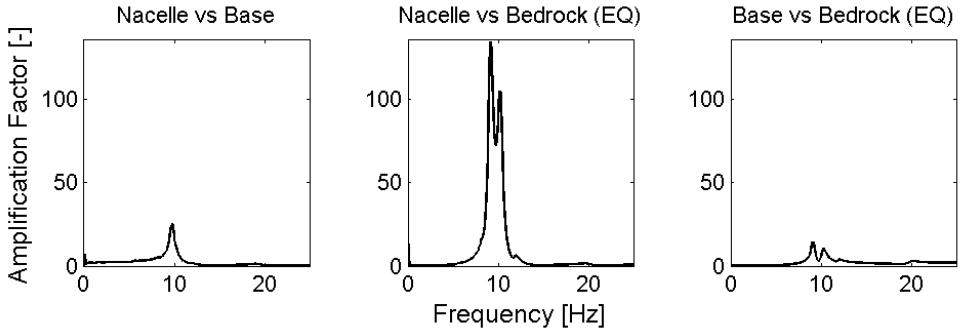

Figure 8.2: *Vertical transform function from SAP2000 for the Nahanni earthquake, V_s = 700 m/s (I-V & II-V).*

The nacelle clearly experience very high amplifications of the input motion. A closer look on Figure 8.2 shows large amplifications in the natural frequencies of the wind turbine (Nacelle vs. Bedrock), and it seems that there are two natural frequencies coinciding around 9-10 Hz.

Figure 8.3 shows responses for V_s = 800, 700 and 600 m/s, plotted together in order to show the difference of the response for different soils.

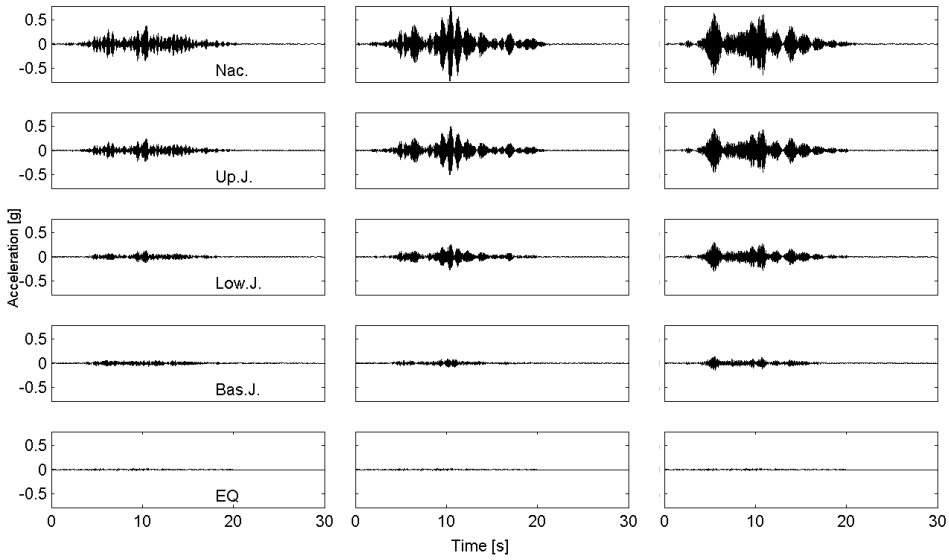

(a) $V_s = 800$ *m/s.* ***(b)*** $V_s = 700$ *m/s.* ***(c)*** $V_s = 600$ *m/s.*

Figure 8.3: *Vertical acceleration for V_s = 800-600 m/s, (I-V & II-V).*

The amplification of input acceleration is clearly exhibited in all the plots. Studying the responses along the turbine tower can indicate input acceleration very close to resonance, as some beating phenomenon seems to appear (as some low frequency waves seems present for each soil) [Mansfield and O'Sullivan, 2008].

Figure 8.4 shows responses for V_s = 1000, 500 and 300 m/s, plotted together in order to show the difference of the response for different soils. Note that this figure has different y-axis than Figure 8.3.

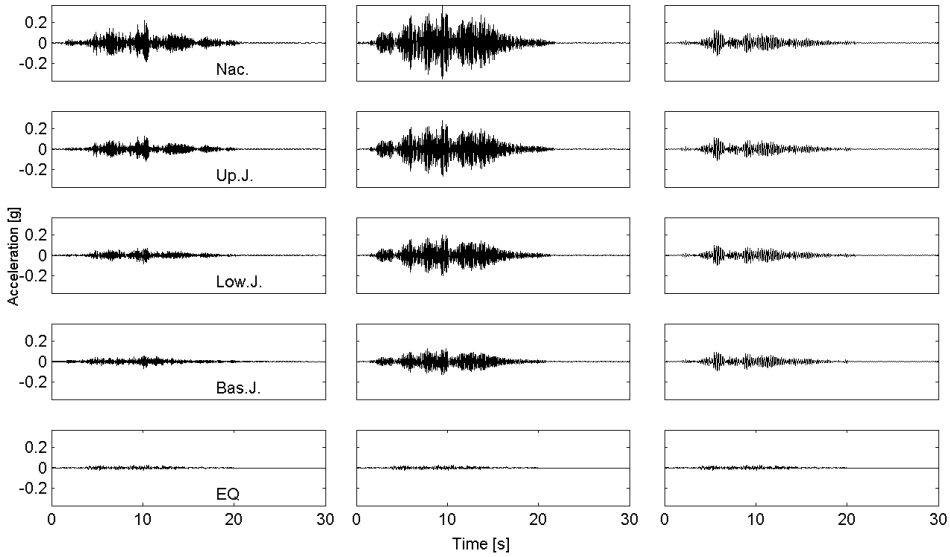

(a) $V_s = 1000$ *m/s.* ***(b)*** $V_s = 500$ *m/s.* ***(c)*** $V_s = 300$ *m/s.*

Figure 8.4: *Vertical acceleration for different V_s (I-V & II-V).*

The amplification is clearly exhibited in Figure 8.4a and 8.4b, while the model containing soil with $V_s = 300$ m/s does not experience as much amplification. It should be noted that these amplifications are not as severe as those presented in Figure 8.3. Detailed plots of the models with $V_s =$ 1000, 800, 600, 500 and 300 m/s are provided in Appendix E.1.1.

As explained in Chapter 5.4, the analysis is purely linear elastic. As such, scaling the response is proportional to scaling the vertical component to a more "realistic" PGA. The original, unscaled, vertical component of the Nahanni earthquake had an PGA of 0,122 [g]. This would imply a peak acceleration in the nacelle of:

Table 8.2: *Scaled vertical accelerations for nacelle from realistic vertical excitation.*

V_s [m/s]	PGA [g]	Nacelle Acc. [g]
1000	0,122	0,967
800		1,680
700		3,471
600		2,828
500		1,639
300		0,555

This would further imply that the nacelle will act more than weightless, and more than double its weight upon the turbine tower. Thus, some considerations must be made for the vertical force in the nacelle-to-tower connection, as elaborated in Chapter 8.1.2.

In addition, it is important to remember that the nacelle contains fine tuned machinery; the gearbox, generator, the shaft, and the rotor connecting the blades to the nacelle. These components could very well be sensitive to shaking, and the vertical component can clearly cause vertical acceleration of a great magnitude in the top of the wind turbine.

8.1.2 Vertical Forces in Turbine Tower

Motivated by the high accelerations in the nacelle due to vertical excitation, the corresponding vertical forces in connections between nacelle-to-tower, and tower-to-base were investigated. As the magnitude of force is of interest at this point, the vertical component of the Nahanni earthquake is scaled to its original PGA of 0,122 [g].

Note that the FEM-model of the tower, created in SAP2000, is discretized into 16 shell elements along the circular section. See Appendix D.3 for further details. As such, the vertical force presented in Figure 8.5 for V_s = 700 m/s represents the shell with the most extreme vertical load, and not the total load upon the top of the turbine tower.

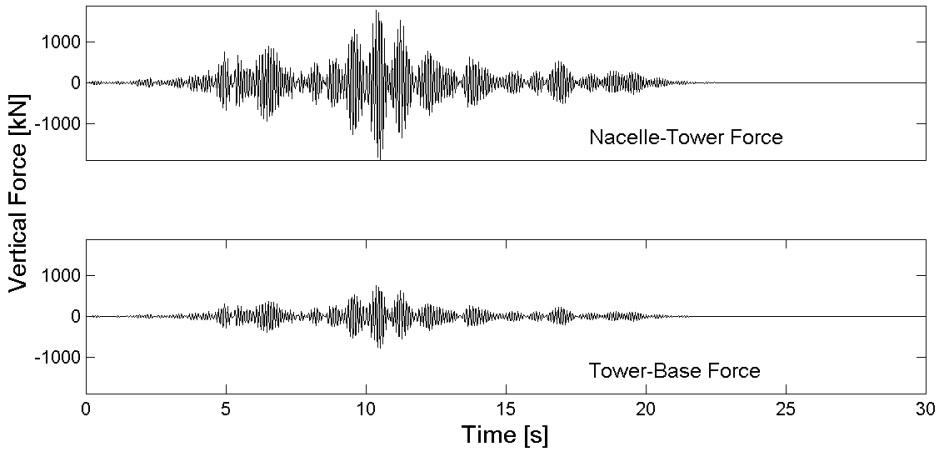

Figure 8.5: *Vertical forces in nacelle and base from SAP2000 for the Nahanni earthquake, V_s = 700 m/s (I-V & II-V), PGA = 0,122 [g].*

It is clear that the nacelle-to-tower connection experience higher vertical forces than the tower-to-base connection. This may lead to further considerations when designing the connection, and check of local buckling for the turbine tower near the connection to the nacelle.

Figure 8.6 shows vertical forces for V_s = 800-600 m/s, plotted together in order to show the difference of the response for different soils.

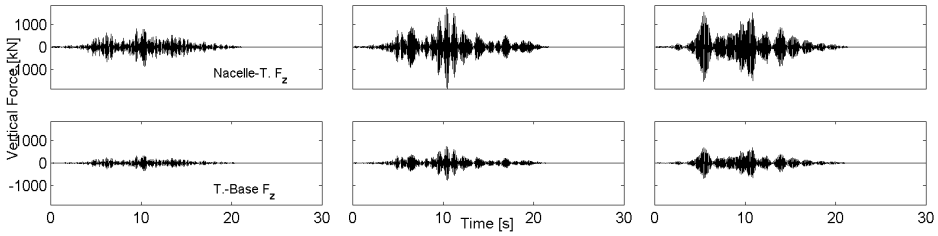

(a) $V_s = 800$ *m/s.* **(b)** $V_s = 700$ *m/s.* **(c)** $V_s = 600$ *m/s.*

Figure 8.6: *Vertical forces for V_s = 800-600 m/s, (I-V & II-V), PGA = 0,122 [g].*

The trend is very similar to Figure 8.3. These high vertical forces may be design driving, especially when combined with other loads on the turbine tower.

Figure 8.7 shows vertical forces for V_s = 1000, 500 and 300 m/s, plotted together in order to show the difference of the response for different soils.

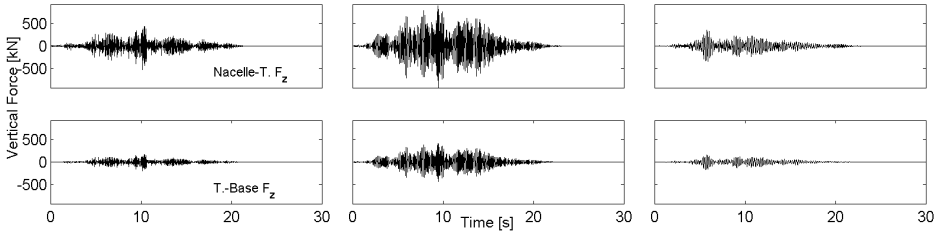

(a) $V_s = 1000$ *m/s.* **(b)** $V_s = 500$ *m/s.* **(c)** $V_s = 300$ *m/s.*

Figure 8.7: *Vertical forces for different V_s (I-V & II-V), PGA = 0,122 [g].*

The trend is very similar to Figure 8.4 – with the highest response for V_s = 1000 and 500 m/s. However the vertical forces from these soils are about half the magnitude of those presented in Figure 8.6.

Buckling & Forces in Turbine Tower

As an elaboration of the results presented in the previous section, the idea to compare the vertical force in turbine tower due to vertical excitation and simulated turbulent wind-induced load was pursued.

Nacelle

Figure 8.8 presents the vertical force in the *connection between nacelle-to-tower*, due to both wind alone and the combination of wind and earthquake. Note that the vertical component of the Nahanni earthquake is scaled up to PGA = 0,122 [g].

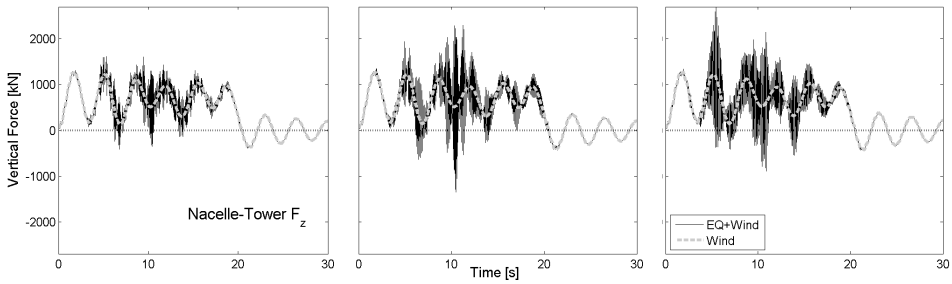

(a) $V_s = 800$ *m/s.* ***(b)*** $V_s = 700$ *m/s.* ***(c)*** $V_s = 600$ *m/s.*

Figure 8.8: *Nacelle: Earthquake and turbulent wind-induced vertical forces for V_s = 800-600 m/s, (I-V & II-V), PGA = 0,122 [g].*

All the models experience additional vertical forces due to the vertical excitation. In fact, the response is more than doubled from the response due to wind only for the model containing soil of V_s = 700 and 600 m/s.

Figure 8.9 presents the vertical force in the *connection between nacelle-to-tower* for V_s = 1000, 500 and 300 m/s.

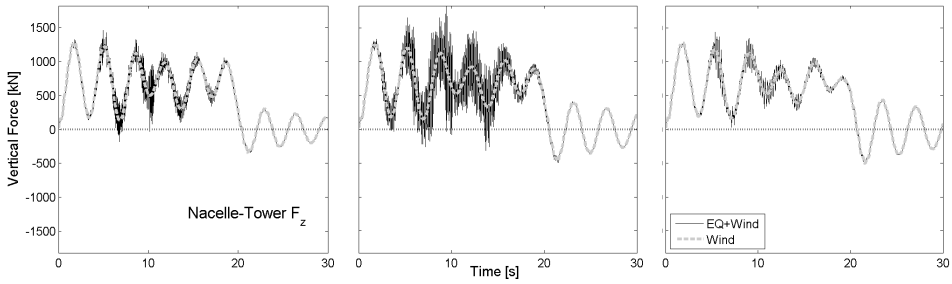

(a) $V_s = 1000$ *m/s.* ***(b)*** $V_s = 500$ *m/s.* ***(c)*** $V_s = 300$ *m/s.*

Figure 8.9: *Nacelle: Earthquake and turbulent wind-induced vertical forces for different V_s (I-V & II-V), PGA = 0,122 [g].*

Especially the model with V_s = 500 m/s experiences additional vertical forces due to the vertical excitation – the response is almost doubled from the response due to wind only. However, the response is still much less than those presented in Figure 8.8.

Base

Figure 8.10 and Figure 8.11 presents the vertical force in the *connection between tower-to-base*, with the same conditions as explained above.

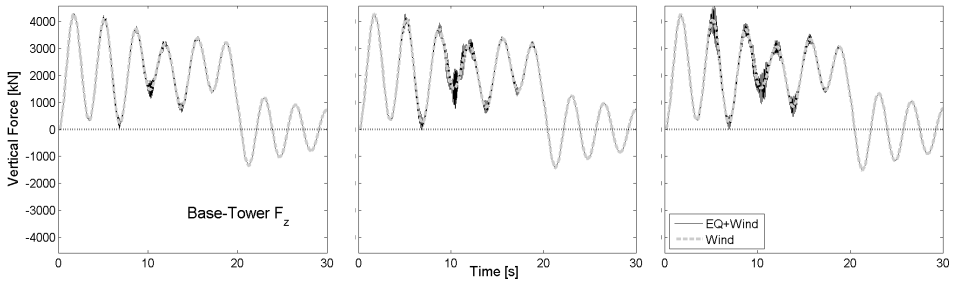

(a) $V_s = 800$ *m/s.* ***(b)*** $V_s = 700$ *m/s.* ***(c)*** $V_s = 600$ *m/s.*

Figure 8.10: *Base: Earthquake and turbulent wind-induced vertical forces or V_s = 800-600 m/s, (I-V & II-V), PGA = 0,122 [g].*

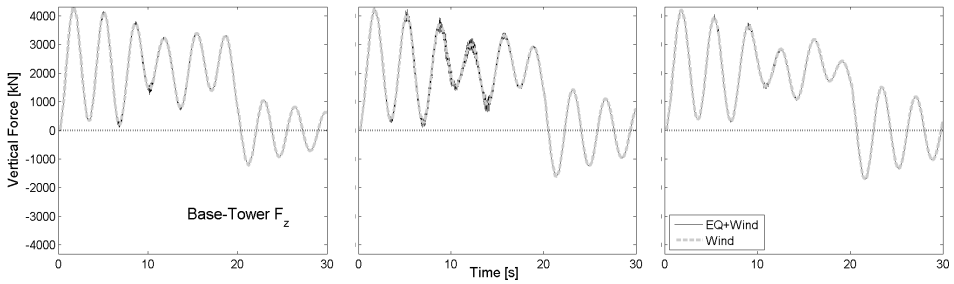

(a) $V_s = 1000$ *m/s.* ***(b)*** $V_s = 500$ *m/s.* ***(c)*** $V_s = 300$ *m/s.*

Figure 8.11: *Base: Earthquake and turbulent wind-induced vertical forces for different V_s (I-V & II-V), PGA = 0,122 [g].*

In contrast to the connection between nacelle and tower, the tower-base connection shows little effect from the vertical earthquake excitation for

either of the soils. The magnitude of wind-induced load is, by far, larger than the magnitude of loads caused by vertical earthquake excitation. These results leads to the motivation of careful judgement of buckling in the turbine tower, especially in the upper parts due to earthquake excitation. A buckling analysis would require a detailed FEM-model, and goes beyond the scope of this thesis.

Note on Radiation Damping

Recognising the severe responses obtained in this chapter, and further recognising the fact that the numerical model does not take into account radiation damping – an alternative approach was investigated in order to indicate the level of radiation damping lost in the model.

As explained in Wilson [2002], a radiation damping factor in the vertical direction (when considering a foundation system consisting of a rigid circular plate) can be expressed as:

$$C_{rad} = 1,79\sqrt{K_v \rho r^3} \tag{8.2}$$

where K_v is the vertical stiffness of the soil, ρ is the mass density of the soil and r is the radius of the rigid circular plate. It should be noted that the model in this thesis contains a monopile foundation, and not a rigid plate. Nonetheless, the above relation is assumed for the purpose of this brief investigation, and r is assumed as the radius of the monopile.

Further explanation on the procedure is provided in Appendix E.1.2. Table 8.3 presents the obtained damping coefficient for the three different soils with the most severe results (V_s = 800-600 m/s). It should be noted that this includes previous assigned modal damping ratios (Table 7.5).

Table 8.3: *Approximation of radiation damping*

Soil V_s $[m/s]$	**Spring-stiffness** K_v $[kN/m]$	**Damping-coefficient** C_{rad} $[kN/(m/s)]$	**Observed Damping** ξ_{tot} [%]
800	$5,13 \cdot 10^7$	$9,42 \cdot 10^4$	2,35
700	$4,04 \cdot 10^7$	$8,36 \cdot 10^4$	2,49
600	$3,09 \cdot 10^7$	$7,31 \cdot 10^4$	2,72

Clearly some additional damping due to radiation damping is lost in the model. The additional damping could lead to somewhat lower responses.

8.1.3 Conclusion & Discussion

The results presented in this section, contains rather surprisingly high acceleration and vertical forces in the turbine tower near the nacelle, induced by vertical earthquake excitation. The PGA of the vertical component of the earthquake was not very high (0,12 [g]), but managed to cause accelerations up to 3,47 [g] in the nacelle (Table 8.2). These results may cause severe amplification of the loads upon the turbine tower from the nacelle, rotor and blades.

The characteristics in the shaking of the nacelle, rotor and blades were not examined, i.e. if these components moved rigidly up and down, or also contained a rocking movement relative to the tower.

The vertical forces presented in Figure 8.8-8.11 included the vertical forces induced by simulated turbulent wind. It was evident that the earthquake excitation contributed very much to the response in the nacelle. In addition, it should be noted that these results did not include horizontal excitation. The horizontal component could indeed contribute to even more vertical forces, especially at the base.

These responses could prove to be important in a design stage of wind turbines of this size. Both for buckling forces in the top of tower, but also of acceleration limits for the fine tuned equipment and shaft in the nacelle, rotor and hub. The response in general also shows the extreme importance of careful and correct considerations of SSI.

The major weakness of the numerical model not including radiation damping should be noted. Total damping was investigated by a crude estimate, and revealed additional damping due to radiation. This extra damping could yield lower responses for the wind turbine in the vertical direction, and should be assessed more correctly in further research.

Even though the vertical component used for analysis in this section matches the response spectra from EC8-1 [2004] quite well (as presented in Chapter 7.2.2), other earthquake records may produce different results.

8.2 Results from Horizontal Set-Up

From the horizontal set-up the dynamic response from earthquake alone, response from earthquake including simulated turbulent wind and response from wind only (static or simulated) were obtained.

8.2.1 Dynamic Response from Earthquake

The wind turbine was excited by the horizontal component of the Nahanni earthquake, and was not subject to any wind load. Referring to Table 5.4, the response was obtained from modeltype I-H (side-side response).

Table 8.4 shows the maximum of responses along the turbine height, in terms of horizontal acceleration, as well as the amplification factor for nacelle to PGA (similar as presented in Equation (8.1)):

Table 8.4: *Summary of acceleration response in the horizontal direction (I-H).*

V_s	PGA (EQ)	Base Jnt.	Lower Jnt.	Upper Jnt.	Nacelle	α_{Nac-EQ}
$[m/s]$	[g]	[g]	[g]	[g]	[g]	[-]
1000		0,172	0,494	0,559	0 190	3,804
500	0,050	0,186	0,244	0,261	0,200	4,004
300		0,174	0,665	0,990	0,372	7,438

The model using modelled soil with a shear wave velocity of 300 m/s experienced severe amplification of the input acceleration, especially for the upper joint. Figure 8.12 shows the response in terms of horizontal acceleration, along the turbine tower height for the model with $V_s = 300$ m/s. Also, Figure 8.13 shows the transform function for the upper joint. Detailed plots of the models with $V_s = 1000$ and 500 m/s are provided in Appendix E.2.1.

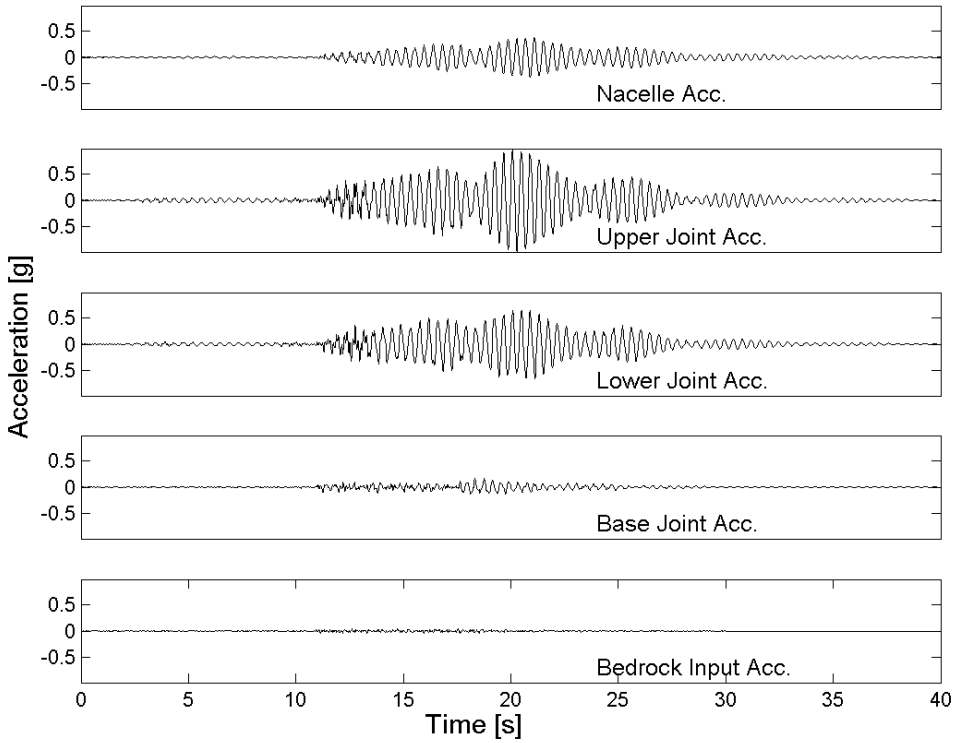

Figure 8.12: *Horizontal time series response from SAP2000 for the Nahanni earthquake, V_s = 300 m/s (I-H).*

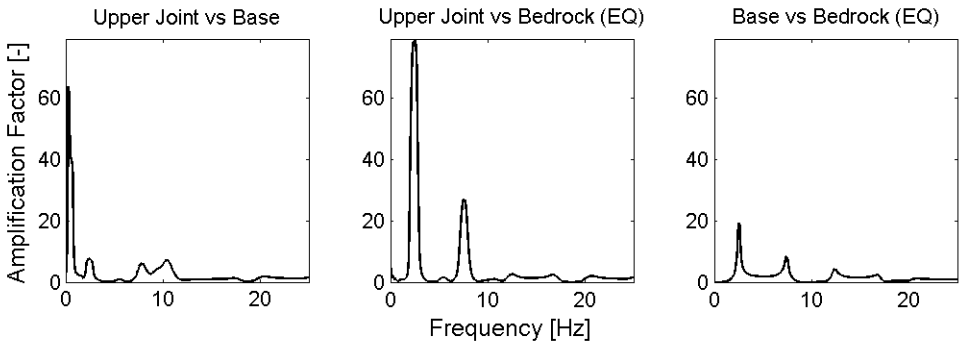

Figure 8.13: *Horizontal transform functions for the Nahanni earthquake, V_s = 300 m/s (I-H).*

The upper joint clearly experience very high amplifications of the input motion, even higher than the nacelle. A closer look on Figure 8.13 shows large amplifications in the natural frequencies of the wind turbine (Upper Joint vs. Bedrock), especially in the 2^{nd} side-side natural frequency ($\approx$ 2,18 Hz). These facts clearly indicates the fact that mainly the 2^{nd} order mode shapes are excited by the input earthquake motion.

The high amplification factor for *Upper Joint vs. Base* close to zero, can be explained some beating phenomenon effect [Mansfield and O'Sullivan, 2008]. The acceleration for the upper joint in Figure 8.12 shows some response of very low frequency, further implying the presence of a beating phenomenon. This is consistent with the observation that the 2^{nd} order natural frequency of the wind turbine is very close to the fundamental natural frequency of the modelled soil with $V_s = 300$ m/s (Figure 5.5 and Table D.1).

However, the amplification shown in the transform function can also be due to various numerical challenges in the algorithm of calculating these transform functions (the algorithm is explained and elaborated in Appendix B.3).

Figure 8.14 shows responses for the three different soils in order to compare the variety of responses due to different soils:

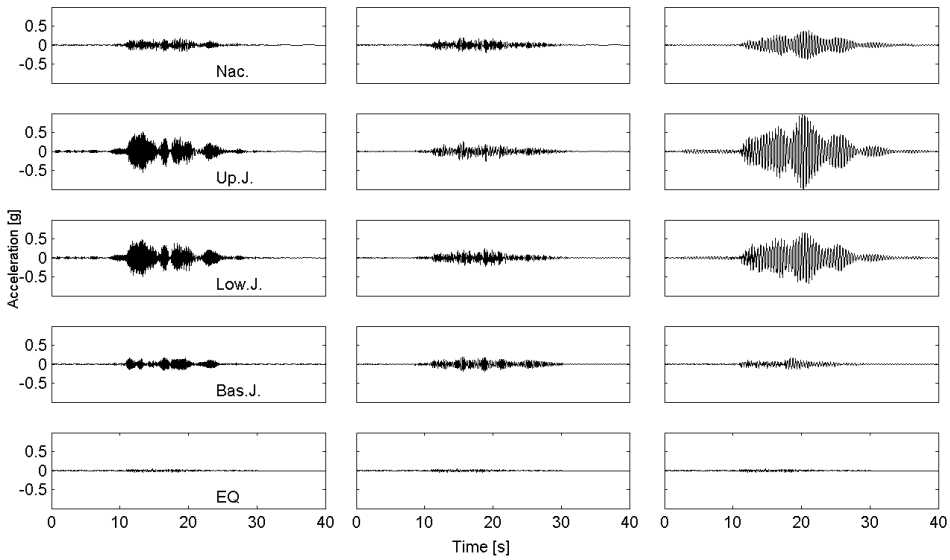

(a) $V_s = 1000$ *m/s.* ***(b)*** $V_s = 500$ *m/s.* ***(c)*** $V_s = 300$ *m/s.*

Figure 8.14: *Horizontal acceleration for different V_s (I-H).*

The amplification is clearly exhibited in Figure 8.14a and 8.14c, while the model containing soil with $V_s = 500$ m/s does not experience as much amplification. It seems that the model containing soil with $V_s = 1000$ m/s also experiences some sort of beating phenomenon, as it seems to experience some waves with low frequency.

Similar as for the vertical component, the horizontal component can be scaled to an original PGA. However, in order to investigate the effect of different sized earthquakes, the horizontal component has been scaled up as follows:

Table 8.5: *Scaled horizontal accelerations for the upper joint from different horizontal excitations (I-H).*

V_s	PGA	Upper Joint Acc.	$\alpha_{Up.J-EQ}$
$[m/s]$	[g]	[g]	[-]
1000		0,559	12,460
500	0,05	0,261	5,810
300		0,990	22,073
1000		1,867	12,460
500	0,15	0,870	5,810
300		3,307	22,073
1000		3,733	12,460
500	0,30	1,741	5,810
300		6,631	22,073
1000		6,222	12,460
500	0,50	2,901	5,810
300		11,022	22,073

The horizontal acceleration for the upper joint is severe when approaching PGA = 0,5 [g]. Most likely the turbine tower would experience some non-linearities at this point. In addition the soil would be likely to yield at these accelerations. Both these non-linearities would absorb energy and reduce the amplification factor. Also, remember that these results are obtained in the side-side direction, not being able to benefit from the higher aerodynamic damping in the fore-aft direction.

Base Moment Demand

As the wind turbines' structural capacity relies on the connection to the base, the moment demand due to earthquake excitation is obtained and presented in Figure 8.15:

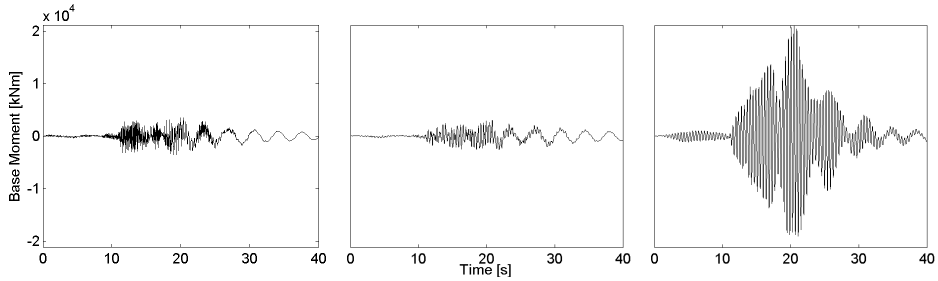

(a) $V_s = 1000$ *m/s.* ***(b)*** $V_s = 500$ *m/s.* ***(c)*** $V_s = 300$ *m/s.*

Figure 8.15: *Moment demand at base for different* V_s *(I-H).*

A trend similar to the acceleration response is evident – a great amplification for the model with soil of $V_s = 300$ m/s. However, it is expected that the moment demand at the base will mainly be driven by wind-induced loads. This is further introduced in the next section, and the base moment demand from combining earthquake and wind-induced load is fully elaborated in Chapter 8.2.3:*Base Moment Demand from Earthquake & Dynamic Wind.*

The base moment demand from Configuration II was also investigated. It showed the same trend, but slightly lower demand. The results is presented in Appendix E.2.1.

8.2.2 Response from Wind-Induced Load

The wind turbine was analysed under two separate load cases: either the simulated turbulent wind-induced load, or the static wind load. Referring to Table 5.4, the response was obtained from modeltype II-H (fore-aft response).

Static Response

Applying a static thrust force of 800 kN (instead of the simulated turbulent wind-induced thrust force), will yield the static response of wind turbine. Thus, comparing the static approach to the dynamic approach can provide valuable knowledge for different structural design procedures.

It should be noted that the applied static thrust force is always equal or higher than the simulated turbulent wind-induced thrust force, that is:

$$F_{thrust,static} \geq F_{thrust,sim}(t) \tag{8.3}$$

$$F_{thrust,static} = 800\ [kN] \tag{8.4}$$

The results are presented in Table 8.6, where u^{nac} represents the displacement of the nacelle, relative to the turbine base.

Table 8.6: *Deflection and base moment for static wind (II-H).*

$\boldsymbol{V_s}$ $[m/s]$	$\boldsymbol{u^{nac}_{wind}}$ $[mm]$	$\boldsymbol{M^{base}_{Ed}}$ $[kNm]$
1000	671	$66,9 \cdot 10^3$
500	704	$66,9 \cdot 10^3$
300	742	$66,8 \cdot 10^3$

Dynamic Response

The simulated turbulent wind (shown in Figure 7.5) will yield a dynamic response in the turbine. The maximum relative displacement of the nacelle and base moment demand are presented in Table 8.8. Note that the results in Table 8.7 and Table 8.8 are taken as maximum values from $\approx$ 5-30 sec, in order to exclude dynamic behaviour at the sudden applying of wind, and the sudden release from the wind-induced load.

Table 8.7: *Deflection and base moment for simulated turbulent wind (II-H).*

V_s $[m/s]$	u_{wind}^{nac} $[mm]$	M_{Ed}^{base} $[kNm]$
1000	820	$106,3 \cdot 10^3$
500	830	$98,3 \cdot 10^3$
300	1010	$98,5 \cdot 10^3$

Analysis showed that the acceleration response was rather independent of soil type. The results are presented in Table 8.8, in terms of horizontal acceleration, as well as the amplification factor for nacelle to base (similar as presented in Equation (8.1)). The results are also graphically presented in Figure 8.16.

Table 8.8: *Summary of acceleration response in the horizontal direction from turbulent wind (II-H).*

V_s [m/s]	PGA (EQ) [g]	Base Joint [g]	Lower Joint [g]	Upper Joint [g]	Nacelle [g]	$\alpha_{Nac-Base}$ [-]
1000		0,001	0,020	0,076	0,125	156,25
500	-	0,003	0,020	0,069	0,113	43,46
300		0,003	0,015	0,050	0,105	26,25

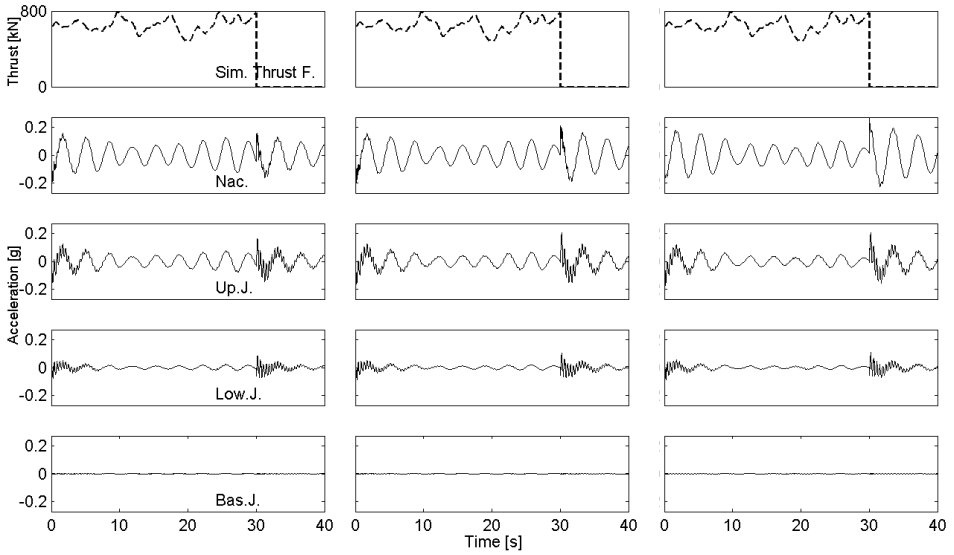

(a) $V_s = 1000\ m/s$. ***(b)*** $V_s = 500\ m/s$. ***(c)*** $V_s = 300\ m/s$.

Figure 8.16: *Turbulent wind-induced horizontal acceleration for different V_s (II-H).*

Clearly, only some minor increase in response is experienced due to the weaker soil. Notice also that the base of the wind turbine is almost at rest, which would indicate a rather low dynamic influence from the operating wind turbine on the surrounding soil.

In the free vibration phase (after 30 sec), the wind turbine shows a sum of two mode shapes; the 1^{st} fore-aft and 2^{nd} fore-aft. The nacelle shows a dominant 1^{st} fore-aft mode shape, while the upper and lower joint shows more contribution from the 2^{nd} fore-aft mode shape. By a quick investigation of the free vibration phase in the nacelle, an indication of the structural damping can be obtained [Chopra, 2012; Humar, 2005]:

$$\xi \approx \ln(\frac{\ddot{u}_i}{\ddot{u}_{i+1}})/2\pi \tag{8.5}$$

$$\xi \approx \ln(\frac{0,129}{0,097})/2\pi \approx 4,6\% \tag{8.6}$$

This is very close to the assigned modal damping ratio for the 1^{st} fore-aft mode shape. The fundamental fore-aft mode shape is (logically) dominant, as

applying a horizontal load in the nacelle is similar as exciting the fundamental mode shape of the wind turbine (or similar as exciting the fundamental mode shape of a cantilever beam with a point mass at the end).

Comparison & Discussion

It is noted that the dynamic analysis produces larger responses than the static analysis. Both in terms of displacement of the nacelle in the fore-aft direction and in terms of base moment demand, M_{Ed}. The difference is summarized in Table 8.9:

Table 8.9: *Summarized difference in static and dynamic wind-induced load (II-H).*

V_s [m/s]	u_{static} [mm]	$u_{dynamic}$ [mm]	**Diff.** [%]	$M_{Ed,static}$ [kNm]	$M_{Ed,dynamic}$ [kNm]	**Diff.** [%]
1000	671	820	22,21	$66,9 \cdot 10^3$	$106,3 \cdot 10^3$	58,89
500	704	830	17,90	$66,9 \cdot 10^3$	$98,3 \cdot 10^3$	46,94
300	742	1010	36,12	$66,8 \cdot 10^3$	$98,5 \cdot 10^3$	47,46

The difference in percentage vary, both between soil types and response types. However, the base moment demand experiences a somewhat large increase of response when accessing the dynamic analysis. On the contrary, the displacement experiences somewhat smaller differences, but the effect is still very noticeable. These results may motivate to either:

1. Make sure to use a sufficiently conservative static load during structural design.
2. Apply a simulated turbulent wind-induced load to get more correct loading, utilizing guidelines like EC1-4 [2004], DNV [2013] etc.

The latter may be preferable as it includes dynamic effects, either alone or in combination with other dynamic loads (as introduced in the next section).

8.2.3 Combined Response of Dynamic Wind & Earthquake

An investigation of the combined effect and contributions of dynamic responses from both wind-induced load and earthquake excitation was conducted. Obtaining the combined response from both simulated turbulent wind-induced load and earthquake excitation, provides knowledge of how much an earthquake will further affect an operating wind turbine.

Acceleration

Referring to Table 5.4, the response was obtained from modeltype II-H (fore-aft response). The horizontal component of the Nahanni earthquake was scaled in order to represent higher PGAs (0,05 - 0,5 [g]). Further the maximum response from the wind turbine was obtained, proving to always be the upper joint in the model containing $V_s = 300$ m/s. The results from wind and earthquake together was then compared to the results from only wind (Table 8.8).

The responses are presented in Table 8.10:

Table 8.10: *Summary of acceleration response in the horizontal direction from turbulent wind and earthquake (II-H).*

PGA (EQ) [g]	**Joint** [-]	V_s $[m/s]$	$\ddot{u}^{joint}_{wind}$ [g]	$\ddot{u}^{joint}_{wind+EQ}$ [g]	**EQ %** [%]	**Wind %** [%]
0,05	Upper J.	300	0,05	0,73	93,14	6,86
0,15	Upper J.	300	0,05	2,38	97,90	2,10
0,30	Upper J.	300	0,05	4,77	98,95	1,05
0,50	Upper J.	300	0,05	7,97	99,37	0,63

The effect of earthquake is quite clear. It dominates the acceleration response even at the lowest PGA, and at the highest PGA the response consist of almost a 100% earthquake excitation. Figure 8.17 through Figure 8.20 shows these results graphically. Notice that the response from wind decays rapidly as the PGA increases:

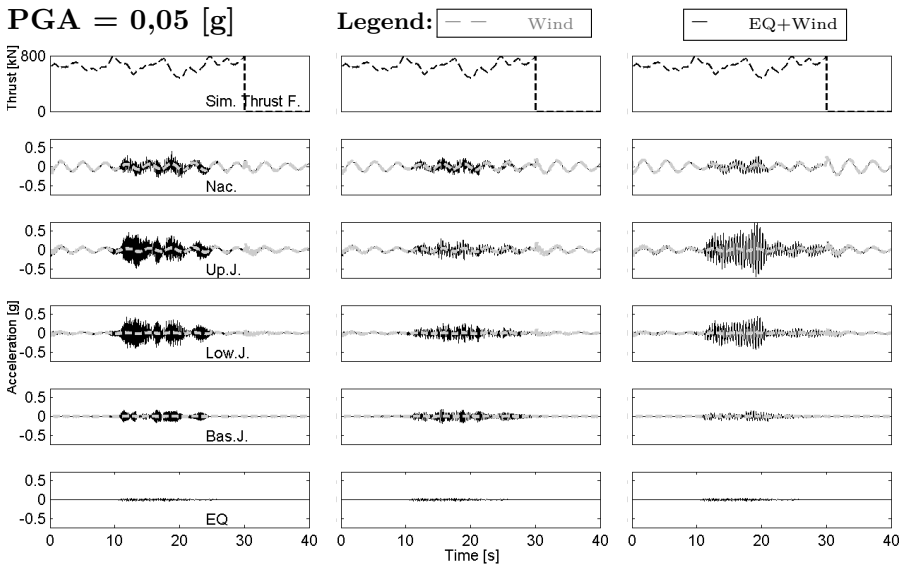

(a) $V_s = 1000\ m/s.$ ***(b)*** $V_s = 500\ m/s.$ ***(c)*** $V_s = 300\ m/s.$

Figure 8.17: *Earthquake and turbulent wind-induced horizontal acceleration for different V_s, PGA = 0,05 [g].*

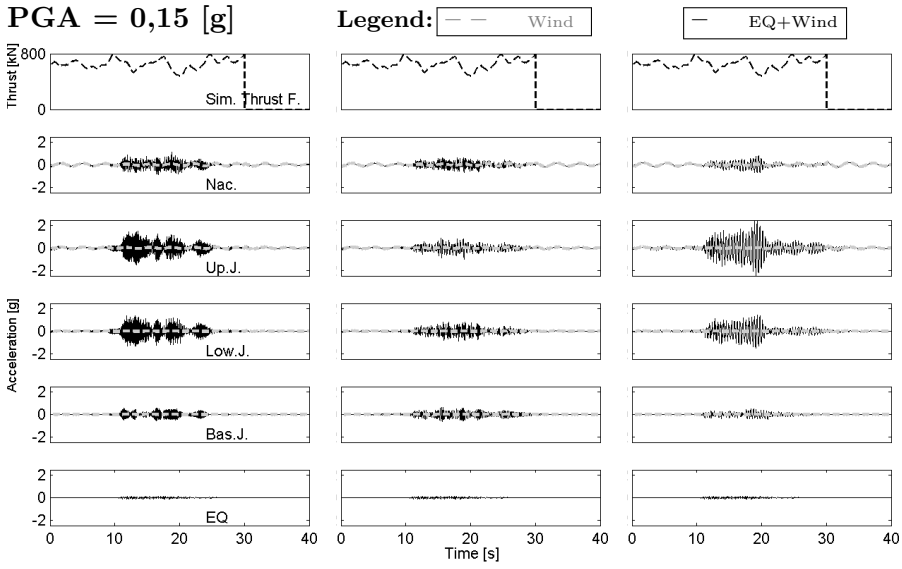

(a) $V_s = 1000\ m/s.$ ***(b)*** $V_s = 500\ m/s.$ ***(c)*** $V_s = 300\ m/s.$

Figure 8.18: *Earthquake and turbulent wind-induced horizontal acceleration for different V_s (II-H), PGA = 0,15 [g].*

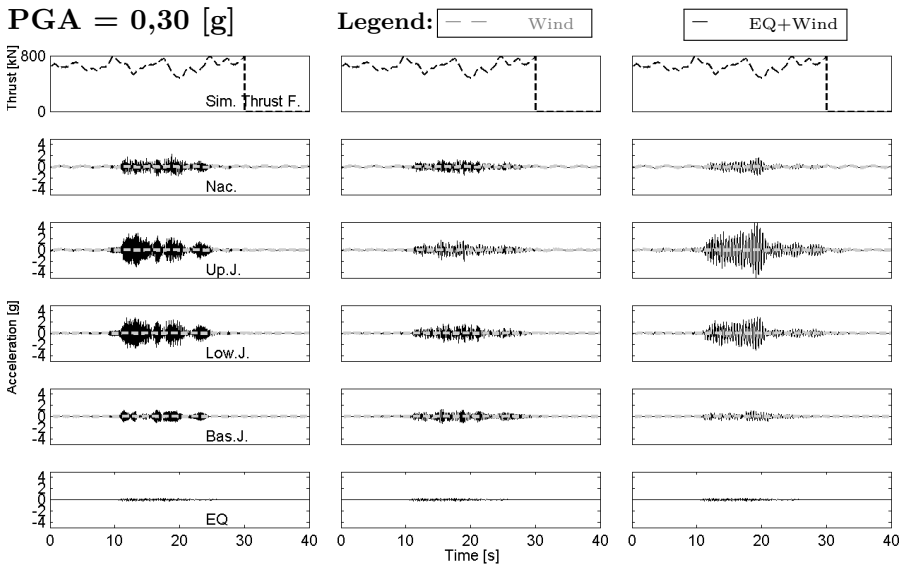

(a) $V_s = 1000$ *m/s.* *(b)* $V_s = 500$ *m/s.* *(c)* $V_s = 300$ *m/s.*

Figure 8.19: *Earthquake and turbulent wind-induced horizontal acceleration for different V_s (II-H), PGA = 0,30 [g].*

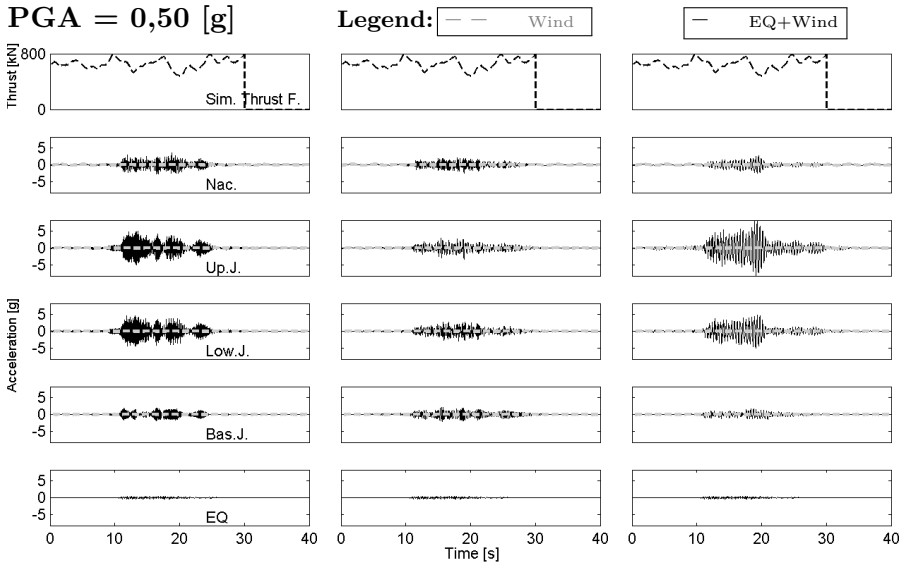

(a) $V_s = 1000$ *m/s.* *(b)* $V_s = 500$ *m/s.* *(c)* $V_s = 300$ *m/s.*

Figure 8.20: *Earthquake and turbulent wind-induced horizontal acceleration for different V_s (II-H), PGA = 0,50 [g].*

These results are not surprising in themselves, as wind contains rather low frequency [Strømmen, 2010] – not inducing high accelerations, and is more likely to excite the fundamental mode shape with corresponding higher damping. Also wind loading does not experience amplification of the modelled system the way the earthquake excitation experiences amplification (through the soil, foundation and structure).

Displacement

As the earthquake excitation proved to be so dominant in acceleration response, data concerning the relative displacement of the wind turbine was investigated. That is; displacement of the wind turbine along its height, relative to its base.

Only displacement from excitation with PGA = 0,50 [g] is presented, as this magnitude of excitation will yield the highest response:

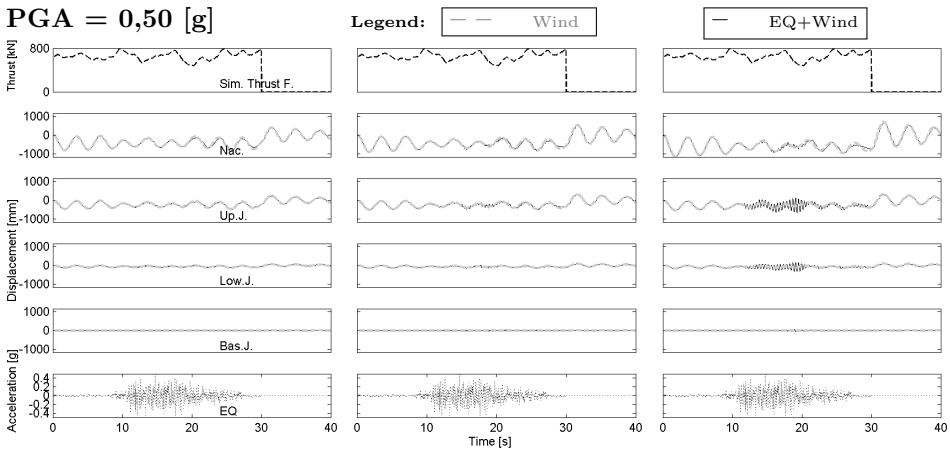

(a) $V_s = 1000$ *m/s.* ***(b)*** $V_s = 500$ *m/s.* ***(c)*** $V_s = 300$ *m/s.*

Figure 8.21: *Earthquake and turbulent wind-induced horizontal displacement for different V_s (II-H), PGA = 0,50 [g].*

In general, it seems that the wind turbine does not experience large deformations due to the earthquake excitation – compared to the deformations from the simulated turbulent wind-induced load. However, for the model containing soil of $V_s = 300$ m/s the earthquake excitation produce some significant contribution to the deformation, especially in the upper and lower joint.

Base Moment Demand from Earthquake & Dynamic Wind

While Chapter 8.2.1:*Base Moment Demand* presented demand for moment capacity in the wind turbine base for earthquake excitation alone, this section presents the demand caused by the combination of both earthquake and the wind-induced load. It is already established that the turbine structure acts like a cantilever beam with a point mass (Chapter 6.1.2), as such the moment in the base is crucial for the capacity of the structure.

Similar as the combined response presented in terms of horizontal acceleration due to wind and earthquake, the results for base moment demand is presented for increasing PGAs. The responses are plotted in Figure 8.22-8.25 in order to get a graphical perspective:

PGA = 0,05 [g]

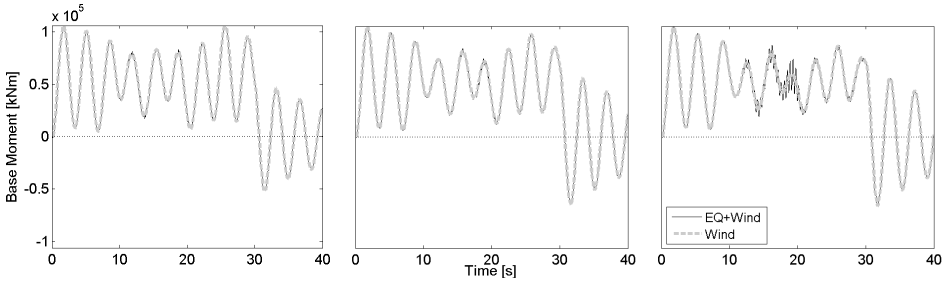

(a) $V_s = 1000$ *m/s.* ***(b)*** $V_s = 500$ *m/s.* ***(c)*** $V_s = 300$ *m/s.*

Figure 8.22: *Earthquake and turbulent wind-induced base moment demand for different V_s (II-H), PGA = 0,05 [g].*

PGA = 0,15 [g]

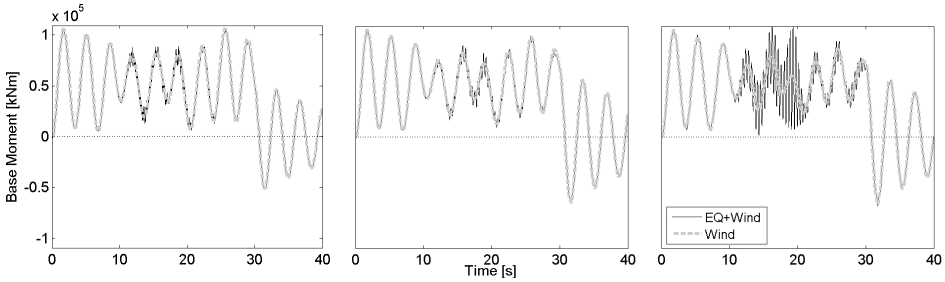

(a) $V_s = 1000$ *m/s.* ***(b)*** $V_s = 500$ *m/s.* ***(c)*** $V_s = 300$ *m/s.*

Figure 8.23: *Earthquake and turbulent wind-induced base moment demand for different V_s (II-H), PGA = 0,15 [g].*

PGA = 0,30 [g]

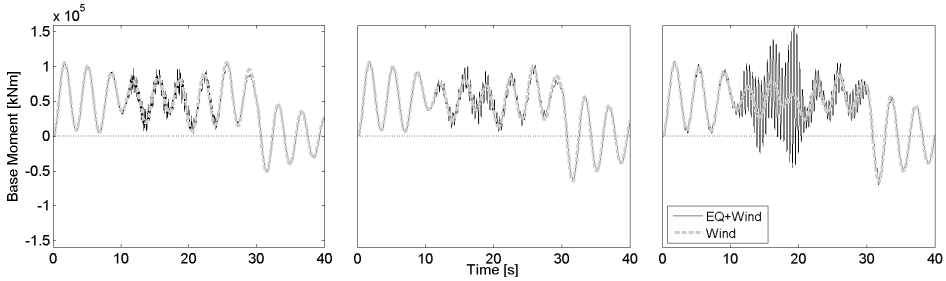

(a) $V_s = 1000$ *m/s.* ***(b)*** $V_s = 500$ *m/s.* ***(c)*** $V_s = 300$ *m/s.*

Figure 8.24: *Earthquake and turbulent wind-induced base moment demand for different V_s (II-H), PGA = 0,30 [g].*

PGA = 0,50 [g]

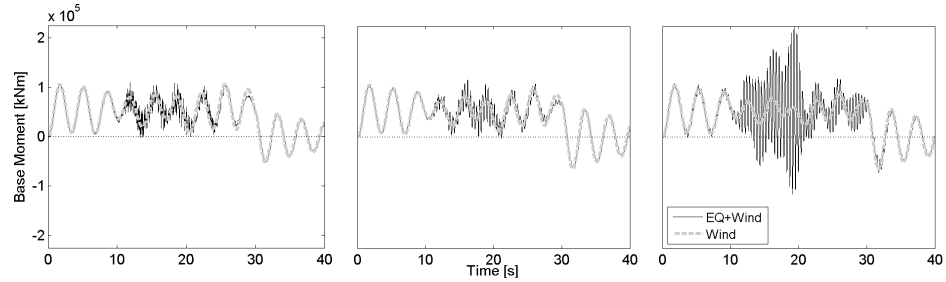

(a) $V_s = 1000$ *m/s.* ***(b)*** $V_s = 500$ *m/s.* ***(c)*** $V_s = 300$ *m/s.*

Figure 8.25: *Earthquake and turbulent wind-induced base moment demand for different V_s (II-H), PGA = 0,50 [g].*

Already at PGA = 0,15 [g] the earthquake affects the moment demand at the base for $V_s = 300$ m/s (Figure 8.23). And at PGA = 0,30-0,50 [g] the contribution from earthquake can be observed even at $V_s = 1000$ m/s.

Table 8.11 presents base moment demand at the time where earthquake alone induces the maximum base moment ($\approx 19,3$ s), and the percentage of contribution from wind, and from earthquake at that time. Note, however, that only the results from the model containing soil with $V_s = 300$ m/s is included as this model exhibited the largest contribution from earthquake.

Table 8.11: *Summary of base moment demand in the horizontal direction from turbulent wind and earthquake for V_s = 300 [m/s], (II-H).*

PGA (EQ) [g]	V_s [m/s]	$\boldsymbol{M_{Ed,wind}}$ [kNm]	$\boldsymbol{M_{Ed,wind+EQ}}$ [kNm]	**EQ %** [%]	**Wind %** [%]
0,05	300	$59,8 \cdot 10^3$	$74,5 \cdot 10^3$	19,80	80,20
0,15	300	$59,8 \cdot 10^3$	$109,3 \cdot 10^3$	45,34	54,66
0,30	300	$59,8 \cdot 10^3$	$158,8 \cdot 10^3$	62,37	37,63
0,50	300	$59,8 \cdot 10^3$	$224,9 \cdot 10^3$	73,44	26,56

Notice the increasing level of contribution from earthquake, up to 73% at PGA = 0,50 [g]. These results leave little doubt that earthquakes can be design-driving factors for moment demand at the base, and shows the importance of accurately assessing soil-structure interaction in the design phase.

8.2.4 Conclusion & Discussion

The results presented in this section are many. The response from horizontal earthquake excitation was presented in terms of horizontal acceleration along the turbine height. The tendency was clear for all soil strengths: high response in the upper and middle joints, but somewhat lower response in the nacelle. This indicates by far that earthquakes mostly will excite the higher order mode shapes and not so much the fundamental mode shapes in regards to wind turbines of this size. In fact, the amplification of response was very severe for the upper joint, indicating a motivation for investigating individual sections of the tower during design. Extreme care should be taken when codes and guidelines indicates that a given number of mode shapes is sufficient for analysing wind turbines.

The difference in response from static wind, or the (equal or less) simulated turbulent wind-induced load was investigated. Both in terms of displacement of the nacelle and base moment demand, the dynamic wind yielded larger responses than the static wind. These results may motivate to show much care during structural design when applying wind-induced loads using structural based software

Lastly, the combined response from simulated turbulent wind-induced load and horizontal earthquake excitation was presented. Overall, the earthquake proved to be very dominant in terms of horizontal acceleration – even at the lowest PGA of 0,05 [g]. On the contrary, earthquake did not affect the displacement as much, as it was highly dominated by wind. In terms of base moment demand, the earthquake showed some contribution, especially for the softest soil. As such, the base moment demand from earthquake may very well be design driving in softer soils.

Even though the problem is not directly presented in this section, the major weakness of the numerical model not including radiation damping should be noted also for the horizontal set-up. This extra damping could yield lower responses for the wind turbine in the horizontal direction, and should be assessed more correctly in further research.

Even though the horizontal component used for seismic analysis in this section matches the response spectra from EC8-1 [2004] quite well (as presented in Chapter 7.2.1), other earthquake records may produce different results.

8.3 Static Wind-Induced Response & Effect of Earthquake

A quick investigation of the effect from earthquake compared to the *statically* applied wind was investigated. Both the displacement along the turbine (relative to its base) and base moment demand were studied. Essentially, the objective was to determine (if) when the response from earthquake would become equal, or greater than the response from static wind, by increasing the PGA (0,05 - 0,85 [g]).

As explained before, the analysis conducted in this thesis are all purely linear elastic. As such, the matter of investigating this subject was fairly easy, as it was just a matter of scaling the obtained responses from previous responses.

8.3.1 Displacement

The displacement in the nacelle is (logically) where the largest displacement from static wind will be present. On the contrary, responses presented in Chapter 8.2.1 and Figure 8.21 showed that the nacelle did not experience that much response from earthquake excitation. Figure 8.26 presents the investigation for displacement in nacelle:

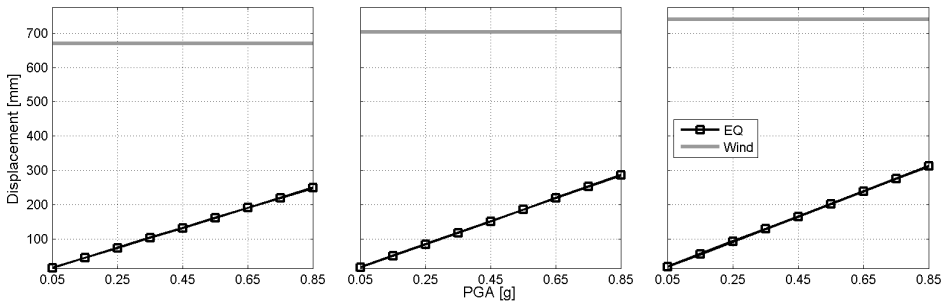

(a) $V_s = 1000$ *m/s.* ***(b)*** $V_s = 500$ *m/s.* ***(c)*** $V_s = 300$ *m/s.*

Figure 8.26: *Effect of earthquake compared to static wind in nacelle displacement, for different V_s (II-H).*

Clearly, the earthquake does not begin to match with the displacement caused by static wind, for any V_s.

On the contrary, displacement caused by earthquake in both the upper and lower joint, proved to de more dominant (as observed in Chapter 8.2.1 and Figure 8.21). Furthermore, the displacement from static wind is much less in these lower joints, as the turbine with applied static wind load resembles a cantilever beam with a point load at the end.

Figure 8.27 and Figure 8.28 presents the investigation for displacement in upper and lower joint, respectively:

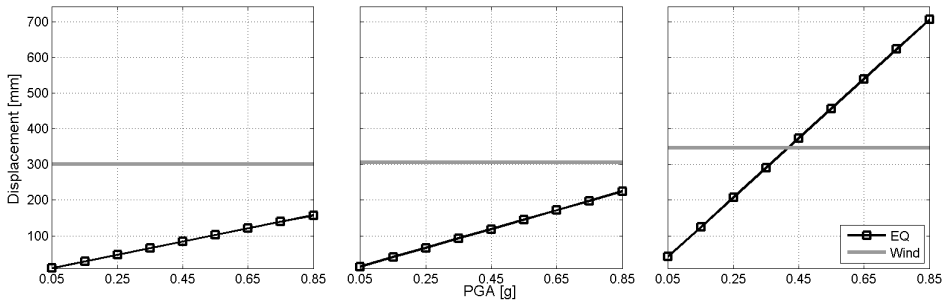

(a) $V_s = 1000$ *m/s.* ***(b)*** $V_s = 500$ *m/s.* ***(c)*** $V_s = 300$ *m/s.*

Figure 8.27: *Effect of earthquake compared to static wind in upper joint displacement, for different V_s (II-H).*

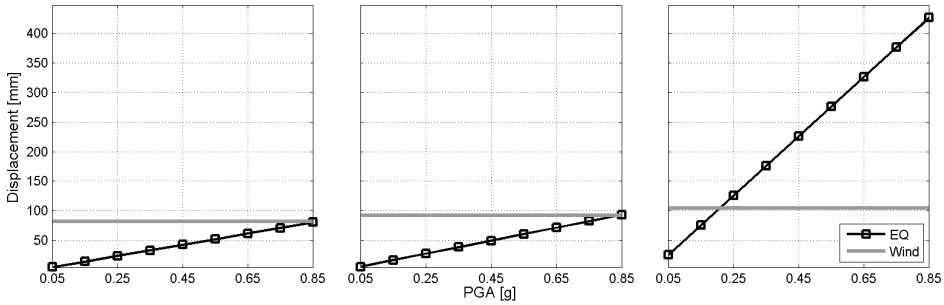

(a) $V_s = 1000$ *m/s.* ***(b)*** $V_s = 500$ *m/s.* ***(c)*** $V_s = 300$ *m/s.*

Figure 8.28: *Effect of earthquake compared to static wind in lower joint displacement, for different V_s (II-H).*

It is evident that earthquake excitation can reach the same level of response as the static wind, in the upper and lower joints. In fact, for the model with $V_s = 300$ m/s, earthquake dramatically exceeds the response from static wind

at rather low values for PGA; approximately 0,40 [g] for the upper joint, and 0,20 [g] for the lower joint. This fact may lead to the belief that earthquake can be a design driving factor for shear forces in the lower parts of the tower – somewhat different than the conclusion in Chapter 8.2.3:*Displacement*.

8.3.2 Base Moment Demand

The base moment demand (i.e. vertical forces in the lower parts of the tower) is a key component in the wind turbine structure and its foundation. The moment demand from static wind proved to be (more or less) independent of the strength of soil (Chapter 8.2.2). However, the moment demand from earthquake proved to be very much dependent of the strength of soil (Chapter 8.2.1).

The investigation of earthquake compared to static wind load is presented in Figure 8.29:

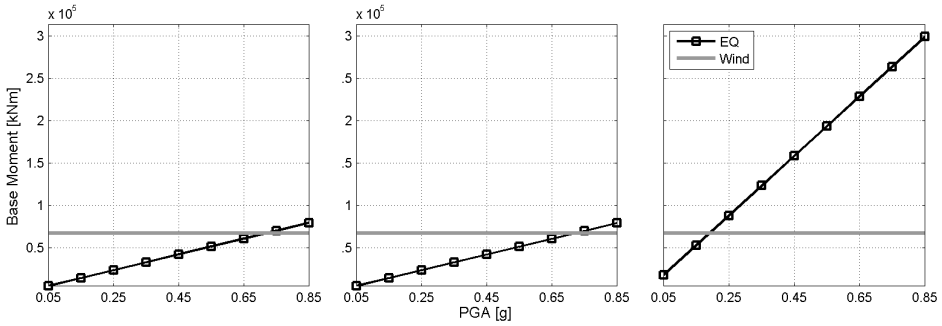

(a) $V_s = 1000$ *m/s.* ***(b)*** $V_s = 500$ *m/s.* ***(c)*** $V_s = 300$ *m/s.*

Figure 8.29: *Effect of earthquake compared to static wind in base moment demand, for different* V_s *(II-H).*

As for the displacement for upper and lower joint, the earthquake can definitively match the response from static wind. It even exceeds the wind response for the stiffer soils of $V_s = 1000$ and 500 m/s. These results are somewhat similar as the conclusion from Chapter 8.2.3:*Base Moment Demand from Earthquake & Dynamic Wind*.

8.3.3 Conclusion & Discussion

Comparison between earthquake induced response to statical applied wind was presented in this section, in terms of displacement and base moment demand. The results for what PGA (if any up to 0,85 [g]) earthquake can match static wind response are summarized in Table 8.12:

Table 8.12: *Summary of response from static wind and earthquake*

V_s	PGA, u_{nac}	PGA, u_{mid}	PGA, u_{low}	PGA, M_{Ed}
$[m/s]$	$[g]$	$[g]$	$[g]$	$[g]$
1000	-	-	-	0,71
500	-	-	0,83	0,71
300	-	0,41	0,20	0,19

As presented in previous sections within this chapter, earthquake responses in the upper and lower joint are quite large, indicating mainly excitation of higher order mode shapes. The responses at these locations proved to be able to match static wind in displacement, as presented in Table 8.12. In particular for weaker soils, earthquake may very well become design driving for shear forces in the middle and lower parts of the tower.

For the bottom joint (base), the earthquake may be design driving factors when considering base moment demand, connection to foundation, and buckling of the lower parts of the tower, especially for weaker soils.

These conclusions further shows the importance of careful considerations of soil-structure interaction early in the design stage. However, remember that the dynamic wind produced larger response – both in displacement and base moment demand – than the static wind. If a dynamic, turbulent wind is proved to be a more correct approach, earthquake may not have that large effect on wind turbines of this size.

8.4 Comparison to Existing Work

This section presents a *brief* comparison to previous work, for some of the most important results and finding introduced in the previous sections.

8.4.1 Comparison for Vertical Response

Not much research and recommendations exists on the vertical response from earthquake excitation on wind turbines. Ritschel et al. [2003] performed various analysis and compared responses to design loads for earthquake in IEC [2005]. The main focus was horizontal response, but vertical force components was reported to be above the design quantities. Ritschel et al. [2003] further discussed that vertical excitation may be important for wind turbines, even for weak earthquakes.

In Prowell et al. [2010b], the reader can be observe a rather large amplification of vertical excitation from bedrock to the top of the modelled 200 m deep soil, due to the vertical component of the 1994 Northridge earthquake. However, further discussion or presentation of vertical response of the wind turbine (same 5-MW reference wind turbine as in this thesis) is not performed.

8.4.2 Comparison for Horizontal Response

Overall, existing research and guidelines concerning wind turbines subject to earthquakes have been focusing on the horizontal response (similar as normal practice in general for earthquake engineering).

In Prowell et al. [2010b] it was concluded that SSI could be of importance in design of base moment demand. Prowell et al. [2010b] further urged for considerations of site-specific soil conditions and for carefully performing seismic analysis for the given site. It was also reported of highest responses near the 2^{nd} order mode shape, suggesting the 2^{nd} mode shapes to be dominant. The general importance of higher order modes of wind turbines in a megawatt-scale has been stated in some amount of research, e.g. Nuta [2010]; Ishihara and Sarwar [2008].

The displacement of the wind turbine due to wind-induced loads was observed (naturally) highest in the nacelle, and with a value $\approx 1/100$ of the turbine height. This result is similar as previous research [Bazeos et al., 2002]. Also, the general importance of carefully and accurately assessing the buckling

analysis for the turbine tower has been stated previously [Lavassas et al., 2003; Bazeos et al., 2002]. In fact, Lavassas et al. [2003] reported special importance of buckling for the upper parts of the turbine tower on a general basis.

Prowell et al. [2010c] conducted independent simulations (i.e. only earthquake or wind) and coupled simulation (i.e. both earthquake and wind, including aerodynamic effects). However, this was done in the aerodynamic software FAST, and was not a direct study of when (and if) earthquake can match the response from wind. Kiyomiya et al. [2002] conducted some comparison between (static) wind and earthquake, and reported base moment demand exceeding allowable moment for input acceleration of $\approx 0{,}6$[g]. This is not dissimilar for some of the results presented in this thesis.

8.4.3 Comparison for Soil-Structure Interaction

A fair amount of previous research has concluded similar to this thesis of the importance of SSI when designing wind turbines, especially for weaker soils as this thesis has stressed [Zhao and Maißer, 2006; Prowell et al., 2010b; Prowell, 2011].

9. Concluding Remarks & Further Research

Throughout the thesis, detailed summary and discussions are provided in each corresponding section. Thus, this chapter is an overview of results relative to the objectives and research questions, and recommendations for further work. For details, the reader is urged to study the *Conclusion & Discussion* within chapters and sections of interest.

9.1 Concluding Remarks

The objectives outlined in Chapter 1.2 were by and large fulfilled. A study of a modern sized wind turbine, interacting with a modelled soil, has yielded results to answer the research questions.

1) Vertical Acceleration: The vertical response of the wind turbine was thoroughly studied. Results were severe accelerations and forces in the upper part of the turbine tower. The acceleration would imply more than doubling the nacelle weight upon the tower, and the nacelle acting weightless.

The importance of vertical acceleration near the nacelle also becomes evident when remembering the fine-tuned equipment in the nacelle, and the large mass from the nacelle, rotor and blades combined.

The study of vertical acceleration exhibited the extreme importance of soil-structure interaction effects, as some soils produced *much* higher responses than other soils. Careful considerations must be taken when the natural frequencies of the structure itself and the soil coincides. However, the reader must take note of the precarious weakness within the combined model of soil and wind turbine as it does not take into account radiation damping.

2) General Seismic Response of Wind Turbines: The results in this thesis can produce two main conclusions for the horizontal excitation of wind turbines. Firstly – similar as for the results from vertical

accelerations – soil-structure interaction was extremely important. Careful considerations must be taken when the natural frequencies of the structure itself and the soil coincides. Amplification of the input motion was severe when natural frequencies of the wind turbine and the modelled soil were close.

Secondly, the importance of recognising that mainly the 2^{nd} and higher order mode shapes are excited when addressing wind turbines of this size, was clear. In general, the highest magnitude of response of horizontal excitation was found in the middle parts of the turbine tower. These results can motivate of careful considerations for the different connections along the tower height. Further, these results should provoke acknowledgement of the importance of critical thinking for the dynamic behaviour of wind turbines – by not simply studying the fundamental frequency and the corresponding mode shape.

3) Effect of Wind & Earthquake: In contrast to the conclusions drawn above, soil-structure interaction did not seem to have as much effect on the wind-induced loads alone. However, it proved important when assessing the level of effect an earthquake can have on a wind turbine, compared to a statically applied wind. Of course, this is related to the extreme importance of soil-structure interaction on seismic loading in general (as explained above).

The dynamic wind-induced load mainly produced large displacements – larger than most of the displacements from earthquake. Also, the dynamic wind-induced load proved to yield larger response than the statically applied wind. This result shows the importance of either; 1) make sure to use sufficient conservative static load, or 2) apply turbulent wind-induce load. However, the aspects on wind-induced load approaches the limit of this thesis, and was not discussed in much detail.

In addition to the results presented above, the utilization of a structural software like SAP2000 was thoroughly validated in modelling wind turbines, with comparison to research involving a model of an actual wind turbine at *University of California, San Diego*. This validation was important to obtain confidence in the results presented for the wind turbine of main interest in this thesis.

9.2 Further Research

The need for further research may seem endless. Directly related to the main results presented here and the research questions, suggestions for further research can be:

1) Vertical Acceleration: Further investigation of vertical response due to seismic excitation in general should be recommended. This would include utilization of different time-series, and more detailed modelling of the upper parts of the turbine tower – including the nacelle, rotor and blades. Furthermore, detailed FEM-models including details of the connection between tower and nacelle could be created in order to check buckling capacity of the upper part of the tower. Also, it is important to remember the tension and compression force already present in the tower due to wind-induced loads.

In addition, the mechanical and electrical equipment within the nacelle and rotor should be checked for the severe vertical acceleration from seismic excitation.

2) General Seismic Response of Wind Turbines: In general, further investigation of soil-structure interaction effects is preferred. This includes (among other aspects) layered soils, better assessment of damping and different foundation types. This could include comparing models containing modelled soil with models utilizing springs and dampers.

Detailed investigation of the local responses due to earthquake excitation of the turbine tower along its height *may* prove interesting. The higher order mode shapes may imply critical points of interest that may differ from typical practice in earthquake engineering (which is traditionally at the base of a structure). This could also include the shadowing effect of the passing blades and the possibility of vortex induced vibrations surrounding the wind turbine.

A (more or less) detailed literature study of guidelines, and how (if) they only utilize a given number of natural frequencies with corresponding mode shapes could prove interesting – especially for structures similar to megawatt-sized wind turbines, that is more likely to excite higher order mode shapes than the fundamental mode shapes. The guidelines could prove to under-estimate and use unfortunate assumptions.

3) Effect of Wind & Earthquake: A thorough study of how to apply

wind-induced loads and aerodynamic effects in structural based software could prove beneficial. This would include detailed study of how to correctly apply aerodynamic damping, either by modal, Rayleigh, Caughey or other damping algorithms. Some level of accuracy is easier to obtain by the use of modal damping (as within this thesis). But this advantage is lost when direct integration is needed.

All in all, a better approach in total should be an objective when studying dynamic response of wind turbines. Correctly including aerodynamics, operational states, modelled soil and earthquake excitation would be beneficial. This should also include correctly assessing the radiation damping in the model, e.g. either by infinite" region of modelled soil, or correct and careful considerations of boundary conditions.

Also, detailed study on the non-linear behaviour of wind turbines would serve the industry. Structures like wind turbines does not normally have much plastic capacity due to its geometry and low ductility.

Bibliography

L.V. Andersen, M.J. Vahdatirad, M.T. Sichani, and J.D. Sørensen. "Natural Freequencies of Wind Turbines on Monopile Foundations in Clayey Soils – A Probabilistic Approach". *Computers and Geotechnics*, 43:1–11, June 2012.

H. Bachman. *Seismic Conceptual Design of Buildings – Basic Principles for Engineers, Architects, Building Owners and Authorities.* Swiss Federal Office for Water and Geology Swiss Agency for Development and Cooperation. BBL, Vertrieb Publikationen, 2003.

N. Bazeos, G.D. Hatzigeorgiou, I.D. Hondros, H. Karamaneas, D.L. Karablis, and D.E. Beskos. "Static, Seismic and Stability Analyses of a Prototype Wind Turbine Steel Tower". *Engineering Structures*, 24(8):1015–1025, 2002.

P.G. Bergan, P.K. Larsen, and E. Mollestad. *Svingning av Konstruksjoner.* Tapir Forlag, 2nd edition, 1993.

V.V. Bertero, F.M. Bendimerad, and H.C. Shah. *Fundamental Period of Reinforced Concrete Moment-Resisting Frame Structure.* The John A. Blume Earthquake Engineering Center, 1988.

E. Booth and D. Key. *Earthquake Design Practice for Buildings.* Thomas Telford Publishing, 2nd edition, 2006.

M. Bruneau, C.-M. Uang, and S.E. Rafael Sabelli. *Ductile Design of Steel Structures.* McGraw-Hill Professional, 2nd edition, 2011.

H. Bungum, C.D. Lindholm, A. Dahle, E. Hicks, H. Høgden, F. Nadim, J.K. Holme, and C. Harbitxz. *Development of a Seismic Zonation for Norway, Report for Norwegian Council for Building Standardization.* NORSAR and Norwegian Geotechnical Institue, 1998.

T. Burton, N. Jenkins, D. Sharpe, and Bossanyi E. *Wind Energy Handbook.* John Wiley & Sons, Ltd, 2nd edition, 2011.

T.G. Carne and A.R. Nord. "Modal Testing of a Rotating Wind Turbine". Technical Report No. SAND82-0631, Sandia National Laboratories, 1983.

A.K. Chopra. *Dynamics of Structures – Theory & Applications to Earthquake Engineering.* Prentice-Hall, Inc., 4th edition, 2012.

R.W. Clough and J. Penzien. *Dynamics of Structures.* Computers and Structures, Inc., 3rd edition, 2003.

R.D. Cook, D.S. Malkus, M.E. Plesha, and R.J. Witt. *Concepts and Applications of Finite Element Analysis.* John Wiley & Sons. Inc., 4th edition, 2002.

CSI. Computers & Structures Inc. CSI Knowledge Base. University of California., 2013. URL `https://wiki.csiberkeley.com/display/kb/Home`.

M. Damgaard, J.K.F Andersen, L.B. Ibsen, and L.V. Andersen. "Natural Frequency and Damping Estimation of an Offshore Wind Turbine Structure". *Proceedings of the Twenty-second (2012) International Offshore and Polar Engineering Conference. Rhodes, Greece.*, June 2012.

M. Damgaard, L.B. Ibsen, L.V. Andersen, and Andersen J.K.F. "Cross-Wind Modal Properties of Offshore Wind Turbines Identified by Full Scale Testing". *Journal of Wind Engineering and Industrial Aerodynamics*, 116: 94–108, 2013.

DNV. *Design of Offshore Wind Turbine Structures.* Det Norske Veritas AS, January 2013.

EC0. *Eurocode 0: Basis of Structural Design.* European Committee for Standarization, 2002.

EC1-4. *Eurocode 1: Actions on Structures – Part 1–4: General Actions, Wind Actions.* European Committee for Standarization, 2004.

EC8-1. *Eurocode 8: Design of Structures for Earthquake Resistance – Part 1: General Rules Seismic Actions and Rules for Buildings.* European Committee for Standarization, 2004.

EC8-6. *Eurocode 8: Design of Structures for Earthquake Resistance – Part 6: Towers, Masts and Chimneys.* European Committee for Standarization, 2005.

D.N. Egglezos and G.D. Bouckovalas. "Analytical Relationships for Earthquake Induced Pore Pressure in Sand, Clay and Silt". *11th European Conference on Earthquake Engineering, Balkema, Rotterdam.*, 1998.

K. Fujii, Y. Tamura, T. Sato, and T. Wakahara. "Wind-Induced Vibration

of Tower and Practical Applications of Tuned Sloshing Damper". *Journal of Wind Engineering and Industrail Aerodynamics*, 33:263–272, 1990.

M. Ghaffar-Zadech and F. Chapel. "Frequency-Independent Impedances of Soil-Structure Systems in Horizontal and Rocking Modes". *Earthquake Engineering & Structural Dynamics*, 11(4):532–540, 1983.

GL. *Guideline for the Certification of Wind Turbines.* Germanischer Lloyd, Hamburg, Germany, 2010.

GL. *Guideline for the Certification of Offshore Wind Turbines.* Germanischer Lloyd, Hamburg, Germany, 2012.

O.T. Gudmestad. "Seismic Design of Facilities for the Oil and Gas Industry, Risk Based Seismic Design Criteria & Upgrading of Existing Facilities". *Journal of Seismology and Earthquake Engineering*, 5(3):55–62, 2003.

M. Hänler, U. Ritschel, and I. Warnke. "Systematic Modelling of Wind Turbine Dynamics and Earthquake Loads on Wind Turbines". *European Wind Energy Conference and Exhibition, European Wind Energy Association, Athens, Greece*, 2006.

B.O. Hardin and V.P. Drnevich. "Shear Modulus and Damping in Soils; Design Equations and Curves". *Journal of Soil Mechanics and Foundation Engineering, Proceedings of ASCE*, 98(7):667–692, 1972.

E. Hau. *Wind Turbines.* Springer-Verlag Berlin & Heidelberg, 2006.

H.M. Hilber, T.J.R. Hughes, and R.L. Taylor. "Improved Numerical Dissipation for Time Integration Algorithms in Structural Dynamics. *Earthquake Engineering and Structural Dynamics*, 5(3):283–292, 1977.

T.J.R. Hughes. *The Finite Element Method: Linear Static and Dynamic Finite Element Analysis.* Prentice-Hall, Inc., 1987.

J. L. Humar. *Dynamics of Structures.* CRC Press, 2nd edition, 2005.

IBC. *International Building Code 2006 - Section 1613 Earthquake Loads.* International Code Council, 2006.

IEC. *IEC 61400-1: Wind Turbines – Part 1: Design Requirements.* International Electronical Commission, 3rd edition, 2005.

IEC. *IEC 61400-3: Wind Turbines – Part 3: Design Requirements for Offshore Wind Turbines.* International Electronical Commission, 3rd edition, 2009.

F. Irgens. *Continuum Mechanics*. Springer-Verlag Berlin & Heidelberg, 2008.

I. Ishibashi and X. Zhang. "Unified Dynamic Shear Moduli and Damping Rations of Sands and Clay". *Soils & Foundations*, 33(1):182–191, 1993.

T. Ishihara and M.W. Sarwar. *"Numerical and Theoretical Study on Seismic Response of Wind Turbines"*. Department of Civil Engineering, The University of Tokyo, 2008.

B.J. Jonkman. "TurbSim User's Guide: Version 1.50". Technical Report No. NREL/TP-500-46198, National Renewable Energy Laboratory, September 2009.

J. Jonkman and M.L. Buhl Jr. "FAST Users Guide". Technical Report No. NREL/EL-500-38230, National Renewable Energy Laboratory, August 2005.

J. Jonkman, S. Butterfield, W. Musial, and G. Scott. "Definition of a 5-MW Reference Wind Turbine for Offshore System Development". Technical Report No. NREL/TP-500-38060, National Renewable Energy Laboratory, February 2009.

O. Kiyomiya, T. Rikiji, and P.H.A.J.M. van Gelder. "Dynamic Response Analysis of Onshore Wind Energy Power Units During Earthquakes and Wind". *Proceedings of the Twelfth International Offshore and Polar Engineering Conference, Kitakyushu, Japan*, 2002.

R.A. Kjørlaug. *Earthquake Engineering – Analysis & Design of Typical Norwegian Buildings*. Norwegian University of Science & Technology, 2012.

S.L. Kramer. *Geotechnical Earthquake Engineering*. Prentice-Hall, Inc., 1st edition, 1996.

M. Kühn. *Dynamics and Design Optimisation of Offshore Wind Energy Conversion Systems*. PhD thesis, Delft University, Wind Energy Research Institute, Netherland, 2003.

D.J. Laino and A.C. Hansen. "User´s Guide to the Computer Software Routines AeroDyn Interface for ADAMS ®". Technical Report Subcontract No. TCX-9-29209-01, Windward Engineering LLC for National Renewable Energy Laboratory, September 2001.

P.K. Larsen. *Dimensjonering av Stålkonstruksjoner*. Tapir Akademiske Forlag, 2nd edition, 2010.

J.P. Lauffer, T.G. Carne, and T.D. Ashwill. "Modal Testing in the Design Evaluation of Wind Turbines". Technical Report No. SAND87-2461, Sandia National Laboratories, 1988.

P.A.A. Laura, J.L. Pombo, and E.A. Susemihl. "A Note on the Vibrations of a Clamped-Free Beam With a Mass at the Free End". *Journal of Sound and Vibrations*, 37(2):161–168, 1974.

I. Lavassas, G. Nikolaidis, P. Zervas, E. Efthimiou, I.N. Doudoumis, and C.C. Baniotopoulos. "Analysis and Design of the Prototype of a Steel 1-MW Wind Turbine Tower". *Engineering Structures*, 25(8):1097–1106, 2003.

P. Leger, E.L. Wilson, and R.W. Clough. "The Use of Load Dependent Vectors for Dynamic and Earthquake Analysis". Technical Report No. UCB/EERC 86-04, Earthquake Engineering Research Center, University of California, Berkeley, California, 1986.

Ø. Løset, M.M. Loo, Å. Lyslo Døssland, M. Gjestvang, A.M. Kanyia, and C. Bråten. *Dimensjonering for Jordskjelv*. Rådgivende Ingeniørers Forening, 2010.

J.E. Luco. "Soil-Structure Interaction Effects on the Seismic Response of Tall Chimneys". *Soil Dynamics and Earthquake Engineering*, 5(3):170–177, 1986.

J.E. Luco. "A Note on Classical Damping Matrices – Authors Reply". *Earthquake Engineering & Structural Dynamics*, 37:1805–1809, 2008a.

J.E. Luco. "A Note on Classical Damping Matrices". *Earthquake Engineering & Structural Dynamics*, 37:615–626, 2008b.

D.J. Malcolm and D.L. Laird. "Modeling of Blades as Equivalent Beams for Aeroelastic Analysis". *ASME Wind Energy Symposium AIAA/ASME, Reno, Nevada, USA*, pages 293–303, 2003.

M. Mansfield and C. O'Sullivan. *Understanding Physics*. John Wiley & Sons Ltd, 2008.

J.F. Manwell, J.G. McGowan, and A.L. Roger. *Wind Energy Explained – Theory, Design & Application*. John Wiley & Sons, Ltd, 1st edition, 2002.

S. Mazzoni, F. McKenna, M.H. Scott, and G.L. Fenves. "OpenSees Command Language Manual. Technical report, University of California, 2006.

P.J. Moriarty and A.C. Hansen. "AeroDyn Theory Manual". Technical

Report No. NREL/EL-500-36881, National Renewable Energy Laboratory, December 2005.

B. Nanda and K.C. Biswal. "Application of Tuned Liquid Damper for Controlling Structural Vibration Due to Earthquake Excitations". *Modern Methods and Advances in Sructural Engineering and Construction, ISEC-6, Zürich*, June 21-26 2011.

E. Nuta. "Seismic Analysis of Steel Wind Turbine Towers in the Canadaian Environment". Master's thesis, University of Toronto, 2010.

U.S. Department of Energy – Wind & Water Power Program. "Building a New Energy Future with Wind Power", 2013.

PEER. Pacific Earthquake Engineering Research Center: NGA Database. University of California, Berkeley, January-June 2013. URL `http://peer.berkeley.edu/nga/`.

I. Prowell. *An Experimental and Numerical Study of Wind Turbine Seismic Behaviour*. PhD thesis, University of California, San Diego, 2011.

I. Prowell and P. Veers. "Assessment of Wind Turbine Seismic Risk: Existing Literature and Simple Study of Tower Moment Demand". Technical report, Sandia National Laboratories, March 2009.

I. Prowell, M. Veletzos, A. Elgamal, and J. Restrepo. "Shake Table Test of a 65kW Wind Turbine and Computational Simulation". *Proceedings of the 14th World Conference on Earthquake Engineering. Beijing, China*, October 2008.

I. Prowell, M. Veletzos, A. Elgamal, and J. Restrepo. "Experimental and Numerical Seismic Response of a 65-kW Wind Turbine". *Journal of Earthquake Engineering*, 13(8):1172–1190, 2009.

I. Prowell, A. Elgamal, and J. Jonkman. "FAST Simulation of Wind Turbine Seismic Response". Technical Report No. NREL/CP-500-46225, National Renewable Energy Laboratory, March 2010a.

I. Prowell, A. Elgamal, and J. Lu. "Modeling the Influence of Soil Structure Interaction on the Seismic Response of a 5MW Wind Turbine". *Fifth International Conference on Recent Advances in Geotechnical Earthquake Engineering and Soil Dynamics*, May 2010b.

I. Prowell, A. Elgamal, H. Romanowitz, J.E. Duggan, and J. Jonkman. "Earthquake Response Modeling for a Parked and Operating Megawatt-

Scale Wind Turbine". Technical Report No. NREL/TP-5000-48242, National Renewable Energy Laboratory, October 2010c.

I. Prowell, A. Elgamal, and C. Uang. "Estimation of Seismic Load Demand for a Wind Turbine in the Time Domain". Technical Report No. NREL/CP-500-47536, National Renewable Energy Laboratory, March 2010d.

I. Prowell, C.-M. Uang, A. Elgamal, J.E. Luco, and L. Guo. "Shake Table Testing of a Utility-Scale Wind Turbine". *Journal of Engineering Mechanics*, 138:900–909, July 2012.

I. Prowell, A. Elgamal, C.-M. Uang, J.E. Luci, H. Romanowitz, and E. Duggan. "Shake Table Testing and Numerical Simulation of a Utility-Scale Wind Turbine Including Operational Effects". *Wind Energy*, (DOI: 10.1002/we.1615), 2013.

Risø. *Guidelines for Design of Wind Turbines*. Det Norske Veritas & Wind Energy Department of Risø National Laboratory, 2002.

U. Ritschel, I. Warnke, J. Kirchner, and B. Meussen. "Wind Turbines and Earthquakes". *Proceedings of the WWEC, Cape Town, South Africa*, 2003.

V.A. Riziotis, S.G. Voutsinas, E.S. Politis, and P.K. Chaviaropoulos. "Aeroelastic Stability of Wind Turbines: the Problem, the Methods and the Issues". *Wind Energy*, 7:373–392, 2004.

E.N. Strømmen. *Theory of Bridge Aerodynamics*. Springer-Verlag Berlin & Heidelberg, 2nd edition, 2010.

E.L. Wilson. *Three-Dimensional Static and Dynamic Analysis of Structures – A Physical Approach With Emphasis on Earthquake Engineering*. Computers and Structures, Inc., 3rd edition, 2002.

R. Wiser and M. Bolinger. "2011 Wind Technologies Market Report". Technical Report No. TP-5000-53474 & DOE/GO-102009-2868, National Renewable Energy Laboratory, 2012.

D. Witcher. "Seismic Analysis of Wind Turbines in the Time Domain". *Wind Energy*, 8(1):81–91, 2005.

D. Wood. *Small Wind Turbines: Analysis, Design and Application*. Springer-Verlag Berlin & Heidelberg, 2011.

X. Zhao and P. Maißer. "Seismic Response Analysis of Wind Turbine Towers Including Soil-Structure Interaction". *Proceedings of the Institute*

of Mechanical Engineers, Part K: Journal of Multi-Body Dynamics, 220 (1):53–61, 2006.

X. Zhao, P. Maißer, and W. Jingya. "A New Multibody Modeling Methodology for Wind Turbine Structures Using a Cardanic Joint Beam Element". *Renewable Energy*, 32(3):532–546, 2007.

A. Global Wind Power Rankings

A.1 Global Wind Power Rankings of 2011

From 2005 through 2008 the U.S. was the leading nation in annual wind power capacity. However, from 2008 through 2011 the U.S. has been second to China [Wiser and Bolinger, 2012].

Table A.1: *International rankings of wind power capacity [Wiser and Bolinger, 2012].*

Annual Capacity (2011, MW)		**Cumulative Capacity (end of 2011, MW)**	
China	17 631	China	62 412
U.S.	6 816	U.S.	46 916
India	3 300	Germany	29 248
Germany	2 007	Spain	21 350
U.K.	1 293	India	16 266
Canada	1 267	U.K.	7 155
Spain	1 050	France	6 836
Italy	950	Italy	6 733
France	875	Canada	5 278
Sweden	763	Portugal	4 214
Rest of World	5 766	*Rest of World*	34 453
TOTAL	41 718	**TOTAL**	240 861

B. Additional Theoretical Aspects

B.1 Vandermonde System for Deciding Damping Ratios

If M modal damping ratios are prescribed, the process of obtaining $\xi = \xi_1, ..., \xi_M$ includes solving Equation (B.1):

$$\begin{bmatrix} 1 & \omega_1^2 & \omega_1^4 & \dots & \omega_1^{2M-2} \\ 1 & \omega_2^2 & \omega_2^4 & \dots & \omega_2^{2M-2} \\ \vdots & \vdots & \vdots & \ddots & \vdots \\ 1 & \omega_N^2 & \omega_N^4 & ... & \omega_N^{2M-2} \end{bmatrix} \begin{Bmatrix} a_0 \\ a_1 \\ \vdots \\ a_{M-1} \end{Bmatrix} = \begin{Bmatrix} 2\omega_1\xi_1 \\ 2\omega_2\xi_2 \\ \vdots \\ 2\omega_M\xi_M \end{Bmatrix} \tag{B.1}$$

$$(N = M = N_{mod})$$

The matrix in Equation (B.1) is a Vandermonde matrix. Under certain conditions the numerical solution of Equation (B.1) may become ill-conditioned [Luco, 2008b].

B.2 Definitions of Some Earthquake Quantities

Definitions of different magnitudes [Kramer, 1996]:

- *Moment magnitude:*

$$M_w = \frac{logM_0}{1.5} - 10.7 \tag{B.2}$$

$$M_0 = \mu AD \tag{B.3}$$

where μ is the rupture strength of the material along the fault, A the rupture area, and D the average amount of slip.

- *Surface wave magnitude:*

$$M_s = logA + 1.66log\Delta + 2.0 \tag{B.4}$$

  Here, A is the maximum ground displacements in micrometers and Δ is the epicentral distance in degrees of the seismometer.

- *Body wave magnitude:*

$$m_b = logA - logT + 0.01\Delta + 5.9 \tag{B.5}$$

  For this magnitude, A is the p-wave amplitude in micrometers. T is the period of the p-wave.

- *Richter local magnitude:* This is defined as the logarithm of the maximum trace amplitude recorded on a Wood-Anderson seismometer located 100 km from the epicentre of the earthquake.

Definitions of some ground motion parameters [Kramer, 1996]:

- *RMS Acceleration:*

$$a_{RMS} = \sqrt{\frac{1}{T_d}\int_0^{T_d}[a(t)]^2 dt} = \sqrt{\lambda_0} \tag{B.6}$$

  T_d is the duration of the strong motion. λ_0 is the average intensity (mean-squared acceleration).

- *Arias Intensity:*

$$I_a = \frac{\pi}{2g}\int_0^{\infty}[a(t)]^2 dt \tag{B.7}$$

B.3 Transform Functions

The Fourier Spectra in this thesis is obtained through *Fourier Amplitude Spectrum*:

Any periodic function that meets certain conditions can be expressed as the sum of a series of sinusoids of different amplitude, frequency and phase. Thus, e.g. an earthquake time series or response time series can be expressed as:

$$\ddot{u}_g(t) \approx c_0 + \sum_{n=1}^{\infty} c_n sin(\omega_n t + \phi_n) \tag{B.8}$$

Normally, for earthquakes $c_0 = 0$, as this represent the average value of the input function from $t = [0, t_{end}]$. Further, c_n is the amplitude of the different Fourier coefficients:

$$c_n = \sqrt{a_n^2 + b_n^2} \tag{B.9}$$

$$a_n = \frac{2}{t_{end}} \int_0^{t_{end}} \ddot{u}_g(t) cos\, \omega_n t\, dt \tag{B.10}$$

$$b_n = \frac{2}{t_{end}} \int_0^{t_{end}} \ddot{u}_g(t) sin\, \omega_n t\, dt \tag{B.11}$$

It is the amplitude which is utilized throughout this thesis. For further reading, see Kramer [1996]; Chopra [2012]; Humar [2005]. Matlab-script for discrete Fourier transform is presented below:

```
function [f,FFourT,fend] = ffourier_trans(A,dt)
% Fast Fourier Transform by Power Spectrum
% Input:
% A = Vector to be performed FFT on [various]
% dt = Size of timestep [s]
% NOT IN USE: freq_end = Last frequency of interest [Hz]
%
% Output:
% f = Frequency-vector of interest [Hz]
% FFourT = Fourier transformed vector
%
% Written by Remi A. Kjoerlaug, March 2013
% Master Thesis on Wind Turbines.

fs = 1/dt;
nyqf = fs/2;
fend = nyqf;
f = linspace(0,fend,round(length(A)/2));
aVf = A - mean(A);
fftaVf = 2*(fft(aVf))/round(length(A));
ak = (imag(fftaVf(1:round(length(A)/2))));
bk = (real(fftaVf(1:round(length(A)/2))));
ck = sqrt(ak.^2+bk.^2);
FFourT = ck;
% END
```

B.4 Matlab Script `Resp_Spec.m`

The following script utilizes Newmarks' method with linearly varying acceleration to obtain maximums responses of a SDOF system with varying natural frequency, in order to produce pseudo acceleration spectra [Chopra, 2012].

```
function [T,Sd,Sa]=Respons_Spec(t,acc,dmp)
% Script that produces Sd and Sa.
% Input:
%
% t = Time vector, uniform timestep
% acc = Acceleration vector
% dmp = Damping [%]
%
% Output:
% T = Natural Periods
% Sd = Response Displacement Spectra
% Sa = Response Acceleration Spectra
%
% Written by Remi A. Kjoerlaug, May 2013
% Master Thesis on Wind Turbines.

%Newmark constants etc.
gamma=1/2; beta=1/6; Tend=5;
xi = dmp/100; dt=t(2)-t(1); T(1)=0;

for i =1:round(Tend/dt); %For every natural period
    m=1;
    omega(i)=2*pi/T(i) ;
    k=omega(i)^2*m;
    c=2*xi*omega(i)*m;
    km=k+gamma/beta/dt*c+1/beta/dt^2*m;
    a=1/beta/dt*m+gamma/beta*c ;
    b=1/2/beta*m+dt*(gamma/2/beta-1)*c ;
        for j =1:(length(acc)-1); %Perform Newmark to obtain dyn. response
            u(1)=0;
            v(1)=0;
            ac(1)=0;
            dpm=(acc(j+1)-acc(j))*m+a*(v(j))+b*ac(j);
            du=dpm/km;
            dv=gamma/beta/dt*du-gamma/beta*v(j)+dt*(1-gamma/2/beta)*ac(j);
            dac=1/beta/dt^2*du-1/beta/dt*v(j)-1/2/beta*ac(j);
            u(j+1)=u(j)+du;
            v(j+1)=v(j)+dv;
            ac(j+1)=ac(j)+dac;
        end
Sd(i)=max(u);           %Maximum displacement for each natural period
Sa(i)=omega(i)^2*Sd(i); %Pseudo acceleration response spectra
T(i+1)=T(i)+dt;
end
Sa(1)=max(abs(acc));
Sa(2)=Sa(1);
Sd=Sd';
Sa=Sa';
T=T';
T(end)=[];

% End
```

C. Elaborated 65-kW Wind Turbine

C.1 Existing Wind Turbine

Figure C.1 shows the 65-kW wind turbine installed at LHPOST@UCSD, and indicates direction of shaking.

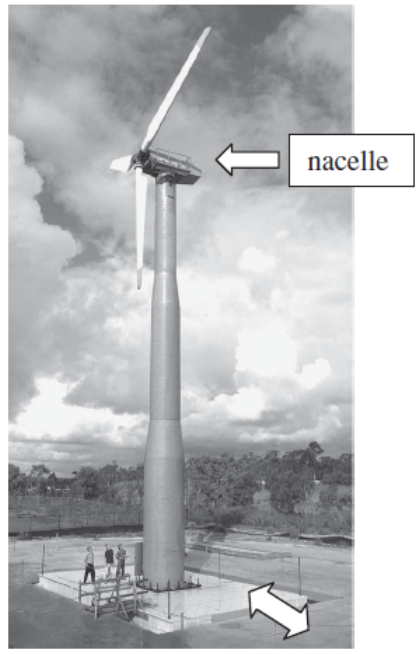

Figure C.1: *Actual 65-kW wind turbine at LHPOST@UCSD [Prowell et al., 2009].*

C.2 2004 Shake Table Test at UCSD

Figure C.2 shows a schematic set-up of the 65-KW wind turbine and the accelerometers used in Prowell et al. [2009]. It also reflects the acceleration output from the SAP2000 analysis conducted in this study.

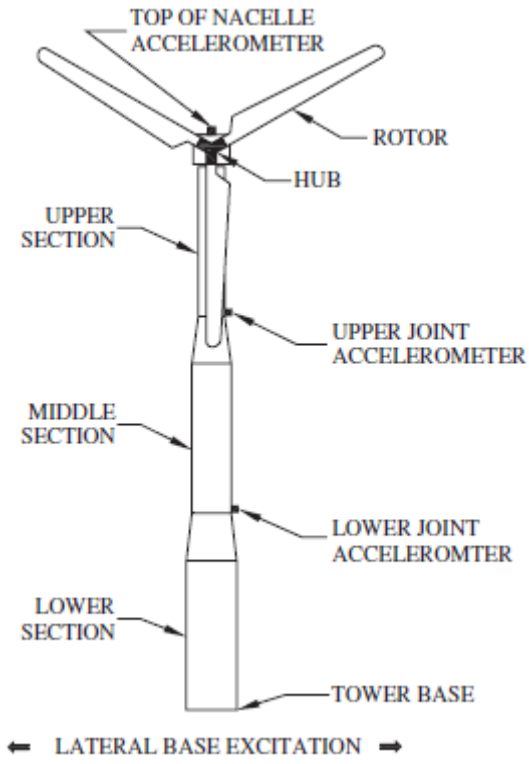

Figure C.2: *Schematic of 65-kW wind turbine [Prowell et al., 2009].*

C.3 Modal Participation Table from this Study

Table C.1 shows modal participation factors for the numerical model of the 65-kW wind turbine, developed in *this study*. Only the ten first modes is showed in Table C.1, as only ten modes is utilized in the modal analysis (as explained in Chapter 4.4.2).

Table C.1: *Modal participation factors for the 65-kW wind in SAP2000.*

Mode #	f_n	U_x	U_y	U_z	R_x	R_y	R_z
[-]	[Hz]	[-]	[-]	[-]	[-]	[-]	[-]
1	1,66	0,0000	0,6527	0,0003	0,9653	0,0000	0,0000
2	1,68	0,6569	0,0000	0,0000	0,0000	0,9672	0,0602
3	9,16	0,0000	0,0228	0,0001	0,0058	0,0000	0,0000
4	11,85	0,0086	0,1319	0,0078	0,0227	0,0015	0,0014
5	11,87	0,1538	0,0074	0,0004	0,0013	0,0267	0,0216
6	18,20	0,0031	0,0000	0,0000	0,0000	0,0003	0,5773
7	26,20	0,0000	0,0298	0,3553	0,0019	0,0000	0,0000
8	32,19	0,0678	0,0002	0,0009	0,0000	0,0033	0,0015
9	32,41	0,0002	0,0377	0,3049	0,0018	0,0000	0,0000
10	46,60	0,0000	0,0135	0,0999	0,0004	0,0000	0,0000

C.4 Meteorological Data from Extended Shake Table Test (2010)

Table C.2 shows gathered meteorological data from Prowell et al. [2013]; the extended shake table test. The wind speed was measured from four local weather stations, and approximated using basic wind theory to the height of the nacelle. Wind direction is relative to the north, and for the configuration for side-side shaking, the turbine itself was 0° from the north. Also, the temperature and relative humidity was measured. Index refers to different tests.

Table C.2: *Meteorological Data from Prowell et al. [2013].*

Index	**Nacelle Wind Speed**	**Wind Direction**	**Temp.**	**Rel. Hum.**
[-]	[m/s]	[°]	[°C]	[%]
1	2,5	209	17	50
2	2,7	195	17	50
3	2,4	203	17	50
4	2,0	211	17	51
5	3,3	262	25	29
6	3,1	268	25	29
7	3,5	197	17	48
8	3,9	198	17	44
9	4,5	203	17	49
10	4,5	203	16	49
11	5,1	207	16	50
12	4,5	204	16	52

D. Elaborated 5-MW Wind Turbine

D.1 Natural Frequencies of Soils & Further Validation of Modelled Soil

Table D.1 presents the first six natural frequencies of a uniform, damped soil on rigid rock based on theory from Kramer [1996], using Equation (5.6) with $n = [0, 5]$.

Table D.1: *Theoretical natural frequencies of soil.*

	V_s	Frequency n [Hz]					
	[m/s]	**0**	**1**	**2**	**3**	**4**	**5**
Horizontal, X	**1000**	8,33	25,00	41,67	58,33	75,00	91,67
	900	7,50	22,50	37,50	52,50	67,50	82,50
	800	6,67	20,00	33,33	46,67	60,00	73,33
	700	5,83	17,50	29,17	40,83	52,50	64,17
	600	5,00	15,00	25,00	35,00	45,00	55,00
	500	4,17	12,50	20,83	29,17	37,50	45,83
	400	3,33	10,00	16,67	23,33	30,00	36,67
	300	2,50	7,50	12,50	17,50	22,50	27,50
	200	1,67	5,00	8,33	11,67	15,00	18,33
	100	0,83	2,50	4,17	5,83	7,50	9,17
Vertical, Z	**1000**	14,43	43,30	72,17	101,04	129,90	158,77
	900	12,99	38,97	64,95	90,93	116,91	142,89
	800	11,55	34,64	57,74	80,83	103,92	127,02
	700	10,10	30,31	50,52	70,73	90,93	111,14
	600	8,66	25,98	43,30	60,62	77,94	95,26
	500	7,22	21,65	36,08	50,52	64,95	79,39
	400	5,77	17,32	28,87	40,41	51,96	63,51
	300	4,33	12,99	21,65	30,31	38,97	47,63
	200	2,89	8,66	14,43	20,21	25,98	31,75
	100	1,44	4,33	7,22	10,10	12,99	15,88

Figure D.1 presents validation for the modelled soil for V_s 800, 700 and 600 m/s. This soil was utilized for the vertical set-up.

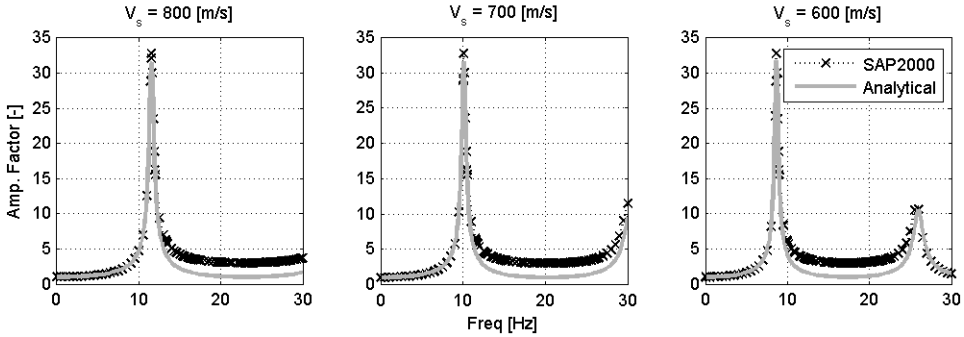

Figure D.1: *Validation for soil with V_s = 800, 700 & 600 [m/s] in SAP2000 in vertical set-up.*

D.2 Matlab Script `wind_simulation.m`

The following script simulates a turbulent wind field, with a given average wind velocity. Mainly, theory from Strømmen [2010] and recommendations from EC1-4 [2004] is applied.

```
% Wind Simulation:
%
% wind_simulation.m:
% simulates a mean wind velocity + turbulent wind
% component and scales the wind to equivalent thrust force.
%
% Written by Remi André Kjørlaug, May 2013
% Master Thesis on Wind Turbines.

clear all
close all
clc

fs = 18; l = 2;                         % Fontsize, linewidth
Size = [100 50 800 500];                % place x, place y, width, height

% Start
t0 = 0; tend = 60; dt = 0.01; t = t0:dt:tend;
u = zeros(size(t));
V = 11.4;                          %Mean wind velocity at operational power

omega0 = 0; omegaend = 20; domega = 0.01; Omega = omega0:domega:omegaend;
N = length(Omega);
```

```
type = input('Simulate new wind, [y] = 1, [n] = 2: ');
if type == 1;   % If simulate new wind

zf = 90;        % Height of turbine
xfLu0 = 100;
zf0 = 10;
z0 = 0.3;       % Friction length
Au = 6.8/(2*pi);

xfLu = xfLu0*(zf/zf0)^0.3;
Iu = 1/log(zf/z0);

dOmega = domega*ones(size(Omega));
dOmega(1) = dOmega(1)/2; dOmega(N) = dOmega(N)/2;

Su = (Iu^2)*V*Au*xfLu*ones(size(Omega))./(1+1.5*Au*Omega*xfLu/V).^(5/3);

for k = 1:N
    u = u + sqrt(2*Su(k)*dOmega(k))*cos(Omega(k)*t+2*pi*rand);
end

U = V + u;
sigmau = std(u);

%Scale to equivalent thrust force
fid = fopen('D:\01. Remi\Dokumenter\00. Master\Matlab\
[......]
WindSpeedRelationships.txt','r');
data = textscan(fid,'%f %*d %*d %*d %f %*d %*d %*d %*d %*d %*d %*d %*d %*d' [......]
,'Delimiter',',','headerLines',2);
fclose(fid);
wind_ref = data{1};
Thrust_ref = data{2};
Utemp = round(U);
T = zeros(size(Utemp));

for i = 1:length(Utemp);
    flag = 0;
    for j = 1:length(wind_ref)-1
        while flag == 0;
            if Utemp(i) ~= wind_ref(j)
                flag = 0;
            else
                flag = 1;
                T(i) = Thrust_ref(j);
            end
            j = j + 1;
         end
    end
    i = i + 1;
end

T = smooth(T,100);

%Save thrust force file
WindSim = fopen('D:\01. Remi\Dokumenter\00. Master\Modell\EarthQuakes\ [......]
```

```
wind_simulation_force_matlab.txt','w');
fprintf(WindSim,'%2.6f\n',T');
fclose(WindSim);
%Save wind velocity file
WindSimVel = fopen('D:\01. Remi\Dokumenter\00. Master\Modell\EarthQuakes\
[......]
wind_simulation_vel_matlab.txt','w');
fprintf(WindSimVel,'%2.6f\n',U');
fclose(WindSimVel);


elseif type == 2; %Use old simulation

    % Wind Vel
fid = fopen('D:\01. Remi\Dokumenter\00. Master\Modell\EarthQuakes\
[......]
wind_simulation_vel_matlab.txt','r');
data = textscan(fid,'%f');
fclose(fid);
U = data{1};
    % Wind Force
fid = fopen('D:\01. Remi\Dokumenter\00. Master\Modell\EarthQuakes\
[......]
wind_simulation_force_matlab.txt','r');
data = textscan(fid,'%f');
fclose(fid);
T = data{1};

end



%
%Plotting

    % Wind velocity
WindSimulSpeed = figure('color','w'); plot(t,U,'color','k','linewidth',l); hold on;
line_rated = line([0 60],[V V]);
set(line_rated,'Linewidth',3,'Color','k','linestyle',':');
title('A Time Domain Simulation of Wind Velocity at Hub Height','fontsize',fs);
legend('Wind velocity','Rated wind velocity','fontsize',fs-2);
ylabel('V+u [m/s]','fontsize',fs-1);
xlabel('Time [s]','fontsize',fs-1);
set(WindSimulSpeed,'Position',Size);
set(WindSimulSpeed,'Paperposition',[0 0 25 8]);
saveas(gcf,['D:\01. Remi\Dokumenter\00. Master\LaTeX\grafer\
[......]
wind_simulation_speed.png'],'png')

    % Force
WindSimulForce = figure('color','w'); plot(t,T,'color','k','linewidth',l);
title('A Time Domain Simulation of Wind Induced Thrust Force','fontsize',fs);
ylabel('Thrust Force [kN]','fontsize',fs-1);
xlabel('Time [s]','fontsize',fs-1);
set(gca,'YTick',[200:200:800]);
set(WindSimulForce,'Position',Size);
set(WindSimulForce,'Paperposition',[0 0 25 8]);
```

```
saveas(gcf,['D:\01. Remi\Dokumenter\00. Master\LaTeX\grafer\
[......]
wind_simulation_force.png'],'png')

    % Fourier Transform
fend = omegaend/(2*pi);
[f,WindF] = ffourier_trans(U,dt);

WindSimSpec = figure('color','w'); plot(f,smooth(WindF,1),'k','linewidth',1);
axis ([0 fend 0 max(WindF+0.1*max(WindF))]);
title('Frequency Power Spectra of Wind','fontsize',fs);
xlabel('Freq [Hz]','fontsize',fs-1); ylabel('Ck [g^{2} \cdot s]','fontsize',fs-1);
set(WindSimSpec,'Position',Size);
set(WindSimSpec,'Paperposition',[0 0 10 10]);
saveas(gcf,['D:\01. Remi\Dokumenter\00. Master\LaTeX\grafer\
[......]
wind_simulation_spectra.png'],'png')

% END
```

D.3 Discretized Wind Turbine Tower

Figure D.2 shows the principle of the discretized turbine tower.

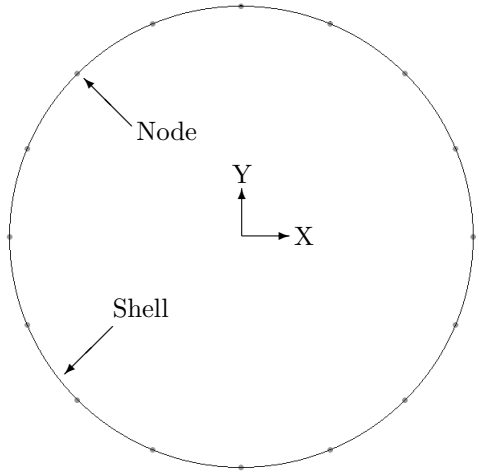

Figure D.2: *Discretized wind turbine tower.*

The same number of shell-elements (16) were utilized for both the 65-kW wind turbine, and the 5-MW wind turbine.

D.4 Ground Types According to Eurocode 8

Table D.2: *Ground types defined in EC8.*

Ground Type	**Description of stratigraphic profile**	$V_{s,30}$ $[ms^{-1}]$	N_{SPT} [blows/30 cm]	c_u [kPa]
A	Rock or other rock-like geological formation, including at most 5 m of weaker material at the surface.	> 800	-	-
B	Deposits of very dense sand, gravel, or very stiff clay, at least several tens of m in thickness, characterised by a gradual increase of mechanical properties with depth.	$360 - 800$	> 50	> 250
C	Deep deposits of dense or medium-dense sand, gravel or stiff clay with thickness from several tens of many hundreds of m.	$180 - 360$	$15 - 50$	$70 - 250$
D	Deposits of loose-to-medium cohesionless soil (with or without some soft cohesive layers), or of predominately soft-to-firm cohesive soil.	< 180	< 15	< 70
E	A soil profile consisting of a surface alluvium layer with $V_{s,30}$ values of type C or D and thickness varying between about 5 m and 20 m, underlain by stiffer material with $V_{s,30} > 800ms^{-1}$.			

$V_{s,30}$ is the average value of propagation velocity of shear waves in the upper 30 m of the soil profile at a shear strain of 10^{-5} or less [EC8-1, 2004]. In this project, $V_{s,30}$ (herein plainly V_s) is the parameter that has been varied in order to study the effects of the different soils.

E. Various Results from Analysis

E.1 Additional Results from Vertical Set-Up

E.1.1 Vertical Acceleration in Turbine Tower

V_s = 1000 m/s:

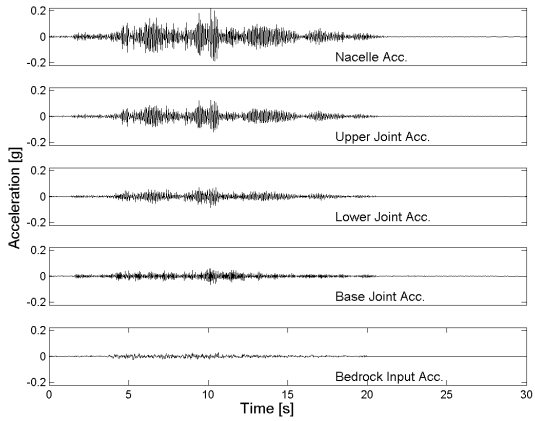

Figure E.1: *Vertical time serie response from SAP2000 for the Nahanni earthquake, V_s = 1000 m/s (Modeltype: I-V & II-V)*

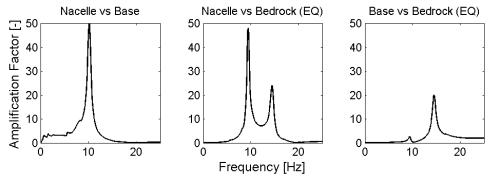

Figure E.2: *Vertical transform function for the Nahanni earthquake, V_s = 1000 m/s (Modeltype: I-V & II-V)*

V_s = 800 m/s:

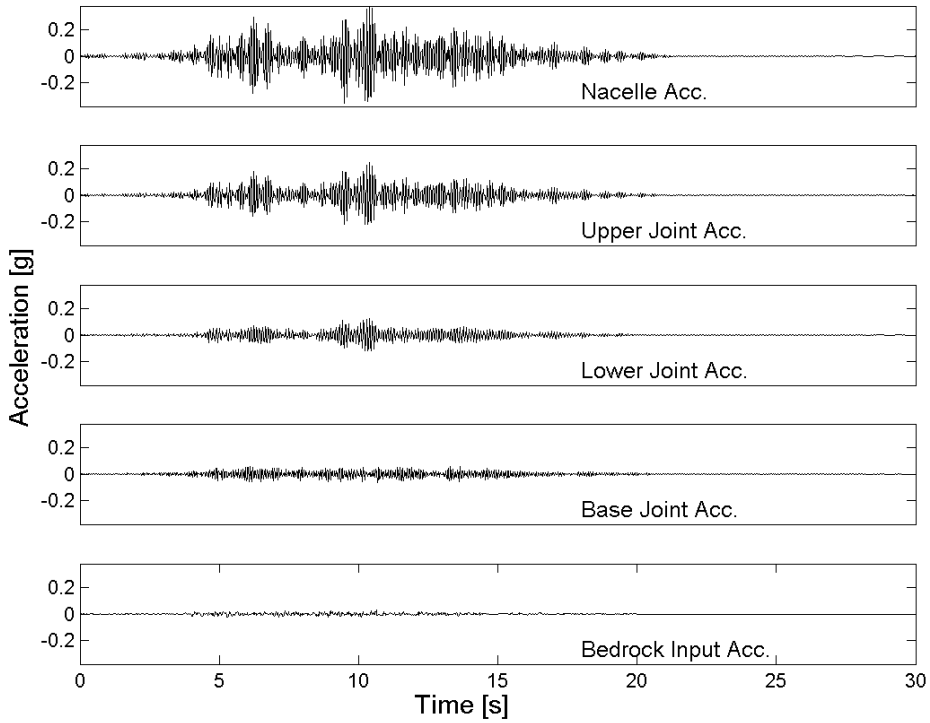

Figure E.3: *Vertical time serie response from SAP2000 for the Nahanni earthquake, V_s = 800 m/s (Modeltype: I-V & II-V)*

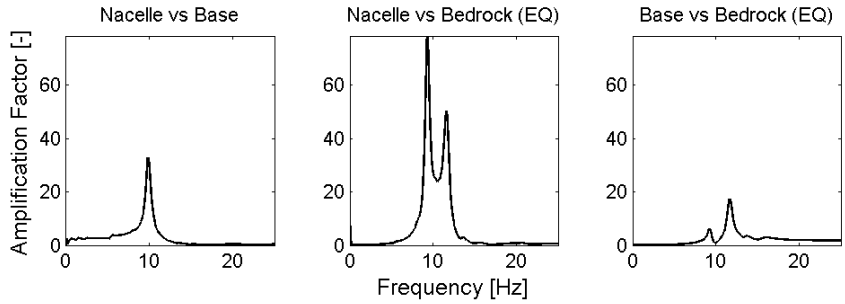

Figure E.4: *Vertical transform function for the Nahanni earthquake, V_s = 800 m/s (Modeltype: I-V & II-V)*

V_s **= 600 m/s:**

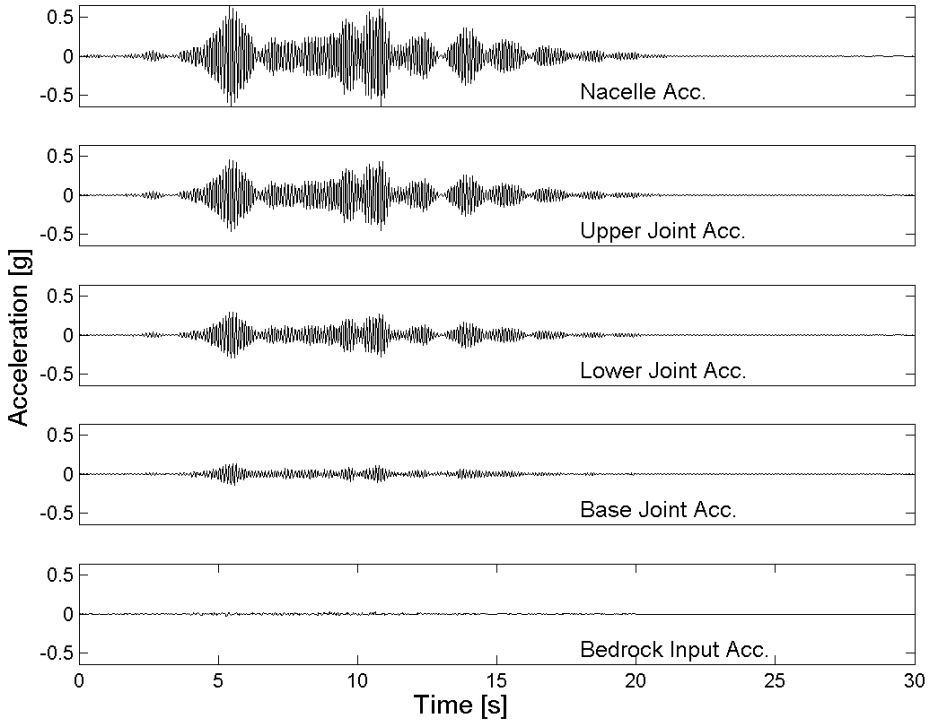

Figure E.5: *Vertical time serie response from SAP2000 for the Nahanni earthquake, V_s = 600 m/s (Modeltype: I-V & II-V)*

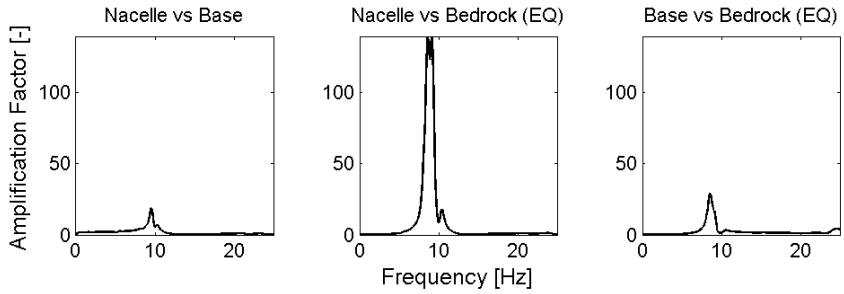

Figure E.6: *Vertical transform function for the Nahanni earthquake, V_s = 600 m/s (Modeltype: I-V & II-V)*

V_s = 500 m/s:

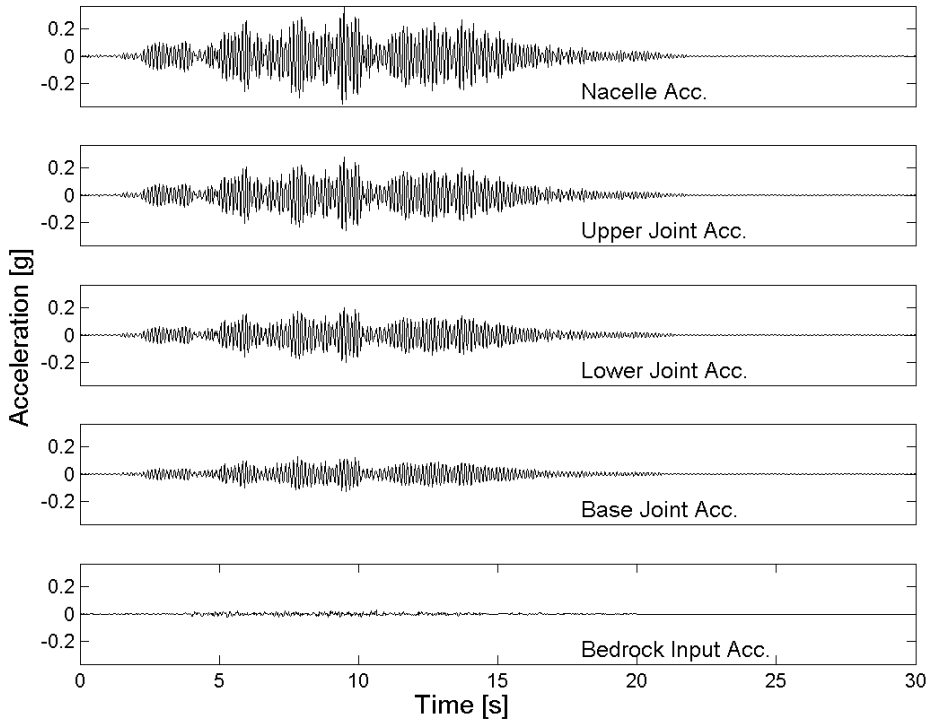

Figure E.7: *Vertical time serie response from SAP2000 for the Nahanni earthquake, V_s = 500 m/s (Modeltype: I-V & II-V)*

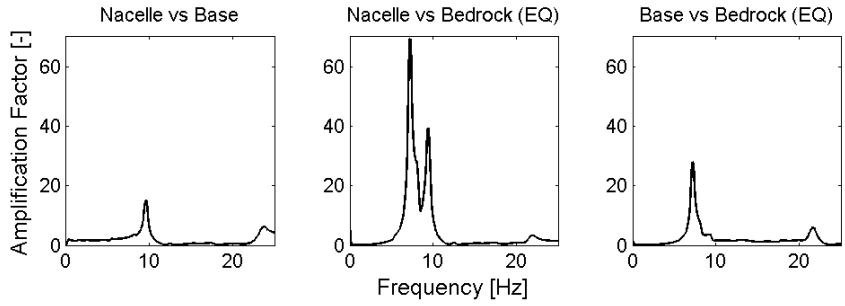

Figure E.8: *Vertical transform function for the Nahanni earthquake, V_s = 500 m/s (Modeltype: I-V & II-V)*

V_s **= 300 m/s:**

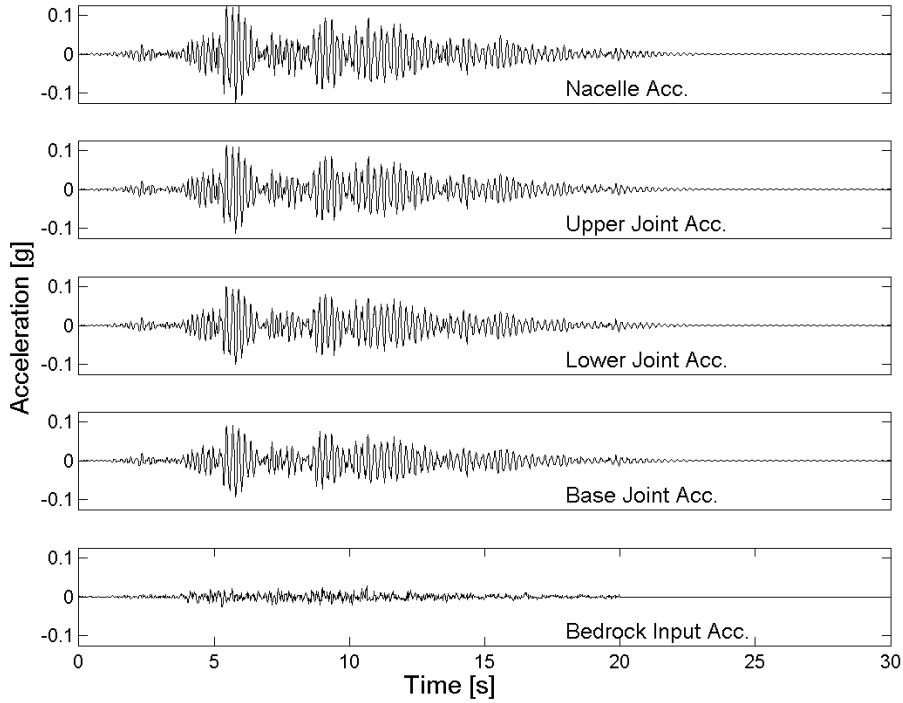

Figure E.9: *Vertical time serie response from SAP2000 for the Nahanni earthquake, V_s = 300 m/s (Modeltype: I-V & II-V)*

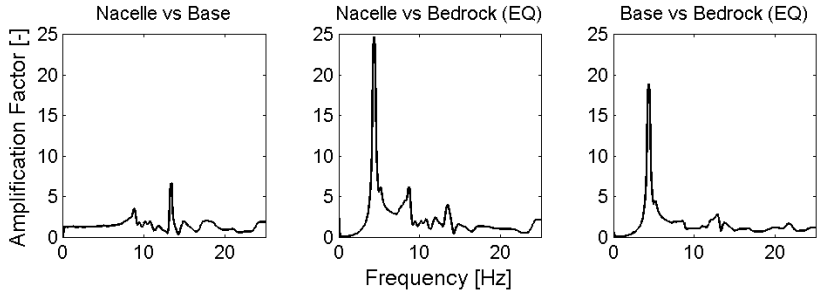

Figure E.10: *Vertical transform function for the Nahanni earthquake, V_s = 300 m/s (Modeltype: I-V & II-V)*

E.1.2 Procedure for Investigating Radiation Damping

If a model containing soil is excited with a frequency higher than the cut-off frequency (Equation (5.6) with $n = 0$ and $V_{s/p} = V_s$), waves will propagate by Rayleigh waves and shear waves.

Similar as Figure 6.8b, a dash-pot with a damping coefficient C (obtained by Equation (8.2)) was added in addition to the already present spring. Further, a ramp-force was applied vertically at the top of the wind turbine. This force was released after 5 s in order to provoke free-vibration phase in the vertical direction.

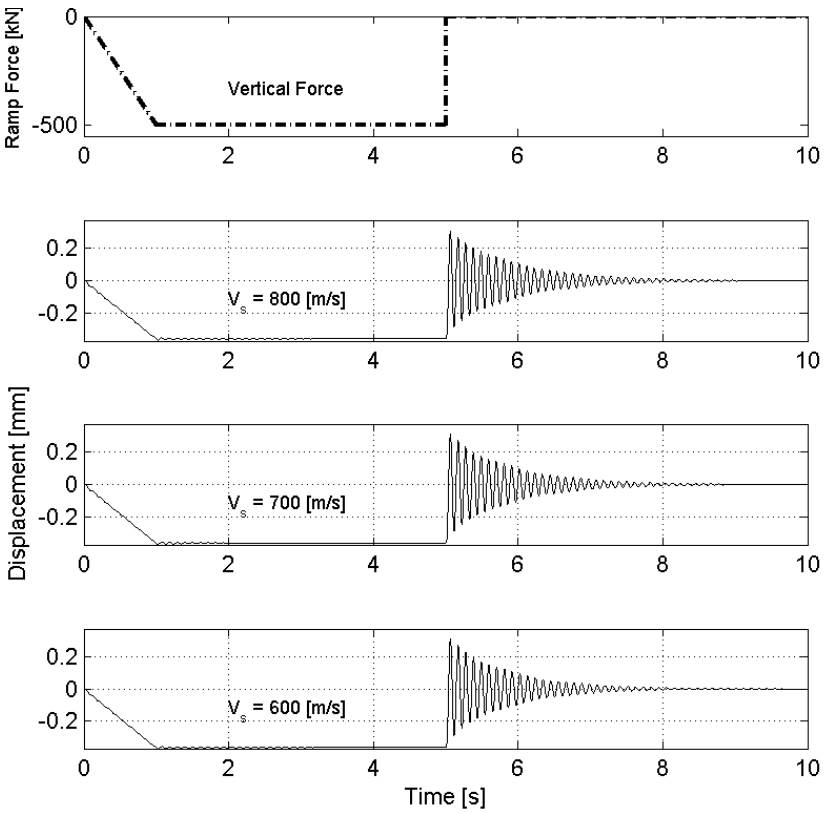

Figure E.11: *Investigation of free-vibration phase and radiation damping (Modeltype: I-V & II-V)*

Further, the logarithmic decrement method [Chopra, 2012] was utilized on the displacement plots in Figure E.11, in order to obtain some information of the magnitude of radiation damping. Results were presented in Table 8.3.

E.2 Additional Results from Horizontal Set-Up

E.2.1 Dynamic Response from Earthquake

V_s = 1000 m/s

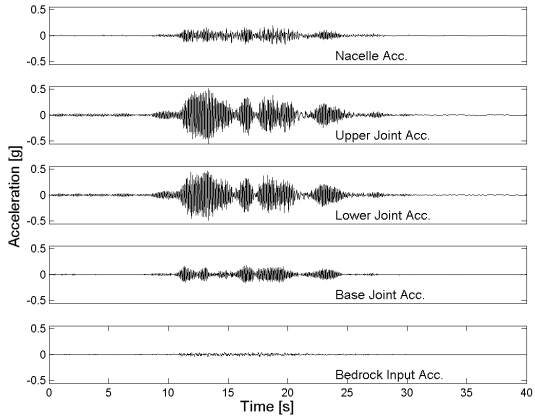

Figure E.12: *Horizontal time series response from SAP2000 for the Nahanni earthquake, V_s = 1000 m/s (Modeltype: I-H)*

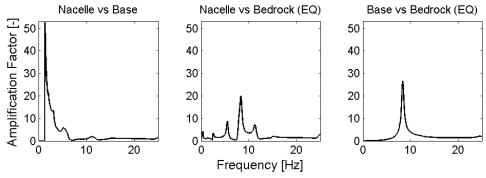

Figure E.13: *Horizontal transform functions for the Nahanni earthquake, V_s = 1000 m/s (Modeltype: I-H)*

V_s **= 500 m/s**

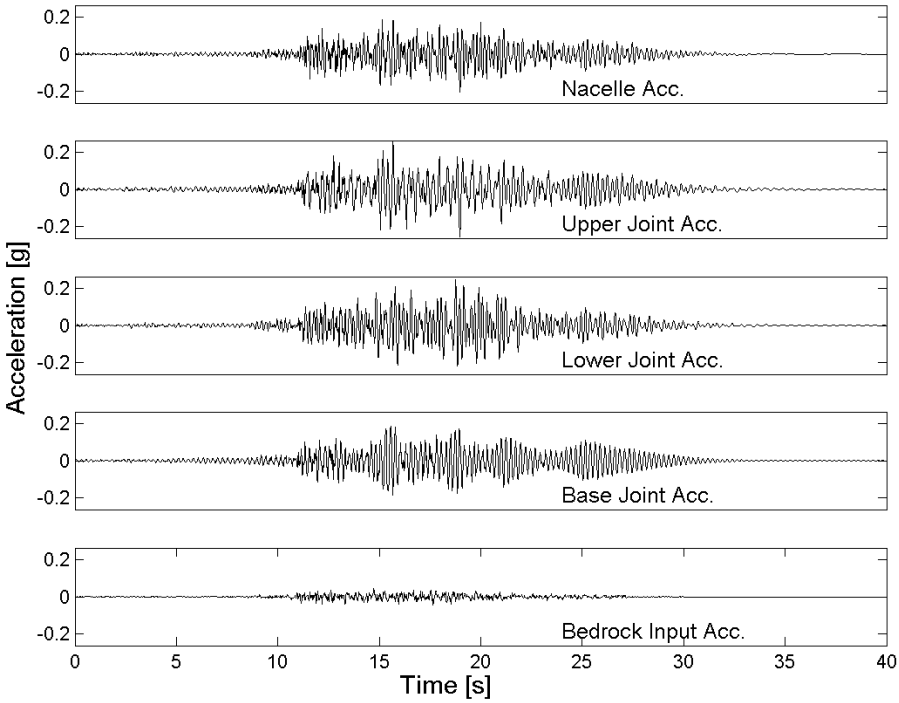

Figure E.14: *Horizontal time series response from SAP2000 for the Nahanni earthquake, V_s = 500 m/s (Modeltype: I-H)*

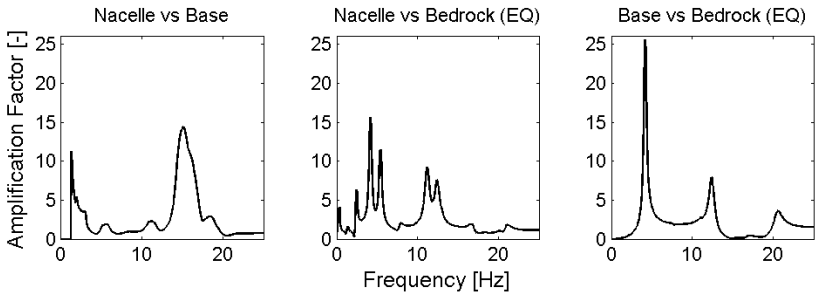

Figure E.15: *Horizontal transform functions for the Nahanni earthquake, V_s = 500 m/s (Modeltype: I-H)*

Base Moment Demand

Base moment demand from Configuration II:

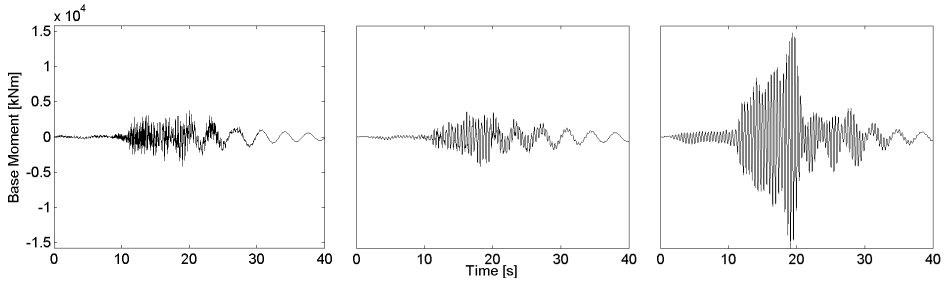

(a) $V_s = 1000\ m/s$. ***(b)*** $V_s = 500\ m/s$. ***(c)*** $V_s = 300\ m/s$.

Figure E.16: *Moment demand at base for different* V_s *(II-H).*

E.3 Further Attachments

For further attachments; script, results, various models, literature and tables, direct contact with the author is preferred.

remi_ak87@hotmail.com